

# Theoretical Explanation of Activation Sparsity through Flat Minima and Adversarial Robustness

Ze Peng<sup>†</sup>      Lei Qi<sup>‡</sup>      Yinghuan Shi<sup>§</sup>      Yang Gao<sup>¶</sup>

6 September 2023

## Abstract

The recent empirical observation [1] of activation sparsity in MLP layers offers an opportunity to drastically reduce computation costs for free. Despite several works attributing it to training dynamics, the theoretical explanation of activation sparsity’s emergence is restricted to shallow networks, small training steps well as modified training, even though the sparsity has been found in deep models trained by vanilla protocols for large steps. To fill the three gaps, we propose the notion of gradient sparsity as the source of activation sparsity and a theoretical explanation based on it that explains gradient sparsity and then activation sparsity as necessary steps to adversarial robustness w.r.t. hidden features and parameters, which is approximately the flatness of minima for well-learned models. The theory applies to standardly trained LayerNorm-ed pure MLPs, and further to Transformers or other architectures if noises are added to weights during training. To eliminate other sources of flatness when arguing sparsities’ necessity, we discover the phenomenon of spectral concentration, i.e., the ratio between the largest and the smallest non-zero singular values of weight matrices is small. We utilize random matrix theory (RMT) as a powerful theoretical tool to analyze stochastic gradient noises and discuss the emergence of spectral concentration. With these insights, we propose two plug-and-play modules for both training from scratch and sparsity finetuning, as well as one radical modification that only applies to from-scratch training. Another under-testing module for both sparsity and flatness is also immediate from our theories. Validational experiments are conducted to verify our explanation. Experiments for productivity demonstrate modifications’ improvement in sparsity, indicating further theoretical cost reduction in both training and inference.

---

<sup>†</sup>State Key Laboratory for Novel Software Technology, Nanjing University; Email: pengze@smail.nju.edu.cn

<sup>‡</sup>School of Computer Science and Engineering, Southeast University; Email: qilei@seu.edu.cn

<sup>§</sup>State Key Laboratory for Novel Software Technology, Nanjing University; Email: syh@nju.edu.cn; Corresponding author

<sup>¶</sup>State Key Laboratory for Novel Software Technology, Nanjing University; Email: gaoy@nju.edu.cn

# Contents

<b>1</b>	<b>Introduction</b>	<b>4</b>
<b>2</b>	<b>Related Works</b>	<b>6</b>
<b>3</b>	<b>Preliminary</b>	<b>7</b>
3.1	Notation . . . . .	7
3.2	Sparsities, Activation Sparsity and Gradient Sparsity . . . . .	9
3.3	Empirically Measuring Sparsity . . . . .	11
3.4	Flat Minima and Stochastic Gradient Noise . . . . .	11
3.5	Random Matrix Theory and Marchenko-Pastur Distribution . . . . .	12
3.6	Adversarial Robustness . . . . .	13
<b>4</b>	<b>Gradiential Explanation of Activation Sparsity</b>	<b>13</b>
4.1	Illustration . . . . .	13
4.2	Gradients w.r.t. Weight Matrices and Zeroth Biases . . . . .	16
4.3	Flat Minima, Implicit Adversarial Robustness and Gradient Sparsity . . . . .	19
4.4	Discussions on Theorem 2 . . . . .	22
4.4.1	Pure MLPs . . . . .	22
4.4.2	Transformers and Other Architectures . . . . .	23
4.4.3	The First Term from Zeroth Biases . . . . .	26
4.5	Spectral Concentration at Initialization . . . . .	27
4.6	Spectral Concentration during Stochastic Training . . . . .	30
<b>5</b>	<b>Experiments for Verification</b>	<b>34</b>
<b>6</b>	<b>Experiments for Productivity</b>	<b>36</b>
6.1	Training from Scratch . . . . .	36
6.2	Finetuning for Sparsity . . . . .	39
<b>7</b>	<b>Empirical Supports for Assumptions</b>	<b>41</b>
7.1	Spectral Increase in $K^l (K^l)^\top \odot M$ . . . . .	41
7.2	Spectral Concentration of $K^l (K^l)^\top$ . . . . .	42
7.3	Assumptions for Theorem 6 . . . . .	42
<b>8</b>	<b>Conclusion</b>	<b>48</b>
	<b>Appendices</b>	<b>54</b>
<b>A</b>	<b>Proof of Lemmas</b>	<b>54</b>
<b>B</b>	<b>More Preliminaries</b>	<b>55</b>
<b>C</b>	<b>Proof of Theorem 6</b>	<b>56</b>
<b>D</b>	<b>Effective Window Size</b>	<b>67</b>

<b>E</b>	<b>Experimental Details</b>	<b>68</b>
<b>F</b>	<b>More Experimental Results</b>	<b>69</b>
<b>G</b>	<b>Theoretically Guided Magic: Massive Perturbation with Small Computation Cost and Good Parallelism</b>	<b>71</b>

# 1 Introduction

Despite the success of overparameterized deep neural networks, how they learn, work and generalize well is not fully understood. Although more than half of parameters and computation are devoted to them [2], even in Transformers, MLP blocks have remained black box for years, blocking interpretation, manipulation and pruning in them. Recently, some works [2], [3] have tried to dive into MLP blocks and reveal its relation with learned knowledge by rewriting MLP blocks of Transformers into an attention mechanism where keys and values are provided by the first and second linear layers, and form a key-value memory that stores learned knowledge.

A more recent work [1] further discovers activation sparsity in MLP blocks, i.e., only a small portions of neurons are activated during inference, within MLP blocks of pure MLP, ResNet, T5, (ReLU) ViT and other architectures on various tasks, without explicit regularization. This discovery not only brings research attention back to MLP blocks when it comes understanding Transformers, but also leads to potential aggressive neuron pruning during inference and thus large reduction in inference cost. Specifically, if pruning is carefully implemented to skip non-activated neurons, theoretically in T5 the inference costs happening in MLP blocks can be astonishingly reduced by about 90%. There is also an increasing tendency of activation sparsity, measured in percentage of zero activations, when models become larger [1], hinting potentially great cost reduction for large models.

However, the emergence of sparsity is not yet fully understood. Several works [1], [4]–[6] have been proposed to explain the emergence of sparsity from training dynamics. [1] explains activation sparsity of the last layer during the first step by exploiting properties of initialization methods and computing gradients. When sharpness-aware optimization is used, [4] finds positive components in gradients that point towards reduction in the norm of activation. However, only a shallow 2-layer MLP is studied in [4]. [5] considers second-order behaviours of SGD and proves sparsity on diagonal 2-layer MLPs, but for general networks it is only conjectured. [6] finds that noises added to samples improve sparsity. However, the noises are manually imposed and are not included in standard augmentations. Although having achieved better understanding on sparsity and training dynamics, these works are still restricted to shallow networks, small steps, or additional regularization or augmentations that cannot be found in ubiquitous training protocols.

Filling the gap between experiments and these theoretical results, we propose a new theoretical explanation that applies to deep networks, large training steps and standard training practices. In particular, we first rewrite the flatness bias of SGD into a tendency to improve implicit adversarial robustness w.r.t. hidden features and parameters. Gradient sparsity and effective gradient sparsity is proposed as the cause of activation sparsity. To support this, we prove a theorem stating that these sparsities can be one of the sources of the implicit adversarial robustness. Since flat minima bias puts constraints on all layers, basing our explanation on this inductive bias allows us reason about deep layers. To eliminate other potential sources of implicit adversarial robustness, we utilize pre-LayerNorm, refer to an already discovered inductive bias called parameter growth [7] and empirically discover a new phenomenon of spectral concentration, i.e., the fraction between the largest and smallest non-zero singular values of the first weight matrices in MLP blocks is not very large. We prove the emergence of spectral concentration at initialization. We also theoretically discuss its re-emergence and maintenance during later training using random matrix theory (RMT) by extracting from stochastic updates two large random matrices, indicating that training stochasticity’s contribution to sparsity is two-folded. Notably, thanks to RMT our formulation of stochastic gradient noises is very direct, without assuming Gaussian or  $\mathcal{S}\alpha\mathcal{S}$  distributions on them.

Following these theoretical insights, we propose two plug-and-play and orthogonal architectural modifications and a drastic modification to improve sparsity, and one under-testing algorithm for both flatness and sparsity, which turn out to be theoretically oriented and greatly ease our formal analyses. The structure of this work is as the following:

- In Section 3, we introduce preliminaries and background information. But in Section 3.2, we propose gradient sparsity, distinguish it with activation sparsity and argue its importance over activation sparsity;
- In Section 4.1, we build an intuitive framework of our explanation from flat minima and implicit adversarial robustness. Two almost plug-and-play architectural modifications, DB-MLP and J-SquaredReLU, are proposed to further improve sparsity and ease formal analyses;
- In Section 4.2, gradients of MLP blocks are computed, laying the basis for latter formal analyses. Effective gradient sparsity is defined in this subsection, and its connection with training updates as well as gradient sparsity is discussed;
- In Section 4.3, we prove Theorem 2 that relates flat minima, implicit adversarial robustness to effective gradient sparsity and activation sparsity by proving relatively tight chained upperbounds among them, demonstrating that sparsity can be the source of implicit adversarial robustness imposed by flat minima;
- In Section 4.4, we instantiate Theorem 2 in several specific settings involving pure MLPs and Transformers. Among them, Theorem 3 proves the tendency toward effective gradient sparsity on pure MLPs with pre-LayerNorms. We argue that effective gradient sparsity is more stable and powerful during the entire training than direct activation sparsity. Theorem 4 deals with Transformers and other architectures by assuming perturbation training like dropout. Another under-testing module called MagicSynapse is immediate after Theorem 4 and is elaborated on in Appendix G. We discuss the effectiveness of our modifications in the rest of this subsection. Aside from effective gradient sparsity, implicit adversarial robustness and flatness can potentially be achieved by reducing norms of a matrix or misaligning gradients with that matrix in the term brought by our modification. To eliminate the first, the discovered phenomenon of parameter growth is utilized. The latter is handled in later subsections;
- Eliminating the latter, we discover another phenomenon in ViTs that most non-zero eigenvalues of the matrix differ by at most 100 times for most of the time, leaving only two possibilities: adversarial robustness is achieved only by (effective) gradient sparsity, or back-propagated gradients are totally lost. In Section 4.5, we prove the emergence of this spectral concentration at initialization, exploiting modern initialization techniques. A drastic architectural modification, wide MLPs, is proposed to fill a gap of theories;
- In Section 4.6 we discuss spectral concentration’s maintenance and re-emergence in latter stochastic training, using random matrix theory by extracting two large random matrices from the updates to the weight matrices;
- In Section 5, we conduct experiments 1) to show that activation sparsity can be lost but gradient sparsity is stable, and 2) to verify our explanation;

- In Section 6, we train modified ViT-Base on ImageNet-1k from scratch to examine the effectiveness of our modifications in the sense of sparsity and further verify our explanation. We also finetune trained weights for sparsity after plugging the two modifications to show their effectiveness;
- In Section 7, assumptions made in Section 4.3 and Section 4.6 are examined empirically.

To summarize our contribution, we propose notions of gradient sparsity, effective gradient sparsity and implicit adversarial robustness. We explain activation sparsity with flat minima and implicit adversarial robustness, and propose three architectural theoretically guided modifications to improve sparsity, as well as an under-testing one for both sparsity and flatness. To our knowledge, we are the first to utilize random matrix theory to reason about inductive bias during stochastic training. As a result, the modeling of stochastic gradient noises (SGN) is very direct and avoids any debatable SGN modeling like Gaussian or  $\mathcal{S}\alpha\mathcal{S}$  model. Experiments show that our explanation is more applicable than other potential ones and our modification further improves activation sparsity by a large margin.

## 2 Related Works

In this section, we list works of the same topic as ours. Section 3 contains works of different topics that our explanation depends on, we omit their details for simplicity here.

In our point of view, the research of activation sparsity in MLP modules starts from the discovery on the relation between MLP and knowledge gained during training. [3] first rewrites MLPs in Transformers into an unnormalized attention mechanism where queries are inputs to the MLP block while keys and values are provided by the first and second weight matrices instead of inputs. So MLP blocks are key-value memories. [2] pushes forward by detecting how each key-value is related to each question and provides a method to surgically manipulate answers for individual questions in Q&A tasks. These works reorient research attention back to MLPs, which are previously shadowed by self-attention.

Recently, comprehensive experiments conducted by [1] demonstrate activation sparsity in MLPs is a prevail phenomenon in various architectures and on various CV and NLP tasks. [1] also eliminates alternative explanations and attributes it solely to training dynamics. The authors explain the sparsity theoretically with initialization and by calculating gradients, but their explanation is restricted to the last layer and the first step because in later steps the independence between weights and samples required by the explanation is broken. They also notice that some activation functions, such as tanh, hinder the sparsity (Fig B.3(c) in [1]), but did not elaborate on it. Compared to [1], our explanation applies to all layers and large steps, and account for the activation functions' critical role on activation sparsity.

Following [1]'s empirical discoveries, [4] shows that sharpness-aware (SA) optimization has stronger bias toward activation sparsity. They explain theoretically by calculating gradients and finding that SA optimization imposes in gradients a component toward reducing norms of activations. However, their explanation is still conducted on shallow 2-layer pure MLPs, and requires SA optimization which is not included in standard training practice. Compared to [4], we explain *deep* networks as long as there are MLPs, and substitute flat minima for SA optimization.

A more recent work [6] holds a similar point with us that the sparsity is a resistance to noises. However, noises are manually imposed in [6] and not included in standard data augmentations. We

substitute gradient noise from SGD or other stochastic optimizers for them. [5] proves sparsity on 2-layer diagonal MLPs, recognizes an important Hadamard product structure that guards sparsity, and conjectures similar things to happen in more general networks. A similar Hadamard product shows up in our explanation and fulfills [5]’s conjecture in deep and general architectures.

[8] studies the adversarial robustness of Mixture of Experts (MoE) models brought by architecture-imposed sparsity. [8] inspires us to relate sparsity with adversarial robustness, although we do it reversely. It is the major inspiration of our results.

To sum up, compared to existing explanatory works, our explanation applies to deep networks and large training steps, and sticks to standard training procedures.

There are other works that are not devoted to activation sparsity but are related to our work. [9] formulates, with Shapley value, and proves that there are sparse “symbols” as groups of patches that are the only major contributors to the output of any well-trained and masking-robust AIs. [9] provides a sparsity independent of training dynamics. Their theory focuses on symbols and sparsity in inputs, which is inherently different from ours.

In Primer [10], several architectural changes given by model searching include a new activation function Squared-ReLU. In this work, we induce a similar squared ReLU activation but with non-zero part shifted left and use it to guide the search for flat minima and gradient/activation sparsity. [10] demonstrates impressive improvement of Squared-ReLU in both ablation and addition experiments, and our work provides a potential explanation for this improvement.

### 3 Preliminary

Before starting, we concisely introduce elements that build our theory. We start from basic symbols and concepts of sparsities, go through bias toward flat minima, adversarial robustness and random matrix theory that deals with large random matrices.

#### 3.1 Notation

We use  $x, y$  to indicate samples and labels, respectively, and  $\mathcal{D} = \{(x_s, y_s) : 1 \leq s \leq |\mathcal{D}|, s \in \mathbb{N}^+\}$  for the training dataset. We restrict focus on activation sparsity on *training* samples, as implicitly done in [1], [4], so we do not introduce symbols for testing set. Lowercase letters such as  $f$  are used to indicate unparameterized models and those subscripted by parameter  $\theta$ , such as  $f_\theta$ , indicate parameterized ones. Classification task is assumed, so  $f_\theta$  is assumed to output a probability distribution over the label space, and the probability of label  $y$  is denoted by  $f_\theta(y | x)$  or  $f(y | \theta, x)$ , with  $\sum_y f(y | \theta, x) = 1$ . Let  $\mathcal{L}$  be a certain loss, then  $\mathcal{L}(f_\theta, (x_s, y_s))$  is the loss of  $f_\theta$  on sample  $(x_s, y_s)$ . If  $l$  is a scalar function of matrix or vector  $X$ , we use  $\frac{\partial l}{\partial X} := \left[ \frac{\partial l}{\partial X_{i,j}} \right]_{i,j}$  to denote the partial derivatives of  $l$  w.r.t.  $X$ ’s entries collected in the same shape, while  $\nabla_{\text{vec}(X)} l(X)$  is used after vectorization.  $\text{Diag}(x)$  is used to transform a vector into a diagonal matrix. We use subscription to indicate substructures of matrices, i.e.,  $X_i$  is the  $i$ -th row of matrix  $X$  while  $X_{:,j}$  is its  $j$ -th column. The Hessian of scalar function  $l$  w.r.t. to vectorized parameter  $\theta$  is  $H_\theta := \left[ \frac{\partial^2 l}{\partial \theta_i \partial \theta_j} \right]_{i,j}$ . Through out this work the scalar function in the Hessian will be the empirical loss  $\mathbf{E}_{(X,Y) \sim \mathcal{D}} [\mathcal{L}(f_\theta, (X, Y))]$ . We assume models are stacked with similar modules, each of which contains at least one MLP block. The layer index is indicated with supscription  $l$ . We assume the hidden features of models on *single* samples are (column) vectors  $x^l$ , as in pure MLPs, or stacked vectors, i.e., matrix  $X^l$ , where the

$j$ -th column  $x_j^l := X_{:,j}^l$  is the vector for the  $j$ -th token in Transformers. A vanilla  $\text{MLP}^l$  block in the  $l$ -th layer contains two linear layers  $\text{MLP}_K^l$  and  $\text{MLP}_V^l$ , each with a learnable matrix  $K^l \in \mathbb{R}^{n^l \times d^l}$  or  $V^l \in \mathbb{R}^{d^l \times n^l}$  of weights, a bias  $b_K^l \in \mathbb{R}^{n^l}$  or  $b_V^l \in \mathbb{R}^{d^l}$ .  $\text{MLP}_K^l$  has a non-linear activation function  $\sigma$  while  $\text{MLP}_V^l$  does not. Following terminology of [2], [3],  $\text{MLP}_K^l$  is called a “key” layer while  $\text{MLP}_V^l$  is called a “value” layer, whose weights are called “keys” or “values”, respectively. They compute the next hidden feature as the following:

$$A^l := \text{MLP}_K^l(X^{l-1}) := \sigma(K^l X^{l-1} + b_K^l), \quad (1)$$

$$Z^l := \text{MLP}_V^l(A^l) := V^l A^l + b_V^l, \quad (2)$$

$$Z^l = \text{MLP}^l(X^{l-1}) = \text{MLP}_V^l(\text{MLP}_K^l(X^{l-1})). \quad (3)$$

For non-stacked vector hidden features  $x^{l-1}$ , the above equations simplifies to

$$\alpha^l := \text{MLP}_K^l(x^{l-1}) := \sigma(K^l x^{l-1} + b_K^l) = [\sigma(\langle K_i^l, x^{l-1} \rangle + (b_K^l)_i)]_i \in \mathbb{R}^{n^l}, \quad (4)$$

$$z^l := \text{MLP}_V^l(\alpha^l) := \sigma(V^l \alpha^l + b_V^l) = [\sigma(\langle V_i^l, \alpha^l \rangle + (b_V^l)_i)]_i \in \mathbb{R}^{d^l}, \quad (5)$$

where  $K_i^l, V_i^l$  are the  $i$ -th rows of weights  $K^l, V^l$ . In above equations,  $A^l$  and  $\alpha^l$  are called the activation pattern of  $l$ -th MLP block. Usually the shapes of  $K^l$ s and  $V^l$ s are identical across different MLP blocks so we drop superscriptions  $l$  in  $n^l$  and  $d^l$ . In Section 4.4, we will investigate the implications of Theorem 2 under a notion of “pure” MLP. Our definition of it is models where weight matrices are updated by only one hidden vector or token during backward propagation. Under this definition, the most primitive fully connected network with stacked linear layers and activation functions is pure MLP, while CNNs, Transformers and MLP-Mixers are not because hidden features are split into multiple vectors or tokens and each MLP block must process multiple of them.

During proof, we frequently use the properties of matrix traces due to its connection with (elementwise) norm of vectors and matrices. Unless explicitly pointed out,  $\|\cdot\|_p$  for vectors is  $L_p$  norm, and  $\|\cdot\|_q$  for matrices is Schatten  $q$ -norm, i.e.,  $L_q$  norm of singular values. In the main text, only real matrices are involved and only  $L_2$  matrix norm is used for matrices. So particularly, elementwise  $L_2$  norm for matrix, or Frobenius norm, of vector  $x$  or matrix  $X$  can be computed by trace:

$$\text{tr}(x^\top x) = \text{tr}(xx^\top) = \|x\|_2^2, \quad (6)$$

$$\text{tr}(X^\top X) = \text{tr}(XX^\top) = \|X\|_2^2, \quad (7)$$

because

$$\text{tr}(A^\top B) = \sum_{i,j} A_{i,j} B_{i,j}. \quad (8)$$

This argument also indicates that elementwise  $L_2$  norm coincides with Schatten 2-norm by noticing  $X^\top X$ 's eigenvalues are squared singular values of  $X$  and are summed by the trace. Therefore, in



later proofs we use trace to express  $L_2$  norms and use a bunch of trace properties, for example its linearity

$$\text{tr}(aA + bB) = a\text{tr}(A) + b\text{tr}(B) \quad (9)$$

and the famous cyclic property with products

$$\text{tr}(ABC) = \text{tr}(CAB). \quad (10)$$

When trace is combined with Hadamard product  $\odot$ , i.e., elementwise product, there is

$$\text{tr}\left(A^\top(B \odot C)\right) = \sum_{i,j} A_{i,j}B_{i,j}C_{i,j} = \text{tr}\left(B^\top(A \odot C)\right) = \text{tr}\left(C^\top(A \odot B)\right). \quad (11)$$

When  $A, B$  are real symmetric positive semi-definite, the trace of their product can be bounded by their minimum eigenvalue and individual traces:

$$\text{tr}(AB) \geq \lambda_{\min}(A)\text{tr}(B), \quad (12)$$

where  $\lambda_{\min}(\cdot)$  indicates the smallest eigenvalue of a matrix. Finally, Hadamard product can be related to matrix products with diagonal matrices:

$$\text{Diag}(x)A\text{Diag}(y) = (xy^\top) \odot A. \quad (13)$$

This is because LHS scales rows of  $A$  first and then scales its columns, while RHS computes the scaling factors for elements in  $A$  first and then scale them in the Hadamard product.

### 3.2 Sparsities, Activation Sparsity and Gradient Sparsity

In the most abstract sense, sparsity is the situation where most elements in a set are zero. Many kinds of sparsity exist in neural networks such as weight sparsity, dead neuron, attention sparsity and activation sparsity [11]. The most static one is weight sparsity, where many elements in weight matrices are zero [12]. More dynamic ones found in hidden features are of more interests because they lead to potential pruning but without damaging model capacity. An example of them is attention sparsity found in attention maps of Transformers that many previous sparsity works [13]–[15] focus on.

The activation sparsity of our focus is the phenomenon where activations in MLPs of trained models contain only a few non-zero elements as in Definition 1

**Definition 1** (Activation Sparsity). *Recall the definition of activation pattern*

$$\alpha^l := \text{MLP}_K^l(x^{l-1}) := \sigma\left(K^l x^{l-1} + b_K^l\right) = [\sigma(\langle K_i^l, x^{l-1} \rangle + (b_K^l)_i)]_i \in \mathbb{R}^n. \quad (14)$$

*For uniformity, define activation sparsity pattern of  $\text{MLP}^l$  on sample  $X^0$  at unstacked vector hidden feature  $x^{l-1}$  to be the activation pattern  $\alpha^l$ .*

*Activation sparsity is the phenomenon that most entries in activation sparsity patterns are zero for most samples and hidden vectors. For mathematical convenience, squared  $L_2$  norm  $\|\alpha^l\|_2^2$  is used as a proxy for activation sparsity.*

Activation sparsity is observed in pure MLPs, CNNs such as ResNet, MLP blocks in Transformers, and channel mixing blocks in MLP-Mixers [1]. Note that activation sparsity cannot be explained by dead neurons or extreme weight sparsity, because every neuron has its activation for some sample [1]. Also be noted that it is not done simply by weight decay [4] but by moving pre-activations towards negative direction in ReLU networks. Activation sparsity potentially allows *dynamic* aggressive neuron pruning during inference with zero accuracy reduction [1]. Similar sparsity can be imposed by architectural design such as Mixture of Experts (MoE) [16]–[18], where each block is equipped with multiple MLPs and tokens are dynamically routed to only 1 or 2 of them. However, MoE has to deal with discrete routing that unstables the training, and emergent imbalanced routing that makes only one expert live and learn. Emergent activation sparsity has no such concerns and can also emerge within each of the experts, and thus still deserves attention even combined with MoE.

We further propose gradient sparsity as the nature of activation sparsity. Gradient sparsity is that most elements in the derivatives  $\sigma'(K^l x^{l-1} + b^l)$  of activations are zero as in Definition 2.

**Definition 2** (Gradient Sparsity). *Let  $\gamma^l$  to be the entrywise derivatives of activation in  $\text{MLP}^l$  with activation function  $\sigma$ , i.e.,*

$$\gamma^l := \sigma' \left( K^l x^{l-1} + b_K^l \right) = [\sigma' (\langle K_i^l, x^{l-1} \rangle + (b_K^l)_i)]_i \in \mathbb{R}^n. \quad (15)$$

*If the model uses stacked hidden features, then let  $\Gamma^l$  be the stacked version. Define gradient sparsity pattern of  $\text{MLP}^l$  on sample  $X^0$  at vector hidden feature  $x^{l-1}$  to be  $\gamma^l$ .*

*Gradient sparsity is the phenomenon where most entries in gradient sparsity pattern  $\gamma^l$  are zero for most samples and hidden vectors. For mathematical convenience, squared  $L_2$  norm  $\|\gamma^l\|_2^2$  is used as a proxy for gradient sparsity.*

For activation functions like ReLU, gradient sparsity coincides with activation sparsity and gives birth to the latter, and the coincidence is why only activation sparsity is proposed in previous empirical works such as [1]. We argue gradient sparsity is more essential and stable than direct activation sparsity. Our theoretical analyses will show that gradient sparsity is a stable cause of activation sparsity through their coincidences, although there is unstable but direct implicit regularization on activation sparsity. Experiments for validation in Section 5 show activation can be manipulated to be dense by gradient sparsity.

Here, we argue the practical importance of gradient sparsity over activation sparsity. Interestingly, activation sparsity itself can be generalized and thus leads to gradient sparsity. To prune most neurons, one actually does not need exact activation sparsity where most activations are zero, but only the fact that most activations have the *same* (possibly non-zero) value that can be *known a priori*. If so, activations can be shifted by the a priori most-likely activation to obtain the exact activation sparsity followed by pruning, and adding the sum of key vectors multiplied by that value back can compensate the shift. If certain regularities of the activation function (for example, being monotonically increasing like ReLU) can be assumed, then these most-likely activations must reside in a contiguous interval in activation function’s domain, which leads to gradient sparsity. The conversed version of this argument also shows that gradient sparsity leads to pruning during inference. Therefore, gradient sparsity is closer to a sufficient and necessary condition for massive pruning, while the activation sparsity is only a sufficient condition much farther from being necessary. Moreover, gradient sparsity also allows aggressive neuron pruning during *training*, which is

more beneficial for researchers in the era of large models. Therefore, more attention should be paid on gradient sparsity.

A more generalized version, effective gradient sparsity, is the sparsity defined on the Hadamard product, or entrywise product, between the gradient sparsity pattern  $\gamma^l$  and the gradient w.r.t. to the activation. Exactly how and why it is defined can be found in Definition 3 to avoid confusion. Using this notion of sparsity, better theoretical results can be obtained. Making these theoretical shift practically meaningful, gradient w.r.t. activation allows further pruning because neurons with near-zero gradients w.r.t. to themselves 1) have little influence on the output during forward propagation and 2) have little contribution to gradients back propagated to shallower layers. As one shall see in Section 4.2, from a theoretical and interpretational view, effective gradient sparsity is also what MLP blocks try to bear in their key matrices.

### 3.3 Empirically Measuring Sparsity

[1] utilizes the percentage of nonzeros in activations on testing samples as a simple measurement of sparsity in ReLU network. We adopt a similar measure but it is also conducted on *training* samples in each batch and we observe its revolution during the entire training. We additionally observe training sparsity in order to see how potentially well gradient sparsity reduces training cost, and we restrict samples to those in the current batch because in practical training, samples outside the batch will not be used and are irrelevant to actual training costs. Sparsity is further averaged across layers and integrated across the steps to approximate the overall reduction in MLPs’ training costs. Since it contains extreme statistics such as in diagonality ratios, Layer 12 is excluded from observation.

### 3.4 Flat Minima and Stochastic Gradient Noise

One of the accounts for good generalization unexpected by traditional statistical learning theory in deep networks is the implicit regularization introduced by architectures, training procedures, etc. One of the most considered is the inductive bias toward flat minima, i.e., loss minima given by SGD are very likely to be flat. This flatness in training loss landscape indicates that the loss landscape nearby the minima will not rise acutely due to distribution shift and explains small loss increase and good generalization in testing [19].

Bias toward flat minima is usually considered due to stochastic gradient noises (SGN) introduced by SGD or other stochastic optimizers, which drives the parameter to escape from sharp minima [20]. Although SGD is usually considered to have stronger flatness bias, parameters optimized by other adaptive optimizers such as Adam still escape sharp minima, only in a slower manner [20].

In works that study SGN and flat minima like [20], [21], the updates of SGD at step  $t$  are often written as

$$\theta^{t+1} = \theta^t - \eta \nabla_{\theta} \mathcal{L}(\theta) + \eta U^t, \quad (16)$$

where  $\mathcal{L}(\theta) := \mathbf{E}_{(X,Y)} [\mathcal{L}(f_{\theta}, (X, Y))]$  is the full-batch gradient, and noise term  $U^t := \nabla_{\theta} \mathcal{L}(\theta) - \frac{1}{|B_t|} \sum_{s \in B_t} \nabla_{\theta} \mathcal{L}(\theta, (x_s, y_s))$  is the difference between full-batch gradient and the gradient provided by the current batch  $B_t$ . If samples in batches are uniformly sampled, the expected mini-batch gradient  $\sum_{s \in B_t} \nabla_{\theta} \mathcal{L}(\theta, (x_s, y_s))$  is naively  $\nabla_{\theta} \mathcal{L}(\theta)$  and the noise  $U^t$  is centered by definition.  $U^t$  is previously modeled by Gaussian distribution as a result of the Central Limit Theorem. Recent works [20], [21] argue that it should better be modeled with symmetric  $\alpha$ -stable ( $S\alpha\mathcal{S}$ ) distribution

based on Generalized Central Limit Theorem where finite variance is not necessary. Under this model, the noise norm is long tailed and expected norm can be very large, since an  $\mathcal{S}\alpha\mathcal{S}$  distribution has infinite variance if it is not Gaussian.

In this work we only rely on the empirical and theoretical results that parameters are optimized toward flat minima. Using random matrix theory, we are allowed to model SGN in the most direct way without relying Gaussian or  $\mathcal{S}\alpha\mathcal{S}$  distribution, by assuming gradient vectors are uniformly and independently (conditionally, when previous updates are conditioned on) sampled from a pool of possible gradients produced by the entire finite training dataset and the model parameter before the update.

Following theoretical works on information bottlenecks [22]–[24], we use the nuclear norm of Hessian at a minimum to measure how flat the minimum is. When a local minimum is reached the Hessian is real symmetric and positive semi-definite, so the nuclear norm equals to its trace, i.e.

$$\|H_\theta\|_* = \text{tr}(\sqrt{H_\theta^* H_\theta}) = \sum_i |\lambda_i| = \sum_i \lambda_i = \text{tr}(H_\theta), \quad (17)$$

where  $\lambda_i$  is the  $i$ -th largest eigenvalues of  $H_\theta$ , and the trace is used to measure flatness. We assume as [22]–[24] that this trace is suppressed during stochastic training.

### 3.5 Random Matrix Theory and Marchenko-Pastur Distribution

The latter half of our theory explaining sparsity’s tendency during stochastic training is based on spectral analysis on sample covariance matrix of large random matrices, which are the main focus of random matrix theory (RMT). Particularly about the most classic setting, consider a sequence of random matrices  $\{X^p \in \mathbb{C}^{p \times n}\}_p$  with size increasing to infinity, where all entries in the sequence are centered, standardized and I.I.D. sampled, and  $n = n(p) = \Theta(p)$  increases linearly with  $p$ . The sample covariance of  $X^p$  is  $S^p := \frac{1}{n} X^p (X^p)^\top$ . To measure their spectral properties, define the empirical spectral distribution  $F^{S^p}(x) := \frac{1}{p} \sum_i \mathbf{I}[\lambda_i(S^p) \leq x]$  and corresponding density  $f^{S^p}$  of eigenvalues for each matrix  $S^p$ . Note that  $F^{S^p}$  is a random variable as  $S^p$ ’s function, but Marchenko and Pastur [25] proved that when  $p$  goes to infinity,  $F^{S^p}$  converges to a non-random distribution later named as Marchenko-Pastur distribution, formally stated in Theorem 1.

**Theorem 1** (Marchenko–Pastur distribution [26]). *Let  $X_{i,j}$ ,  $1 \leq i \leq p, 1 \leq j \leq n$ , be I.I.D. complex random variables with  $\mathbf{E}[X_{i,j}] = 0$  and  $\mathbf{E}[X_{i,j}^2] = 1$ . Let  $X^p := [X_{i,j}]_{i,j} \in \mathbb{R}^{p \times n}$  be the matrix comprised of these random variables. Let  $\lambda_k(\cdot)$  be the  $k$ -th largest eigenvalues of the symmetric matrix*

$$S^p := \frac{1}{d} X^p (X^p)^\top, \quad (18)$$

*and define its empirical spectral distribution (ESD) by*

$$F_p(x) = F^{S^p}(x) = \frac{1}{p} \sum_{k=1}^p \mathbf{I}[\lambda_k(S^p) \leq x]. \quad (19)$$

*and corresponding density  $f_p = f^{S^p}$ .*

When  $p, n \rightarrow \infty$  with  $p/n := c$ ,  $f^p \rightarrow f$  in probability, where density  $f$  of Marchenko-Pastur distribution is defined by

$$f(x) = \frac{1}{2xc\pi} \sqrt{(b-x)(x-a)} \mathbf{I}[a \leq x \leq b] + \mathbf{I}[x \geq 1] \cdot \left(1 - \frac{1}{c}\right) \delta(x), \quad (20)$$

$a = (1 - \sqrt{c})^2$ ,  $b = (1 + \sqrt{c})^2$ , and  $\delta$  is the Dirac delta function.

We will discover  $X^p(X^p)$ -like matrices products in Section 4.5 and Section 4.6, and apply generalized Theorem 1 to them, for example at initialization and in stochastic additive updates, given that hidden features are of several hundreds dimensions and there are millions of steps involved in training. We consider large random matrices as a powerful tool in analyzing behaviors of deep models given their high dimension and randomness.

### 3.6 Adversarial Robustness

It is well known that deep models are prone to adversarial attacks, i.e., small changes in inputs may result in large changes in output or classification. Most works on adversarial attack and robustness consider perturbations at the beginning of the network. Given the layered structure of deep networks, we naturally consider perturbations to hidden intermediate features, simulated by perturbations on parameters in shallower layers. We refer to them as implicit adversarial attacks and implicit adversarial robustness and see (effective) gradient sparsity as a necessary step in resistance of them. Following works connecting flat minima to adversarial robustness [27], we use squared  $L_2$  norm  $\left\| \frac{\partial \mathcal{L}(f_{\theta_s}(x_s, y_s))}{\partial x^l} \right\|_2^2$  of derivatives w.r.t. hidden features on *individual samples* to measure adversarial robustness for mathematical convenience.

## 4 Gradiential Explanation of Activation Sparsity

Before starting the formal analysis of emergence of activation sparsity, we provide intuitive framework of our explanation. Slight architectural changes in MLPs, which ease theoretical analyses, are also already available under this intuitive illustration. Another radical change is proposed after more detailed analyses.

### 4.1 Illustration

Deep networks are built by stacking. Between layers, hidden intermediate features are generated and passed to deeper parts of the network. The first important intuition is that the output of shallower layers can be seen as the input of deeper layers, which allows us to see shallower layers as a part of “inputs” to deeper layers and apply notions previously defined at the real inputs  $x^0$ , for example, the notion of (implicit) adversarial robustness.

For deeper layers to have adversarial robustness, a way is to reduce the norm of activations’ derivatives, because the gradients w.r.t.  $x^{l-1}$  is calculated by multiplying the gradients to  $x^l$  with derivatives of the activations and weights. So by suppressing gradient norm of activations to extreme, i.e., promoting gradient sparsity, adversarial robustness increases for sure. Note that good sparsity and implicit adversarial robustness do not necessarily hinder approximability because they only implies local flatness and naturally distinct samples differ so much that there are multiple

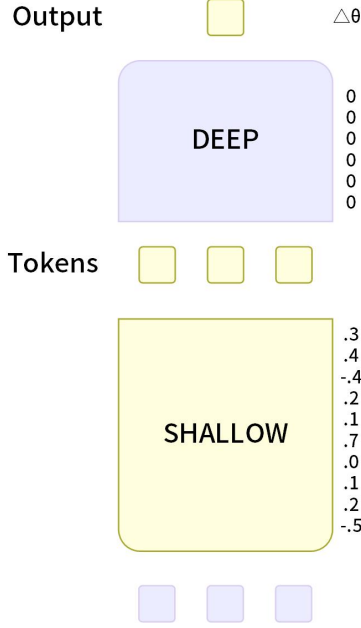


Figure 1: The illustration of virtual perturbations to shallow layers. Given a trained parameter at a flat minimum, if a small change around 0 in shallow parameters is added, the loss will not drastically increase due to the flatness. This virtual perturbation is illustrated by yellow shallow parts, their outputs and the final output, as well as blue and frozen deeper layers and inputs. The minor increase in loss indicates that the deep layers have to learn adversarial robustness.

flat regions between them in the output-input landscape, i.e., approximability can be achieved by drastically changing which neurons are activated [7].

Without explicit adversarial training, adversarial samples may come from perturbations in shallower layers. The inputs to deeper layers are not static and even not stable, because gradient noises in stochastic training are driving the parameters to run around randomly, which give birth to adversarial robustness. Note that the idea of wrapping perturbations in weights into hidden features has been used by [23], where this technique is implicitly applied to define representation information bottleneck, but [23] did not explicitly consider the perturbations to shallow parameters as those to hidden features. This explains how deep neural networks gain implicit adversarial robustness and then gradient sparsity from stochastic optimization in standard training.

From a more static point of view, i.e., considering the parameter after training, we model the perturbations in a virtual way as illustrated in Fig. 1. If the trained parameter is a flat minimum, then slight changes in its parameters do not drastically increase loss. Changes restricted to the shallow layers inherit this property and apply virtual perturbations to the shallow layers and to inputs for deep layers. As explained before, the deep layers must have learned implicit adversarial robustness to ensure flatness w.r.t. virtually perturbed inputs for deep layers. This intuition leads to the notion of flat minima and we will follow it in Section 4.3 by proving that both implicit adversarial robustness and some sparsity-related inner products are upperbounded by the measure of flatness, i.e.,  $\text{tr}(H_\theta)$ .

Following this line, one question to answer is how diverse the perturbations are to hidden features. In contrast with explicit adversarial training where perturbations are directly added

to  $x^0$ , perturbations to parameters have to go through low-rank linear operations and non-linear operations, which hinders the expressibility of parameter perturbations. To make things worse, some parameters are itself low-dimensional compared to hidden dimensions, e.g. convolution kernels in CNN, making it impossible to cover all potential explicit adversarial attacks. We consider this problem extremely severe in CNN because normally a small ( $\sim 4 \times 4$ ) convolution kernel should be responsible for a large feature map. This problem in Transformers is moderate because there are seemingly full-dimensional parameters (e.g. weights and bias in value matrices and MLPs), but all tokens are subject to the same parameter and it is low in this stacking dimension. Pure MLPs have the smallest problem because its weights and biases are full-dimensional and there are only one vector of features, but the perturbations are subjected to activation functions.

To alleviate these problems, we propose Doubly Biased MLP (DB-MLP) by introducing an extra bias  $D^l$  or  $d^l$ , called zeroth bias (ZB) due to its position, before other operations. ZB is a matrix of the same shape with hidden features if they are matrices of stacked tokens, i.e.

$$\text{DB-MLP}^l(X^{l-1}) := \text{MLP}^l(X^{l-1} + D^l), \quad (21)$$

where  $D^l$  is the zeroth bias of current DB-MLP. For hidden features of single vectors, it writes

$$\text{DB-MLP}^l(x^{l-1}) := \text{MLP}^l(x^{l-1} + d^l) = \sigma(K^l(x^{l-1} + d^l) + b^l). \quad (22)$$

For vector hidden features the zeroth bias removes the hindering effect of activation functions on last layer's bias  $b^{l-1}$ , and for matrix hidden features,  $D^l$  of the same shape allows full-dimensional perturbations. Note that zeroth biases are added to hidden features, meaning that they share gradients. This property will ease the analyses bridging flatness and implicit adversarial robustness.

Another implication of the above illustration is that activation function matters in gradient and/or activation sparsity. In Section 5, we design strange activation to differentiate gradient and activation sparsity and show that activation sparsity is lost to reach gradient sparsity defined by the activation. On the other hand, one problem of common ReLU and GELU is that their derivatives are almost piecewisely constant for most regions, having difficulties to guide the second-order search for flat minima. By squaring ReLU, which coincides with [10], the non-constant derivatives of activations provide a guidance to sparser neighbours, and  $\Omega(x)$ -large derivatives for large activations drive the parameters into sparse ones. However, in experiments we found that the derivatives are too small around zero-activation and provide little drive toward sparsity, so we shift the non-zero parts left and give

$$\text{J-SquaredReLU}(x) := \begin{cases} 0 & x < 0, \\ \frac{1}{2}((x+1)^2 - 1) & x \geq 0, \end{cases} \quad (23)$$

where "J" means jumping across the ignored interval  $[0, 1]$  and  $\frac{1}{2}$  is used to calibrate derivatives at  $x = 0$  to 1, approximating ReLU's and GELU's behaviors near 0.

One of the benefits of our architectural modifications is that they are plug-and-play, not only for training from scratch, but also for directly loading weights of vanilla architectures with changes plugged in and finetuning for sparsity, given that  $D^l$  and  $d^l$  can be initialized to 0 for any weights, and J-SquaredReLU approximates ReLU or GELU to the first order. Due to their simplicity, they are also likely orthogonal to other potential methods.

Now we have established the framework of our explanation. A formal analysis following this framework, based on DB-MLP, is conducted in the following three subsections. We will first

calculate gradients in MLP blocks. As the start of the analyses, we relate flatness to implicit adversarial robustness, and then implicit adversarial robustness to gradient sparsity in Section 4.3. After that, we exclude alternative sources of implicit robustness and flatness. To give the most general form of results, we assume DB-MLP in later subsections, if MLP is not explicitly pointed out. To obtain results for MLP, simply remove the ZB-related term (usually the first term) in inequalities.

## 4.2 Gradients w.r.t. Weight Matrices and Zeroth Biases

Since we are interested in the flat minima, gradients will be heavily involved. Therefore, we will compute gradients and updates to weight matrices in this subsection. We will also define the notion of effective gradient sparsity and argue its practical and theoretical importance, justifying our theories that is built on effective gradient sparsity.

Let  $\text{MLP}_*^l$  be any sublayer of the block  $\text{MLP}^l$ , whose weight matrix is  $W^l$ . Let  $g_{*,i}^l$  be the gradient w.r.t. the output of  $\text{MLP}_*^l$  on sample  $(x_s, y_s)$  at a hidden vector  $u_i^l$ , where  $u_i^l$  abstracts  $x^{l-1}$  or  $\alpha^l$ . Let  $G_*^l$  be the stacked version of  $g_{*,i}^l$  and  $U^l$  be that of  $u_i^l$ .

One can compute the gradient w.r.t.  $W^l$  on a hidden vector input  $u^l$  by

$$\left(g_{*,i}^l \odot \sigma_i^l\right) \left(u_i^l\right)^\top, \quad (24)$$

where  $\sigma_i^l = \gamma^l$  for weight matrices, while  $\sigma^l$  is  $[1]_{i \in \{1, \dots, d\}}$  for value matrices since there are no activation functions in value layers. Summing updates from all single hidden vectors to obtain gradients of sample  $(x_s, y_s)$  gives

$$\frac{\partial \mathcal{L}(\theta, (x_s, y_s))}{\partial W^l} := \sum_i \left(g_{*,i}^l \odot \sigma_i^l\right) \left(u_i^l\right)^\top = \left(G_*^l \odot \Sigma^l\right) \left(U^l\right)^\top. \quad (25)$$

The gradients w.r.t. to zeroth biases are also computed, if they exist.

$$\frac{\partial \mathcal{L}(\theta, (x_s, y_s))}{\partial d^l} = \left(J_{\mathcal{L}}\left(\alpha^l\right) J_{\alpha^l} \left(K^l \left(x^l + d^l\right) + b_K^l\right) J_{K^l(x^l + d^l) + b_K^l} \left(d^l\right)\right)^\top \quad (26)$$

$$= \left(\left(g_{K,i}^l\right)^\top \text{Diag}\left(\gamma^l\right) K^l\right)^\top = \left(K^l\right)^\top \left(g_{K,i}^l \odot \gamma^l\right). \quad (27)$$

Instantiating these results on key and value matrices obtains Lemma 1

**Lemma 1** (Gradients w.r.t. Weight Matrices). *The gradients w.r.t. weight matrices in  $\text{MLP}^l$  of sample  $(x_s, y_s)$  are*

$$\frac{\partial \mathcal{L}(\theta, (x_s, y_s))}{\partial K^l} = \left(G_K^l \odot \Gamma^l\right) \left(X^{l-1}\right)^\top, \quad (28)$$

$$\frac{\partial \mathcal{L}(\theta, (x_s, y_s))}{\partial V^l} = G_V^l \left(A^l\right)^\top. \quad (29)$$

If  $\text{MLP}^l$  is DB-MLP, then there is further

$$\frac{\partial \mathcal{L}(\theta, (x_s, y_s))}{\partial D^l} = \left(K^l\right)^\top \left(G_K^l \odot \Gamma^l\right). \quad (30)$$



Particularly if hidden features are vectors, there are

$$\frac{\partial \mathcal{L}(\theta, (x_s, y_s))}{\partial K^l} = \left( g_K^l \odot \gamma^l \right) \left( x^{l-1} \right)^\top, \quad (31)$$

$$\frac{\partial \mathcal{L}(\theta, (x_s, y_s))}{\partial V^l} = g_V^l \left( \alpha^l \right)^\top, \quad (32)$$

$$\frac{\partial \mathcal{L}(\theta, (x_s, y_s))}{\partial d^l} = \left( K^l \right)^\top \left( g_K^l \odot \gamma^l \right). \quad (33)$$

Lemma 1 introduces a Hadamard product between gradients from deeper layers and the derivatives of the activation in weight layers. We define it as the effective gradient pattern.

**Definition 3** (Effective gradient sparsity). *Define effective gradient patterns of  $\text{MLP}^l$  on sample  $(x_s, y_s)$  at hidden vector  $x^{l-1}$  to be*

$$\eta^l := \text{Diag} \left( g_K^l \right) \gamma^l = g_K^l \odot \gamma^l. \quad (34)$$

Let  $H^l = G_K^l \odot \Gamma^l$  (capitalized “ $\eta$ ” instead of capitalized “ $h$ ”) be its stacked version.

Effective gradient sparsity is that most elements in  $\eta^l$  are near zero for most samples and hidden vectors. For mathematical convenience, define  $\|\eta^l\|_2^2 = \|\text{Diag}(g^l) \gamma^l\|_2^2 = \|g^l \odot \gamma^l\|_2^2$  to be the effective gradient sparsity measured in squared  $L_2$  norm.

This notion first simplifies Lemma 1.

**Lemma 2** (Gradients w.r.t. Weight Matrices, restated with effective gradient sparsity patterns). *The gradients w.r.t. weight matrices in  $\text{MLP}^l$  of sample  $(x_s, y_s)$  are*

$$\frac{\partial \mathcal{L}(\theta, (x_s, y_s))}{\partial K^l} = H^l \left( X^{l-1} \right)^\top, \quad (35)$$

$$\frac{\partial \mathcal{L}(\theta, (x_s, y_s))}{\partial V^l} = G_V^l \left( A^l \right)^\top. \quad (36)$$

$$(37)$$

If there  $\text{MLP}^l$  is DB-MLP, then there is further

$$\frac{\partial \mathcal{L}(\theta, (x_s, y_s))}{\partial D^l} = \left( K^l \right)^\top H^l. \quad (38)$$

Particularly if hidden features are vectors, there are

$$\frac{\partial \mathcal{L}(\theta, (x_s, y_s))}{\partial K^l} = \eta^l \left( x^{l-1} \right)^\top, \quad (39)$$

$$\frac{\partial \mathcal{L}(\theta, (x_s, y_s))}{\partial V^l} = g_V^l \left( \alpha^l \right)^\top, \quad (40)$$

$$\frac{\partial \mathcal{L}(\theta, (x_s, y_s))}{\partial d^l} = \left( K^l \right)^\top \eta^l. \quad (41)$$

This sparsity inherits sparsity in  $\gamma$ s but also allows more “sparsity” due to  $g_K^l$ s. Sparsity in  $g_K^l$  is also meaningful in the sense that if the  $i$ -th entry  $g_i^l$  of  $g_K^l$  is small in magnitude, then 1)  $\alpha_i^l$  does not influence the output much in forward propagation, and 2) there is little contribution of  $i$ -th neuron

in gradients to shallower layers during the backward propagation. Therefore, the  $i$ -th neuron can also be pruned in both training and inference with minor cost in accuracy, and thus this notion is of even more practical value, although  $g^l$  cannot be known before backward propagation. The notion of effective gradient sparsity in  $\eta^l$  considers the two sparsities in a combined manner. This incorporation of gradients of the outputs also reminds us of the improved knowledge attribution method proposed by [2] where not only activation magnitude, but also the gradients of model output w.r.t. the activation are exploited. Last but not least, the effective sparsity hides the complexity of deeper layers and attribute its emergence solely to  $K^l$ , which is somehow shallow despite there being dozens of deeper modules and allows easier theoretical manipulations.

More importantly, effective gradient sparsity pattern is what key layers try to memorize in columns, given in Observation 1.

**Observation 1** (Effective gradient sparsity pattern is memorized in columns of key matrices). *Consider the update of one sample to the key matrix given by Lemma 2*

$$\frac{\partial \mathcal{L}(\theta, (x_s, y_s))}{\partial K^l} = H^l (X^{l-1})^\top = \sum_i \eta_i^l (x_i^{l-1})^\top \quad (42)$$

$$= \begin{bmatrix} \sum_i X_{i,1}^{l-1} \eta_i^l & \cdots & \sum_i X_{i,j}^{l-1} \eta_i^l & \cdots & \sum_i X_{i,d}^{l-1} \eta_i^l \end{bmatrix}. \quad (43)$$

*In the update of each column, a mixture effective gradient sparsity patterns is borne into the key matrix with different weights given by the input.*

Taking a transposed view, key layers also memorize  $x_i^{l-1} \mathbf{s}$ , under the control of  $\eta_i^l \mathbf{s}$ .

**Observation 2** (Effective sparsity gradient pattern controls row memorization in key matrices). *Consider the update of one sample to the key matrix given by Lemma 2*

$$\frac{\partial \mathcal{L}(\theta, (x_s, y_s))}{\partial K^l} = H^l (X^{l-1})^\top = \sum_i \eta_i^l (x_i^{l-1})^\top \quad (44)$$

$$= \begin{bmatrix} \sum_i H_{j,i}^l (x_i^{l-1})^\top \end{bmatrix}_j. \quad (45)$$

*In the update of each row, a mixture of inputs is borne into the key matrix, weighted by entries of effective gradient sparsity pattern.*

Similar things also happen in value matrices but with  $g_V^l$ s and  $\alpha^l$ s memorized. It is interesting to see that linear layers are trying to resemble the gradients back-propagated to them. This observation may leads to a notion of pseudo gradients which can be calculated as soon as the forward propagation finishes. Maybe a portion of samples can be trained by these pseudo gradients to save computation budgets. However, this is out of our scope and is left for future works to explore.

Note that effective gradient sparsity pattern is not directly related to activation sparsity under common activation functions, so we keep the notion of gradient sparsity as well. The gap is due to the Hadamard product with  $g_K^l$ .  $g_K^l$  can cause effective gradient sparsity without gradient sparsity on  $\gamma^l$  by 1) reducing the norm of itself, or 2) misalign itself with  $\gamma^l$ . The first possibility can be eliminated by the phenomenon of parameter growth already discovered in [7]. This indicates that the norm of Transformers' parameters will increase even under weight decay and normalization.

Since gradients are obtained by multiplying parameters and hidden features,  $\|g_K^l\|_2^2$  is also likely to increase. We empirically examine it in Section 7.1 where  $\text{tr}(M_i^l) := \text{tr}\left(g_{K,i}^l (g_{K,i}^l)^\top\right) = \|g_{K,i}^l\|_2^2$  is observed to increase. For the second possibility,  $\gamma^l$  will have small value at least at entries where  $g_K^l$  has large magnitude so gradient sparsity in large and moderate entries of  $g_K^l$  is still encouraged. An informal argument for the rest of the entries is that, if the  $i$ -th entry in  $\eta^l$  is near zero, then during the row memorization described by Observation 2, little change is imposed by  $x^{l-1}$  to the  $i$ -th row of  $K^l$ . When next time  $x^{l-1}$  arrives, although with changes due to shallower layers, it is very likely the  $i$ -th row in  $K^l$  forgets  $x^{l-1}$  and  $(K^l x^{l-1})_i = \langle K_i^l, x^{l-1} \rangle$  is very close to 0, leading to activation sparsity in  $\alpha^l$ , and thus gradient sparsity in  $\gamma^l$  if common activation functions are used.

### 4.3 Flat Minima, Implicit Adversarial Robustness and Gradient Sparsity

As discussed in Section 4.1, we start from  $\text{tr}(H_\theta)$  and relate it to implicit adversarial robustness for some hidden feature  $x^l$ , or  $\mathbf{E}_{(X,Y)} \left[ \left\| \frac{\partial \mathcal{L}}{\partial x^l} \right\|_2^2 \right]$ . Cross Entropy loss is assumed under classification task. Note that aside from explicit classification tasks, token classification and Cross Entropy loss form the basis for many self supervision objectives in NLP pretraining, including causal language modeling and mask language modeling. Therefore this assumption has implication across broad practical scenarios. Assuming  $\mathcal{L} = \mathcal{L}_{\text{CE}} = -\log f(y | \theta, x)$ , the Hessian writes

$$\nabla_\theta^2 \mathbf{E}_{(X,Y)} [-\log f(Y | \theta, X)] = -\mathbf{E}_{(X,Y)} [\nabla_\theta^2 \log f(Y | \theta, X)], \quad (46)$$

which, together with  $\mathbf{E}_{(X,Y)} \left[ \left\| \frac{\partial \mathcal{L}}{\partial x^l} \right\|_2^2 \right]$ , reminds us of the famous equality of Fisher’s Information Matrix, i.e.

$$\mathcal{I}(\theta) = -\mathbf{E}_X [\nabla_\theta^2 \log g_\theta(X)] = \mathbf{E}_X \left[ \left( \frac{\partial g_\theta(X)}{\partial \theta} \right) \left( \frac{\partial g_\theta(X)}{\partial \theta} \right)^\top \right], \quad (47)$$

the trace of RHS of which is exactly the expected squared norm of the gradients. So following the classic proof of this equality, we connect flatness measured by Hessian trace to the norm of gradients in Lemma 3.

**Lemma 3** (Flatness and samplewise gradient norm). *Assume  $f_\theta$  is a neural network parameterized by  $\theta$ , trained by Cross Entropy loss  $\mathcal{L}_{\text{CE}}$ . Given  $H_\theta$  being the Hessian matrix of loss at  $\theta$ , there is*

$$\text{tr}(H_\theta) = \mathbf{E}_{(X,Y) \sim \mathcal{D}} \left[ \|\nabla_\theta \mathcal{L}_{\text{CE}}(\theta, (X, Y))\|_2^2 \right] - \mathbf{E}_{(X,Y) \sim \mathcal{D}} \left[ \frac{\text{tr}(\nabla_\theta^2 f(Y | \theta, X))}{f(Y | \theta, X)} \right]. \quad (48)$$

Further for well learned models, i.e.,  $f_\theta(Y | X) \approx \mathcal{D}(Y | X)$  for all training samples, there is

$$\text{tr}(H_\theta) \approx \mathbf{E}_{(X,Y) \sim \mathcal{D}} \left[ \|\nabla_\theta \mathcal{L}_{\text{CE}}(\theta, (X, Y))\|_2^2 \right]. \quad (49)$$

The proof of it can be found in Appendix A. This lemma invokes a samplewise point of view of Hessian and flatness, which is more close to adversarial attacks because they are added in a samplewise manner. Aside from implication in the context of sparsity, Lemma 3 indicates that a flat minima also provides solutions that are locally good for most single samples.

After that we move perturbations from parameters to hidden features in Lemma 4.

**Lemma 4** (Gradient norm and implicit adversarial robustness). *Let  $f_\theta$  be a neural network parameterized by  $\theta$ , and the parameters for the  $l$ -th layer is  $\theta_l$ . Let DB-MLP <sup>$l$</sup>  be a doubly biased MLP in  $f_\theta$  whose input is  $X^{l-1}$ , zeroth bias is  $D^l$ . Then there is*

$$\|\nabla_{\theta_l} \mathcal{L}_{\text{CE}}(\theta, (x, y))\|_2^2 \geq \|\nabla_{X^{l-1}} \mathcal{L}_{\text{CE}}(\theta, (x, y))\|_2^2 + \left\| H^l \left( X^{l-1} \right)^\top \right\|_2^2 + \left\| G_V^l \left( A^l \right)^\top \right\|_2^2. \quad (50)$$

If MLP <sup>$l$</sup>  is not doubly biased, then the first term in RHS simply disappears.

*Proof.* By noticing  $\theta_l$  contains at least  $K^l, V^l$  and  $D^l$ , there is

$$\|\nabla_{\theta_l} \mathcal{L}_{\text{CE}}\|_2^2 \geq \|\nabla_{D^l} \mathcal{L}_{\text{CE}}\|_2^2 + \|\nabla_{K^l} \mathcal{L}_{\text{CE}}\|_2^2 + \|\nabla_{V^l} \mathcal{L}_{\text{CE}}\|_2^2. \quad (51)$$

Consider how  $X^{l-1}$  is processed in DB-MLP <sup>$l$</sup> : It is added with  $D^l$  before any other operations. So there is  $\nabla_{D^l} \mathcal{L}_{\text{CE}} = \nabla_{X^{l-1}} \mathcal{L}_{\text{CE}} = \nabla_{X^{l-1} + D^l} \mathcal{L}_{\text{CE}}$ . Combining Lemma 2 for the second and the third terms, the lemma follows.  $\square$

From the proof of Lemma 4 we can see that the zeroth biases avoid tedious linear or non-linear operations and drastically ease our analysis. This implies that we can design theoretically oriented architecture that allows easy theoretical analysis.

We then connect implicit adversarial robustness to gradient sparsity.

**Lemma 5** (Implicit adversarial robustness and gradient sparsities). *Under the same condition of Lemma 4, together with the assumption that in DB-MLP <sup>$l$</sup>  the weight matrix is  $K^l \in \mathbb{R}^{n \times d}$  and  $\gamma^l$  is the entrywise derivatives of activations, there is*

$$\|\nabla_{x^{l-1}} \mathcal{L}_{\text{CE}}(\theta, (x, y))\|_2^2 = \left( \gamma^l \right)^\top \left( \left( K^l (K^l)^\top \right) \odot M^l \right) \gamma^l = \left( \eta^l \right)^\top K^l \left( K^l \right)^\top \eta^l, \quad (52)$$

if hidden features are vectors, where  $M^l := g^l (g^l)^\top$  is a symmetric positive semi-definite matrix of rank at most 1,  $\odot$  denotes Hadamard product, i.e., entrywise product.

If hidden features are matrices, then there is

$$\|\nabla_{X^{l-1}} \mathcal{L}_{\text{CE}}(\theta, (x, y))\|_2^2 = \text{tr} \left( H^l \left( H^l \right)^\top K^l \left( K^l \right)^\top \right). \quad (53)$$

*Proof.* By Lemma 2, the gradients w.r.t.  $d^l$  is

$$\frac{\partial \mathcal{L}_{\text{CE}}(\theta, (x, y))}{\partial d^l} = \left( K^l \right)^\top \eta^l. \quad (54)$$

Similar to the proof of Lemma 4,  $x^{l-1}$  and  $d^l$  share the same gradient, so

$$\nabla_{x^{l-1}} \mathcal{L}_{\text{CE}} = \frac{\partial \mathcal{L}_{\text{CE}}(\theta, (x, y))}{\partial x^{l-1}} = \left( K^l \right)^\top \eta^l. \quad (55)$$

Now we can compute the squared norm of gradients by its relation with trace

$$\|\nabla_{x^{l-1}} \mathcal{L}_{\text{CE}}\|_2^2 = \text{tr} \left( \left( \nabla_{x^{l-1}} \mathcal{L}_{\text{CE}} \right)^\top \nabla_{x^{l-1}} \mathcal{L}_{\text{CE}} \right) \quad (56)$$

$$= \text{tr} \left( \left( \eta^l \right)^\top K^l \left( K^l \right)^\top \eta^l \right) \quad (57)$$

$$= \left( \eta^l \right)^\top K^l \left( K^l \right)^\top \eta^l. \quad (58)$$

To see how  $M^l := g_K^l (g_K^l)^\top$  emerges, expand the definition of  $\eta^l$  and obtain

$$\|\nabla_{x^{l-1}} \mathcal{L}_{\text{CE}}\|_2^2 = (\eta^l)^\top K^l (K^l)^\top \eta^l \quad (59)$$

$$= (\text{Diag}(g_K^l) \gamma^l)^\top K^l (K^l)^\top (\text{Diag}(g_K^l) \gamma^l) \quad (60)$$

$$= (\gamma^l)^\top \text{Diag}(g_K^l) K^l (K^l)^\top \text{Diag}(g_K^l) \gamma^l \quad (61)$$

$$= (\gamma^l)^\top \left( g_K^l (g_K^l)^\top \odot K^l (K^l)^\top \right) \gamma^l \quad (62)$$

$$= (\gamma^l)^\top \left( M \odot K^l (K^l)^\top \right) \gamma^l, \quad (63)$$

where the second last step is to apply Eq. (13). Note that  $M^l$ 's rank is at most 1.

When hidden features are matrices,  $\|\nabla_{X^{l-1}} \mathcal{L}_{\text{CE}}\|_2^2$  sums the gradient norms for every hidden vectors, which leads to

$$\|\nabla_{X^{l-1}} \mathcal{L}_{\text{CE}}\|_2^2 = \sum_i \|\nabla_{x_i^{l-1}} \mathcal{L}_{\text{CE}}\|_2^2 = \text{tr} \left( \sum_i (\eta_i^l)^\top K^l (K^l)^\top \eta_i^l \right) \quad (64)$$

$$= \text{tr} \left( \left( \sum_i \eta_i^l (\eta_i^l)^\top \right) K^l (K^l)^\top \right) \quad (65)$$

$$= \text{tr} \left( H^l (H^l)^\top K^l (K^l)^\top \right). \quad (66)$$

□

Combining Lemma 3, Lemma 4 and Lemma 5 together, we have the main theorem.

**Theorem 2** (Flatness, implicit adversarial robustness and sparsities). *Let  $f_\theta$  be a well-learned neural network parameterized by  $\theta$ , trained under Cross Entropy loss  $\mathcal{L}_{\text{CE}}$ . Let  $H_\theta$  be the Hessian matrix w.r.t. parameters at  $\theta$ . Let DB-MLP<sup>*l*</sup> be a doubly biased MLP in  $f_\theta$  whose input is  $x^{l-1}$ . There is*

$$\text{tr}(H_\theta) \geq \sum_l \left( \mathbf{E} \left[ \|\nabla_{x^{l-1}} \mathcal{L}_{\text{CE}}(\theta, (X, Y))\|_2^2 \right] + \mathbf{E} \left[ \|H^l (X^{l-1})^\top\|_2^2 \right] + \mathbf{E} \left[ \|G_V^l (A^l)^\top\|_2^2 \right] \right) \quad (67)$$

$$= \sum_{i,l} \mathbf{E} \left[ (\eta_i^l)^\top K^l (K^l)^\top \eta_i^l \right] + \sum_l \mathbf{E} \left[ \|H^l (X^{l-1})^\top\|_2^2 \right] + \sum_l \mathbf{E} \left[ \|G_V^l (A^l)^\top\|_2^2 \right], \quad (68)$$

where  $M^l$  is a symmetric positive semi-definite matrix of rank at most 1. The first term can also be expressed by  $(\gamma_i^l)^\top (K^l (K^l)^\top \odot M_i^l) \gamma_i^l$ . Further by Schur's Theorem,  $(K^l (K^l)^\top) \odot M_i^l$  is also positive semi-definite.

This chained upperbounds connect flatness and implicit adversarial robustness to effective gradient sparsity (the first two term in Eq. (68)) and as well as activation sparsity (the last term in Eq. (68)), indicating that both gradient and activation sparsity can be sources of implicit adversarial robustness and flatness. If flatness is achieved, then it is possibly done through (effective)

gradient sparsity and activation sparsity. Note that this bound is very tight because MLPs take a large portion of parameters [2] even in Transformers, so by Cauchy’s Interlace Theorem most large eigenvalues of  $H_\theta$  are retained in the submatrix of MLP parameters. Therefore to achieve flatness, the terms in Eq. (68) must be suppressed.

#### 4.4 Discussions on Theorem 2

In this section, we discuss the implications of Theorem 2 under several particular specific settings, including pure MLPs, pure pre-LayerNorm-ed MLPs, Transformers and Transformers with hypothetical massive perturbation training. We point out their tendency toward effective gradient sparsity, which leads to gradient and activation sparsity as discussed in Section 4.2, among which effective gradient sparsity is more stable.

##### 4.4.1 Pure MLPs

The last two terms in Eq. (68) have similar forms, so we inspect them together. To have a clearer understanding on them, first consider the situations where models use vector hidden features in Corollary 1

**Corollary 1** (Flatness, and gradient and activation sparsity in pure MLPs). *Inherit the assumptions of Theorem 2. Assume additionally that the model uses vector hidden features, then there is*

$$\text{tr}(H_\theta) \geq \sum_l \mathbf{E} \left[ \left( \eta^l \right)^\top K^l \left( K^l \right)^\top \eta^l \right] + \sum_l \mathbf{E} \left[ \left\| x^{l-1} \right\|_2^2 \left\| \eta^l \right\|_2^2 \right] + \sum_l \mathbf{E} \left[ \left\| g_V^l \right\|_2^2 \left\| \alpha^l \right\|_2^2 \right]. \quad (69)$$

*Proof.* With hidden vectors,  $\left\| H^l \left( X^{l-1} \right)^\top \right\|_2^2$  reduces to

$$\left\| H^l \left( X^{l-1} \right)^\top \right\|_2^2 = \left\| \eta^l \left( x^{l-1} \right)^\top \right\|_2^2 = \text{tr} \left( \left( \eta^l \left( x^{l-1} \right)^\top \right)^\top \eta^l \left( x^{l-1} \right)^\top \right) \quad (70)$$

$$= \text{tr} \left( x^{l-1} \left( \eta^l \right)^\top \eta^l \left( x^{l-1} \right)^\top \right) = \text{tr} \left( \left( \eta^l \right)^\top \eta^l \left( x^{l-1} \right)^\top x^{l-1} \right) \quad (71)$$

$$= \left\| \eta^l \right\|_2^2 \left\| x^{l-1} \right\|_2^2. \quad (72)$$

$\left\| G_V^l \left( A^l \right)^\top \right\|_2^2$  can be reduced similarly.  $\square$

If normalization layers are imposed, for example LayerNorm layers before MLP blocks, then  $\left\| x^{l-1} \right\|_2^2 = d$  will not change during training, directly leading to effective gradient sparsity. Since key matrices also take a large portion of parameters, flatness in these parameters must be achieved as well and  $\text{tr}(H_{\theta_K})$  is not too small from  $\text{tr}(H_\theta)$ , the second term alone will have strong tendency to decrease. Therefore, a rigorously proved, strong and stable tendency of pure pre-LayerNorm-ed MLPs toward effective gradient sparsity is presented in Theorem 3.

**Theorem 3** (Flatness, and gradient and activation sparsity in pure MLPs with pre-LayerNorms). *Inherit the assumptions of Theorem 2. Assume additionally that the model uses vector hidden*

features and LayerNorm layers, with affine transformation turned off, are imposed before every MLP block. Temporarily assume non-DB-MLP models are used, then there is

$$\text{tr}(H_\theta) \geq d \sum_l \mathbf{E} \left[ \|\eta^l\|_2^2 \right]. \quad (73)$$

Or more tightly,

$$\text{tr}(H_{\theta_K}) \geq d \sum_l \mathbf{E} \left[ \|\eta^l\|_2^2 \right], \quad (74)$$

where  $\theta_K$  is the collection of all parameters in all key matrices.

If DB-MLPs are used and LayerNorm layers are placed before zeroth biases, by clipping the norm of columns in zeroth biases to  $c$ , there will be

$$\text{tr}(H_{\theta_K}) \geq (\sqrt{d} - c)^2 \sum_l \mathbf{E} \left[ \|\eta^l\|_2^2 \right]. \quad (75)$$

LayerNorm places quite strong and stable drive towards effective gradient sparsity, if they are placed right before (DB-)MLP blocks and affine factors are turned off to avoid their reduction due to updates or weight decay. Theorem 3 can be one explanation of benefits of LayerNorms and the practice to exclude their parameters from weight decay.

The last term in Eq. (69) relating activation sparsity is less ensured as the second term, because gradient norm may change drastically. If a local minimum is reached and the minimum is flat, then the gradient will be small for individual samples, as discussed in Lemma 3. Plus the first term, we conclude that (effective) gradient sparsity is more stable and significant than direct activation sparsity. This will be empirically verified in Section 5 where gradient sparsity competes over activation sparsity when they differ.

#### 4.4.2 Transformers and Other Architectures

When stacked hidden features are used, for example in Transformers, the discussion is more tricky. It is possible that gradients of different hidden vectors cancel each other in

$$H^l \left( X^{l-1} \right)^\top = \sum_i \eta_i^l \left( x_i^{l-1} \right)^\top. \quad (76)$$

We can only rigorously conclude a possibly loose lowerbound with  $\|\eta_i^l\|_2^2$  in Corollary 2.

**Corollary 2** (Flatness, and gradient and activation sparsity in Transformers). *Inherit assumptions from Theorem 2, then there is*

$$\text{tr}(H_\theta) \geq \sum_{i,l} \mathbf{E} \left[ \left( \eta_i^l \right)^\top K^l \left( K^l \right)^\top \eta_i^l \right] \quad (77)$$

$$+ \sum_l \mathbf{E} \left[ \lambda_{\min} \left( \left( X^{l-1} \right)^\top X^{l-1} \right) \sum_i \|\eta_i^l\|_2^2 \right] \quad (78)$$

$$+ \sum_l \mathbf{E} \left[ \lambda_{\min} \left( \left( G_V^l \right)^\top G_V^l \right) \sum_i \|\alpha_i^l\|_2^2 \right], \quad (79)$$

where  $\lambda_{\min}(\cdot)$  indicates the minimum eigenvalue of a matrix.

*Proof.*

$$H^l (X^{l-1})^\top = \text{tr} \left( \left( H^l (X^{l-1})^\top \right)^\top H^l (X^{l-1})^\top \right) \quad (80)$$

$$= \text{tr} \left( (X^{l-1})^\top X^{l-1} (H^l)^\top H^l \right). \quad (81)$$

The last term can be similarly rearranged. Applying Eq. (12) to both of them and noticing  $\text{tr} \left( (H^l)^\top H^l \right) = \sum_i \|\eta_i^l\|_2^2$  finish the proof.  $\square$

There are tricky ways to bypass the cancelling, however. For example, consider augments conducted on hidden features such as dropout. They effectively duplicate the parameter into  $k$  views and perturb each view independently (using dropout, rows of weight matrices are randomly pruned) if there are  $k$  hidden vectors. If flatness can be extended to these effective duplicated parameters, i.e., if there is still flatness when we really duplicate the weight matrices and assign one token for each matrix, then each view is only handling one hidden vectors and we can repeat Corollary 1. However, traditional dropout may hinders the sparsity by eliminating activations and forcing the model to back up the representation. A soft dropout by slightly perturbing before activation function is more preferable. Moreover, the perturbation should better be conducted on weight matrices in an entrywise manner, otherwise the gradients w.r.t. these perturbations still involve summation and cancelling. Under this hypothetical massive perturbation, we assume flatness can be obtained w.r.t. duplicated parameters, because in the real model losses are suppressed even under independent perturbation so the effective model is not sensitive to changes in individual parameter duplicates. This intuition leads to Lemma 6.

**Lemma 6** (Flatnesses of massively perturbed model and perturbation-induced effective model). *Assume weight matrices are perturbed by Gaussian noise independently for each hidden vector, i.e., the perturbed MLP<sub>\*</sub><sup>l</sup> outputs*

$$\sigma \left( [\hat{W}^{l,1}x_1 \quad \dots \quad \hat{W}^{l,i}x_i \quad \dots \quad \hat{W}^{l,k}x_k] + b^l \right) \quad (82)$$

for input hidden matrix  $X = [x_1 \quad \dots \quad x_i \quad \dots \quad x_k]$ , where  $\hat{W}^{l,i} := W^l + E^{l,i}$ , and  $E^{l,1}, \dots, E^{l,k}$  are  $k \times n \times d$  independent centered Gaussian variables with variance  $\sigma^2$ . Let random variable  $E$  denote the collection of all perturbations. Let  $\hat{\theta}$  be the collection of proxied parameters, where  $\hat{W}^{l,i}$ s are taken into consideration instead of  $W^l$ , while other parameters are inherited from  $\theta$ .

Let  $g_{\tilde{\theta}}$  be the effective parameter by duplicating each weight matrix  $W^l$  for  $k$  times into  $\tilde{W}^{l,1}, \dots, \tilde{W}^{l,k}$ , each of which deals with exactly one hidden vector  $x_i$  during inference.

Then

$$\frac{1}{\sigma^2} \mathbf{E}_{(X,Y),E} \left[ (\mathcal{L}(f_\theta, E, (X,Y)) - \mathcal{L}(f_\theta, 0, (X,Y)))^2 \right] + ndLk \cdot o(1) \quad (83)$$

$$= \sum_l \sum_{W \in \{K,V\}} \sum_i \mathbf{E} \left[ \left\| \frac{\partial \mathcal{L}(f_\theta, 0, (X,Y))}{\partial \hat{W}^{l,i}} \right\|_2^2 \right] = \sum_l \sum_{W \in \{K,V\}} \sum_i \mathbf{E} \left[ \left\| \frac{\partial \mathcal{L}(g_{\tilde{\theta}}, (X,Y))}{\partial \tilde{W}^{l,i}} \right\|_2^2 \right], \quad (84)$$

where  $\mathcal{L}(f_\theta, E, (X,Y))$  indicates the loss of  $f_\theta$  on sample  $(X,Y)$  when perturbation is  $E$ ,  $L$  is the number of MLP layers. If Cross Entropy loss is assumed and  $f_\theta$  is well learned when perturbations



are removed then by Lemma 3 applied to  $g_{\tilde{\theta}}$ ,

$$\frac{1}{\sigma^2} \mathbf{E}_{(X,Y),E} \left[ (\mathcal{L}_{\text{CE}}(f_{\theta}, E, (X, Y)) - \mathcal{L}_{\text{CE}}(f_{\theta}, 0, (X, Y)))^2 \right] + ndLk \cdot o(1) \quad (85)$$

$$= \sum_l \sum_{W \in \{K,V\}} \sum_i \mathbf{E} \left[ \left\| \frac{\partial \mathcal{L}_{\text{CE}}(f_{\theta}, 0, (X, Y))}{\partial \hat{W}^{l,i}} \right\|_2^2 \right] = \sum_l \sum_{W \in \{K,V\}} \sum_i \mathbf{E} \left[ \left\| \frac{\partial \mathcal{L}_{\text{CE}}(g_{\tilde{\theta}}, (X, Y))}{\partial \tilde{W}^{l,i}} \right\|_2^2 \right] \quad (86)$$

$$\leq \mathbf{E} \left[ \left\| \frac{\partial \mathcal{L}_{\text{CE}}(f_{\theta}, 0, (X, Y))}{\partial \hat{\theta}} \right\|_2^2 \right] = \mathbf{E} \left[ \left\| \frac{\partial \mathcal{L}_{\text{CE}}(g_{\tilde{\theta}}, (X, Y))}{\partial \tilde{\theta}} \right\|_2^2 \right] \approx \text{tr}(H_{\tilde{\theta}}) \quad (87)$$

$$(88)$$

*Proof.* By construction of  $g_{\tilde{\theta}}$ , gradients w.r.t.  $\hat{W}^{l,i}$  and  $\tilde{W}^{l,i}$  share the same path in  $f_{\theta}$  and  $g_{\tilde{\theta}}$ . If the same sample is used and the perturbation is removed, then they are equal.

We can approximate  $\mathcal{L}(f_{\theta}, E, (x, y))$  from  $\mathcal{L}(f_{\theta}, 0, (x, y))$  by

$$(\mathcal{L}(f_{\theta}, E, (x, y)) - \mathcal{L}(f_{\theta}, 0, (x, y)))^2 = \left( (\nabla_{\text{vec}(E)} \mathcal{L}(f_{\theta}, 0, (x, y)))^{\top} \text{vec}(E) + o(\|\text{vec}(E)\|_2) \right)^2 \quad (89)$$

$$= \left( (\nabla_{\text{vec}(E)} \mathcal{L}(f_{\theta}, 0, (x, y)))^{\top} \text{vec}(E) \right)^2 + o(\|\text{vec}(E)\|_2^2) \quad (90)$$

$$(91)$$

Since Gaussian  $\text{vec}(E)$  has covariance  $\sigma^2 I$ ,  $\nabla_{\text{vec}(E)}^{\top} \mathcal{L} \times \text{vec}(E)$  is also Gaussian whose variance is

$$\sigma^2 (\nabla_{\text{vec}(E)} \mathcal{L}(f_{\theta}, 0, (x, y)))^{\top} (\nabla_{\text{vec}(E)} \mathcal{L}(f_{\theta}, 0, (x, y))) = \sigma^2 \|\nabla_{\text{vec}(E)} \mathcal{L}\|_2^2. \quad (92)$$

Taking expectation over noises  $E$ , there is

$$\mathbf{E}_E \left[ (\mathcal{L}(f_{\theta}, E, (x, y)) - \mathcal{L}(f_{\theta}, 0, (x, y)))^2 \right] \quad (93)$$

$$= \sigma^2 \|\nabla_{\text{vec}(E)} \mathcal{L}(f_{\theta}, 0, (X, Y))\|_2^2 + o(ndLk\sigma^2) \quad (94)$$

$$= \sigma^2 \|\nabla_{\text{vec}(\tilde{W})} \mathcal{L}(f_{\theta}, 0, (X, Y))\|_2^2 + o(ndLk\sigma^2), \quad (95)$$

where  $\tilde{W}$  denote the collection of all  $\tilde{W}^{l,i}$ s. The rest of the proof is easy according to the equivalence between  $g_{\tilde{\theta}}$  and  $f_{\theta}$  with perturbations removed.  $\square$

**Remark 1.** Although  $\text{tr}(H_{\tilde{\theta}})$  is involved by an inequality, considering the large portion of  $\tilde{W}$  parameters,  $\sum_l \sum_{W \in \{K,V\}} \sum_i \mathbf{E} \left[ \left\| \frac{\partial \mathcal{L}_{\text{CE}}(g_{\tilde{\theta}}, (X, Y))}{\partial \tilde{W}^{l,i}} \right\|_2^2 \right]$  can in fact represent  $\text{tr}(H_{\tilde{\theta}})$  well. If this argument is not satisfying, then perturb all parameters in the same way so that “ $\leq$ ” becomes “ $=$ ”.

So by training a weight-perturbed non-pure-MLP network to have low losses, we are helping its pure-MLP equivalence reaching flat minima, where effective gradient sparsity can be directly obtained in Theorem 4. If we assume  $\frac{1}{\sigma^2} \mathbf{E}_{(X,Y),E} \left[ (\mathcal{L}_{\text{CE}}(f_{\theta}, E, (X, Y)) - \mathcal{L}_{\text{CE}}(f_{\theta}, 0, (X, Y)))^2 \right] \leq \text{tr}(H_{\tilde{\theta}})$  is indeed suppressed during training because losses are suppressed to near-zero values, then Theorem 4 is meaningful.

**Theorem 4** (Flatness, and gradient and activation sparsity under massive weight perturbations). *Inherit the assumptions of Theorem 2 as well as notations in Lemma 6. Further assume that weight matrices are independently perturbed before multiplying with any individual hidden vectors during training, then*

$$\frac{1}{\sigma^2} \mathbf{E}_{(X,Y),E} \left[ (\mathcal{L}(f_\theta, E, (X, Y)) - \mathcal{L}(f_\theta, 0, (X, Y)))^2 \right] + ndLk \cdot o(1) \quad (96)$$

$$= \sum_{i,l} \mathbf{E} \left[ \left( \eta_i^l \right)^\top K^l \left( K^l \right)^\top \eta_i^l \right] + \sum_{i,l} \mathbf{E} \left[ \left\| x_i^{l-1} \right\|_2^2 \left\| \eta_i^l \right\|_2^2 \right] + \sum_{i,l} \mathbf{E} \left[ \left\| g_{V,i}^l \right\|_2^2 \left\| \alpha_i^l \right\|_2^2 \right] \quad (97)$$

$$\leq \text{tr} \left( H_{\tilde{\theta}} \right), \quad (98)$$

where  $\tilde{\theta}$  stands for the perturbation-induced effective parameter where weight matrices are really duplicated so that each of them serves one hidden vector/token. If no-affine pre-LayerNorms are applied, there is further

$$\frac{1}{\sigma^2} \mathbf{E}_{(X,Y),E} \left[ (\mathcal{L}(f_\theta, E, (X, Y)) - \mathcal{L}(f_\theta, 0, (X, Y)))^2 \right] + ndLk \cdot o(1) \quad (99)$$

$$= \sum_{i,l} \mathbf{E} \left[ \left( \eta_i^l \right)^\top K^l \left( K^l \right)^\top \eta_i^l \right] + (\sqrt{d} - c)^2 \sum_{i,l} \mathbf{E} \left[ \left\| \eta_i^l \right\|_2^2 \right] + \sum_{i,l} \mathbf{E} \left[ \left\| g_{V,i}^l \right\|_2^2 \left\| \alpha_i^l \right\|_2^2 \right] \quad (100)$$

$$\leq \text{tr} \left( H_{\tilde{\theta}} \right), \quad (101)$$

$$(102)$$

where  $c = 0$  if non-DB-MLPs are used, otherwise  $c$  is the norm bound of columns in zeroth biases.

Aside from Transformers, massively perturbed CNNs, MLP-Mixers and other potential architectures apply, as long as they have MLP blocks and the perturbed loss is small enough. Additionally, this bound is also very tight by tightness of Lemma 6 or by counting parameters, so perturbed error's reduction or the flatness of the effective model inevitably leads to reduction in sparsity. A simple algorithm MagicSynapse is immediate after Lemma 6 and Theorem 4, which is listed in Appendix G in order not to disrupt the presentation of major theoretical results.

#### 4.4.3 The First Term from Zeroth Biases

Now we look back to the first term in Eq. (68). Although the first term seems to have minor weight compared the others, either by counting parameters or decomposing eigenvalues of  $K^l \left( K^l \right)^\top$  (see Fig. 9), it is still worth investigating since it leads to another phenomenon of spectral concentration in  $K^l \left( K^l \right)^\top$  and introduces random matrix theory to reason about training dynamics.

In the first term, since the gradient of the inner product w.r.t.  $\eta^l$  is

$$2K^l \left( K^l \right)^\top \eta^l, \quad (103)$$

there is an *overall* positive tendency toward sparsity if  $\text{tr} \left( H_\theta \right)$  is suppressed, because  $\left( \eta^l \right)^\top 2K^l \left( K^l \right)^\top \eta^l$  is non-negative, i.e., partial derivatives w.r.t.  $\eta^l$  are always overall positive if they are weighted by values in  $\eta^l$  themselves.

It is better to reach a non-overall conclusion. Moreover, there are two possibilities that can also achieve implicit adversarial robustness: reducing the norm of  $K^l (K^l)^\top$ , or misalign the non-null space of  $K^l (K^l)^\top$  with  $\eta^l$ . The first alternative can already be eliminated by parameter growth observed in [7], where Transformers are observed to have increasing parameter norms during training. We also empirically verify this phenomenon under CV settings and show that the trace, or the sum of eigenvalues, will not decrease drastically during training in Section 7.1, even under weight decay. Another possible elimination is normalization layers, which make parameters scale-invariant and introduce normalized effective parameters [28] with moderate norms. However, this requires an entire reform of the theory to utilize effective weight matrices so we simply hide normalization layers in  $M$  and leave it, and especially its interaction with weight decay, for future works.

The other alternative is dealt with in the next two subsections, where hidden vectors are abstractly used in proofs but the theories apply to stacked hidden features. To give a brief account, in the following subsections we will prove that non-zero eigenvalues of  $K^l (K^l)^\top$  have similar values. So if gradients have moderate projections in the non-null subspace of  $K^l (K^l)^\top$ , then  $(\eta^l)^\top K^l (K^l)^\top \eta$  can be lowerbounded by  $\lambda r (\eta^l)^\top (\eta^l)$ , where  $r \leq 1$  indicates how much of  $\eta^l$  falls in the non-null space of  $K^l (K^l)^\top$  and  $\lambda$  is the smallest non-zero eigenvalue or some averaged non-zero eigenvalues of  $K^l (K^l)^\top$ , which is not too small compared to the largest one. Assuming gradients are still back-propagated to shallower layers,  $\lambda r (\eta^l)^\top \eta^l$  can only be suppressed by decreasing  $\|\eta^l\|_2^2$  given that  $\lambda$  increases with the trace of  $K^l (K^l)^\top$ . In Section 4.5 we prove this phenomena at initialization in Theorem 5 that the largest eigenvalue is initially at most 9 times than the smallest non-zero one in ViT-Base. The proof is based on Xavier or Kaiming initialization and Marchenko-Pastur distribution from random matrix theory. In Section 4.6, we theoretically discuss its re-emergence during stochastic training. We first rewrite the updates to the weight matrix  $K^l$  into two large random matrices, whose shape is hidden dimension times number of samples used in training. We then extend Marchenko-Pastur distribution in Theorem 6 under dependent and non-asymptotic scenarios to prove an upperbound on the fraction between the largest and smallest non-zero eigenvalues. Conditions and/or assumptions of the theorem are verified empirically in Section 7.3. There are still gaps in combining the two random matrices, so we measure the spectral concentration in  $K^l (K^l)^\top$  empirically in Section 7.2 and leave a more rigorous discussion for future works.

## 4.5 Spectral Concentration at Initialization

In this section, we prove that  $K^l (K^l)^\top$  has eigenvalues that are close to each other, at least at initialization. With effective gradient sparsity measured by  $\|\eta^l\|_2^2$ , this spectral concentration allows us to approximate the first term in RHS of Eq. (68) with  $\lambda r (\eta^l)^\top \eta^l$ , which is almost directly effective gradient sparsity measured in  $L_2$  norm.

To reach this goal, recall Marchenko–Pastur distribution in Theorem 1 that reveals the asymptotic spectral distribution of random matrices’ product. Applying Theorem 1 to  $K^l (K^l)^\top$  initialized by Xavier or Kaiming initialization, we obtain Lemma 7.

**Lemma 7** (Initial Spectral Property of  $K^l (K^l)^\top$ ). *Assume  $n \neq d$ . Let  $K^l \in \mathbb{R}^{n \times d}$  be the weight matrix initialized by (Gaussian, uniform, or other distribution-based) Xavier or Kaiming initialization. When  $n, d \rightarrow \infty$  with  $d/n = 1/c$ , the ratio between the largest and smallest non-zero*

eigenvalues of  $K^l (K^l)^\top$  converges weakly to

$$\frac{\lambda_1 \left( K^l (K^l)^\top \right)}{\min_{k: \lambda_k \left( K^l (K^l)^\top \right) > 0} \lambda_k \left( K^l (K^l)^\top \right)} \leq \frac{(1 + \sqrt{c})^2}{(1 - \sqrt{c})^2}. \quad (104)$$

Regarding zero eigenvalues, if  $d > n$ , there is no zero eigenvalue, and if  $d \leq n$ , the expected portion of zero eigenvalues is  $1 - \frac{1}{c} = 1 - \frac{d}{n}$ .

*Proof.* The initialization methods utilize centered distribution, and thus there is  $\mathbf{E} \left[ K_{i,j}^l \right] = 0$ .

$K^l (K^l)^\top$  differs from  $W$  of Theorem 1 in 1) the shared standard variance of entries not being 1, and 2) the scaling factor  $\frac{1}{d}$ . Since we are only interested in ratio between eigenvalues, these differences of simultaneous scaling can be ignored.

By Eq. (20), we can see that the support of eigenvalues is restricted to  $[a, b] \cup \{0\}$ . As a result, non-zero eigenvalues can only be found in  $[a, b]$ .

When  $c < 1$ , i.e.,  $d > n$ , the support degenerates to  $[a, b]$ . When  $c \geq 1$ , the probability to pick a zero eigenvalue is  $F(0) = \lim_{u \rightarrow 0^+} \int_0^u f(x) dx = \lim_{u \rightarrow 0^+} \int_0^u \left(1 - \frac{1}{c}\right) \delta(x) dx = 1 - \frac{1}{c}$ .  $\square$

Note that Lemma 7 applies to uniform or other base initialization distribution as long as it is centered and entrywisely independent with the same variance. Since  $n, d$  is generally large, even in small model sizes like Small and Base, we believe this lemma applies to common practice. In Base-sized Transformers, it is usually the case where  $n = 3072, d = 768$ , indicating  $1 - \frac{768}{3072} = \frac{3}{4}$  of eigenvalues are 0, while the rest of them varies up to the ratio of  $\frac{(1 + \sqrt{\frac{1}{4}})^2}{(1 - \sqrt{\frac{1}{4}})^2} = 9$ . This is a surprisingly small value compared to the number of dimensions.

Effective gradient sparsity patterns have great affinity to  $K^l (K^l)^\top$ , allowing Theorem 5.

**Theorem 5** (Spectral Properties of  $K^l (K^l)^\top \odot M$  at Initialization). *Assume  $d \neq n$  and they are sufficiently large.  $K^l \in \mathbb{R}^{n \times d}$  is initialized as in Lemma 7. Let  $M^l = g^l (g^l)^\top$ ,  $\gamma^l$  and  $\eta^l$  be those defined previously.*

*If  $d > n$  then there is*

$$\left( \gamma^l \right)^\top \left( \left( K^l (K^l)^\top \right) \odot M^l \right) \gamma^l = \left( \eta^l \right)^\top K^l (K^l)^\top \eta^l \quad (105)$$

$$\geq \lambda_n \left( K^l (K^l)^\top \right) \cdot \left\| \eta^l \right\|_2^2, \quad (106)$$

where  $n$ -th eigenvalue  $\lambda_n \left( K^l (K^l)^\top \right)$  is moderate and cannot be arbitrarily small because

$$\frac{\lambda_1}{\lambda_n} \leq \left( \frac{1 + \sqrt{c}}{1 - \sqrt{c}} \right)^2, \quad (107)$$

where  $c = d/n$ .

If  $n > d$ , let  $K^l = U\Sigma V^\top$  be the singular value decomposition of  $K^l$ . The result is restricted to the projection to the subspace expanded by  $(U^\top)_{1:d}$ , i.e.,

$$(\gamma^l)^\top \left( \left( K^l (K^l)^\top \right) \odot M^l \right) \gamma^l = (\eta^l)^\top K^l (K^l)^\top \eta^l \quad (108)$$

$$\geq \lambda_d \left( K^l (K^l)^\top \right) \cdot \left\| (U^\top)_{1:d} \eta^l \right\|_2^2, \quad (109)$$

where  $d$ -th eigenvalue  $\lambda_d \left( K^l (K^l)^\top \right)$  satisfies

$$\frac{\lambda_1}{\lambda_d} \leq \left( \frac{1 + \sqrt{c}}{1 - \sqrt{c}} \right)^2, \quad (110)$$

where  $c = d/n$ .

For demonstration, when  $\{n, d\} = \{3072, 768\}$ , the ratio upperbound is 9.

*Proof.* The proof is straightforward after Theorem 1, by noting that when  $n > d$  there are exactly  $(1 - \frac{1}{c})n = n - d$  zero eigenvalues in  $K^l (K^l)^\top$ , or equivalently  $d$  non-zero eigenvalues in  $K^l (K^l)^\top$ .  $\square$

There is still gap between  $\lambda_r (\eta^l)^\top \eta^l$  and current practices where  $d < n$  and there are a lot of zero eigenvalues in  $K^l (K^l)^\top$ , but Theorem 5 is perfectly useful for wide MLPs where  $d > n$ . Therefore, we propose a drastic architectural modification called wide MLP where  $d > n$ , i.e., model dimension is larger than hidden dimension in MLP blocks. Aside from more powerful motivation toward sparsity, wide MLPs also allow rows in  $K^l$  to be mutually orthogonal and permit perfect sparsity, which is impossible when  $n > d$ .

In non-wide MLPs, we believe that since  $K^l (K^l)^\top$  are randomly initialized and samples are randomly selected, there are moderate projections of  $\eta^l$  into the non-null subspace of  $K^l (K^l)^\top$ . Another supporting intuition is that although  $\sigma'$  is not identity or linear, the derivatives of common activation functions are often monotonically increasing and form an approximation to its inputs. This approximation is better when part of the activation derivatives are linear, as in the case of Squared-ReLU[10] and our J-SquaredReLU. Therefore, taking  $\sigma'$  to  $K^l x + b^l$ , which already falls near the subspace expanded by  $(U^\top)_{1:d}$ , does not deviate far from the subspace. Observation 1 also supports this moderate projection dynamically because if  $\eta^l$  is in the null space, it will be borne into every column of the key matrix and next time it will have non-zero projections if  $\eta^l$  does not change too much after one epoch and the column memory is not blurred too severely. Repeatedly memorizing different  $\eta^l$  will make the non-null space of  $K^l (K^l)^\top$  a mixture of the majority  $\eta^l$ 's provided by the training dataset. The empirical evidence for this is that  $(\eta^l)^\top K^l (K^l)^\top \eta^l$ , according to the derivation in Lemma 5, is actually the norm of gradients back propagated to shallower layers. Extreme cases where  $\eta^l$  are contained only in null space of  $K^l (K^l)^\top$  result in zero gradients for shallower layers, which rarely happens. If no residual connection is involved this insight strongly augments the spectral explanation. The detailed and formal analysis of the zero eigenvalues especially when there are residual connections is left for future empirical and theoretical works. For now we can simply cover the gap with wide MLPs.

## 4.6 Spectral Concentration during Stochastic Training

In this subsection, we discuss how spectral concentration re-emerges during later stochastic training.

First recall the Marchenko-Pastur distribution in Theorem 1. The condition of random centered matrices in Theorem 1 invites another randomness other than initialization to the party, i.e., stochastic gradient noise (SGN) brought by stochastic optimizers. After  $t$  updates,  $K^l$  can be written as the sum of random initialization, stochastic gradient noises and full-batch gradients that are not as stochastic as the two former terms, i.e.

$$K^{l,t} = K^{l,0} - \underbrace{\sum_{i=1}^t U_{K^l}^i}_{\text{stochastic, centered}} - \sum_{i=1}^t \frac{\partial \mathcal{L}(\theta^t)}{\partial K^l} \quad (111)$$

As discussed in Section 3.4,  $U_{K^l}^i$  is by definition centered. If it can be assumed that the  $\mathcal{S}\alpha\mathcal{S}$  SGN with large variance and noise norm shadows full-batch gradient, then  $K^{l,t}$  is the sum of two centered random matrix with a slight non-stochastic bias, to which Marchenko-Pastur distribution would approximately apply if further entries in  $U_{K^l}^i$  shared similar variance and were sampled independently. [29] and works cited in it have tried to relax independence condition of Theorem 1, but it is still far from applying relaxed Marchenko-Pastur distribution here. Aside from waiting for this mathematical progress, we build empirical basis in Section 7 where at all steps, in  $K^l (K^l)^\top$ , there is a stable portion of near-zero eigenvalues as in Theorem 5 across most layers, and the majority of non-zero ones, with significant gap with near-zero ones, vary up to a ratio of  $< 100$  for most of the time. It is not surprising that this effect empirically sustains and even becomes stronger at the end of training because model is well-learned by then and the full-batch gradient is of smaller norm.

To have a more satisfying discussion, we propose a extended version of Marchenko-Pastur distribution and find a re-directed view on stochastic gradients to apply it. To this end, what conditions and/or assumptions can stochastic training provide must be figured out first.

Observing the structure of MLP or DB-MLP layers, the most essential operation involving weight matrix  $K^l$  is

$$z^l := K^l u^l, \quad (112)$$

where  $u^l$  is anything that is multiplied with  $K^l$ , abstracting  $x^l$  or  $x^l + d^l$ , and  $z^l$  is the vector passed to the vanilla bias and activation function. This structure gives birth to the update of a sample  $(x_s, y_s)$  to  $K^l$  that writes

$$\Delta K^{l,s} = \frac{\partial \mathcal{L}(\theta, (x_s, y_s))}{\partial z^{l,s}} \times (u^{l,s})^\top \quad (113)$$

$$= \eta^{l,s} (u^{l,s})^\top. \quad (114)$$

At step  $t$  with batch  $B_t$ , the update on  $K^l$  averages these samplewise differences, i.e.

$$\Delta K^{l,t} := \frac{1}{|B_t|} \sum_{s \in B_t} \eta^{l,s} (u^{l,s})^\top \quad (115)$$

$$= \frac{1}{|B_t|} H^t (U^t)^\top, \quad (116)$$

where  $H^t \in \mathbb{R}^{n \times |B_t|}$  (capitalized “ $\eta$ ”) is the matrix consisting of column vectors  $\eta^{l,s}$  for sample  $s$  in the batch  $B_t$ , and  $U^t \in \mathbb{R}^{d \times |B_t|}$  is similarly constructed with  $u^{l,s}$ ,  $s \in B_t$ . It can be seen that another sample covariance matrix of large random matrices emerges in  $\Delta K^{l,t} (\Delta K^{l,t})^\top$ , i.e.,

$$\Delta K^{l,t} (\Delta K^{l,t})^\top = \frac{1}{|B_t|^2} H^t (U^t)^\top U^t (H^t)^\top. \quad (117)$$

Since we are interested in spectral distribution and that cycling a matrix product does not change non-zero eigenvalues, a more desirable form is

$$H^\top H^t (U^t)^\top U^t, \quad (118)$$

and we want to separately investigate the spectral distributions of

$$(H^t)^\top H^t \text{ or spectrally equivalent } H^t (H^t)^\top, \quad (119)$$

$$\text{and, } (U^t)^\top U^t \text{ or spectrally equivalent } U^t (U^t)^\top. \quad (120)$$

Columns, hidden features or gradients of samples, are (conditionally) independently sampled to form a batch, so it is possible to apply some generalized Marchenko-Pastur distribution allowing dependence within a column, e.g., [30]. However, some extension is still needed, so we directly jump to the result for multiple batches and concentrate all technical details in one theorem.

Spectral concentration in  $\Delta K^{l,t} (\Delta K^{l,t})^\top$  hints that in  $K^{l,T} = K^{l,0} + \sum_{t=1}^T \Delta K^{l,t}$ , but it is not half-formally discussed. It turns out that sample covariances of even larger random matrices can be observed in  $K^{l,T} = K^{l,0} + \sum_{t=1}^T \Delta K^{l,t}$  as well:

$$K^{l,T} - K^{l,0} = \sum_{t=1}^T \frac{1}{|B_t|} \sum_{s \in B_t} \eta^{l,s} (u^{l,s})^\top \quad (121)$$

$$= \frac{1}{bT} H^{1:T} (U^{1:T})^\top, \quad (122)$$

where  $T$  is the number of batches,  $b$  is batch size, and  $H^{1:T} := [H^1 \dots H^t \dots H^T]$ , and  $U^{1:T} := [U^1 \dots U^t \dots U^T]$ . This makes

$$(K^{l,T} - K^{l,0}) (K^{l,T} - K^{l,0})^\top = \frac{1}{(bT)^2} H^{1:T} (U^{1:T})^\top U^{1:T} (H^{1:T})^\top \quad (123)$$

another sample covariance matrix of large random matrices. However, the dependence of later columns on earlier columns hinders the formal proof of it, which is modeled in Definition 4. In later formal definitions, theorems and proofs,  $U$  is used to represent both  $H^{1:T}$  or  $U^{1:T}$ ,  $p$  indicates the height of  $U^{1:T}$  or  $H^{1:T}$ , i.e., the hidden dimensions.  $b$  and  $T$  keep their meanings as batch size and total number of batches.

**Definition 4** (Batch Dependence Model). *Let  $U^{1:T} \in \mathbb{R}^{p \times (bT)}$  be a random matrices. Decompose it into blocks with batch size  $b$ , i.e.,*

$$U^{1:T} = [U^1 \quad \dots \quad U^t \quad \dots \quad U^{T-1} \quad U^T], \quad (124)$$

where  $U^t \in \mathbb{R}^{p \times b}$ . If the dependence between elements can be described by SCMs

$$\{u_k^t := f^t(U^1, U^2, \dots, U^{t-1}), \epsilon_k^t : t \in [1, T], k \in [1, b]\} \quad (125)$$

or SCMs that resemble the notion of samples and parameters

$$\{u_k^t := g^t(m^{t-1}), \epsilon_k^t : t \in [1, T], k \in [1, b]\} \cup \{m^t := h^t(m^{t-1}, U^t)\} \quad (126)$$

where  $u_k^t$ s are columns in  $U^t$ ,  $m^t$  is the parameter after step  $t$ ,  $\epsilon_k^t$  are I.I.D. random noises, then  $U^{1:T}$  is a random matrix with batch dependence.

**Remark 2.** Within each batch (i.e., when conditioned on all previous batches), samples are I.I.D. sampled to simulate batch sampling. However, previous samples have trained the parameters and shift distribution of output of shallow layers as well as back-propagated gradients. Therefore, the current batch depends on previous batches.

There are works re-establishing Marchenko-Pastur law with independence condition relaxed to martingale conditions [31], but some conditions in it require entrywise conditional independence. There are also Marchenko-Pastur law for time series [32], [33], but restricted to linear dependence. We adapt proofs in [30], and use  $O(p)$ -anisotropy condition in all samples to extend Marchenko-Pastur distribution under Batch Dependence Model, leading to Theorem 6.

**Theorem 6** (Spectral property of accumulated steps). *Let  $X^{p,b} \in \mathbb{R}^{p \times b}$  be a random matrix whose columns are  $X_{:,j}^{p,b} \in \mathbb{R}^p$ . Assume columns in  $X^{p,bT} \in \mathbb{R}^{p \times bT} = X^p$  are not necessarily independent but forms a batch dependence model as in Definition 4 with step count  $T$  and batch size  $b$ .*

*Let  $x_k^p := X_{:,k}^{p,b}$  be the  $k$ -th column of  $X^p$  and  $x_{t,l}^p := X_{:,l}^{p,t}$  be the  $l$ -th column of batch  $t$  or equivalently the  $k = ((t-1) * b + l)$ -th column  $x_k$  in  $X^{p,b}$ . Supscription  $p$  maybe dropped for convenience.*

*Let  $S^p := \frac{1}{bT} \sum_{k=1}^{bT} x_k x_k^\top$  be the empirical covariance matrix of all random vectors, and  $I_p$  be the compatible identity matrix. Assume  $x_{t,l}$ s' norm is bounded, say by 1, and scale it with*

$$u_{t,l}^p := \sqrt{a} x_{t,l}^p, \quad (127)$$

obtaining  $U^{p,b} = [U^1 \ \dots \ U^t \ \dots \ U^T] = \sqrt{a} \cdot X^p$ , where  $a := \frac{\text{tr}(S^p)}{\text{tr}(S^p S^p)}$ . Let

$$T^p := \frac{1}{bT} \sum_{k=1}^{bT} u_k u_k^\top = a \cdot S^{p,t} \quad (128)$$

be the empirical covariance matrix of all  $u_k^p$ s.

Assume  $a$  is bounded by  $\alpha(p) = O(p)$  and  $\mathbf{E} \left[ \sqrt{p \text{tr}((T^p - I^p)(T^t - I^p))} \right]$  also is upperbounded by  $\beta(p) = O(p)$ .

Further assume that the following function of  $z \in \mathbb{C}^+$  and  $p, b, T \in \mathbb{N}^+$

$$\mathbf{E} \left[ \sum_i \frac{1}{\lambda_i(UU^\top) - z} \right] \quad (129)$$

is always continuous w.r.t.  $z$  for any  $p, b, T$ .



If the above assumptions are satisfied, the non-zero eigenvalue concentrates. To be more specific, let  $\overline{\lambda^{>0}}$  be the mean of non-zero eigenvalues of  $\frac{1}{bT}U^p(U^p)^\top$  and use  $\mathbf{E} \left[ \overline{\lambda^{>0}} \right]^2$  to represent the overall situation of non-zero eigenvalues. Then there is

$$\mathbf{E} \left[ \frac{\mathbf{E} \left[ \overline{\lambda^{>0}} / \sqrt{v} \right]^2}{\left( \frac{\lambda}{\sqrt{v}} \right)^2 + v} \right] \leq \frac{\sqrt{2}}{cv\sqrt{v}} \frac{\alpha^2}{\min(bT, p)^2} \sqrt{c + \frac{(2\sqrt{2} + 2)c\alpha}{vp} + \frac{c\beta}{vp} + \frac{c}{vp}}, \quad (130)$$

$$\mathbf{E} \left[ \frac{\mathbf{E} \left[ \overline{\lambda^{>0}} \right]}{\lambda + \frac{v^2}{\lambda}} \right] \leq \frac{\sqrt{2}}{c\sqrt{v}} \frac{\alpha}{\min(bT, p)} \sqrt{c + \frac{(2\sqrt{2} + 2)c\alpha}{vp} + \frac{c\beta}{vp} + \frac{c}{vp}}. \quad (131)$$

for any  $v > 0$ , where  $\lambda$  is a randomly selected eigenvalue of  $\frac{1}{bT}U^p(U^p)^\top$  and  $c = p/bT$ .

Its proof is left in Appendix C. This concludes that spectral concentration also happens in  $H^{1:T} (H^{1:T})^\top$  and  $U^{1:T} (U^{1:T})^\top$ , as long as the samples during training are diverse enough to have  $O(p)$  anisotropy and  $O(p)$  norm bounds. To empirically verify the applicability of Theorem 6, one needs to compute anisotropy  $\mathbf{E} \left[ \sqrt{p \text{tr} \left( (T^p - I)^\top (T^p - I) \right)} \right]$  and  $\alpha$  from  $u^p$ 's marginal distribution, i.e., by mixing hidden features and back-propagated gradients in parallelly trained models, which is conducted in Section 7.3.

In contrast with conventional results with  $p \rightarrow \infty$  and  $p/bT \rightarrow c$  in RMT, our theorem gives bounds for non-limiting scenarios. One of its benefits in the context of machine learning is that one often are more interested in training behaviours when the total number  $bT$  of training samples increase as the training proceeds while  $p$  is holden still. Nevertheless, the co-increasing scenarios is also of interest, especially in the era of large models [34]. In our result, the spectral concentration is measured by expected fraction between eigenvalues and the expected eigenvalue, but with an extra shadowing parameter  $v$  that may shadow small eigenvalues and decreasing  $v$  to suppress the disturbance loosens the bound. Fortunately, most  $v$  as dominators show up together with  $c$  as numerators, the ratio between hidden dimension and number of training samples used which is often extremely small. If  $\frac{\alpha}{p}$  is also small and decreases as  $p$  is enlarged, as we will show in the experiments, then the bound will be controlled.

It is frustrating to see that the bound diverges as training steps increase due to factor  $\frac{1}{c} = \frac{bT}{p}$ . However, we consider weight decay as an alleviation to this issue. Weight decay effectively introduces a sliding window which reduces the effective  $T$ , because vectors out of the window are exponentially decayed and they have little contribution to the sample covariance matrix. For example, let  $w$  be the parameter of weight decay, then each column in  $H^{1:T}$  or  $U^{1:T}$  becomes  $(\sqrt{1 - \eta w})^{T-t} \eta_{t,l}$  or  $(\sqrt{1 - \eta w})^{T-t} u_{t,l}$ , where  $\eta$  is learning rate and  $w$  is the strength of weight decay. Setting  $r = 1 - \eta w$ , if we consider the tail whose weights' sum is smaller than a threshold  $\tau$  as those out of the window, then the window size  $k$  needs to satisfy  $\sum_{i=k+1}^{\infty} r^i = r^{k+1}/(1 - r) \leq \tau$ , where  $r$  is used to obtain tighter bounds instead of  $\sqrt{r} = \sqrt{1 - \eta w}$  by arguments in Appendix D. One sufficient condition for this is  $k \geq \frac{\ln \tau(1-r)}{\ln r} - 1$ . When  $\tau = 10^{-3}, \eta = 10^{-3}, w = 10^{-1}$ , the effective window size is about 161, 172. When  $w$  increases to 0.3, the effective window size becomes 50, 057. As a result,  $\frac{1}{c}$  is upperbounded by a constant as the training proceeds if weight decay presents.

There are still gaps between full spectral distribution of  $K^l (K^l)^\top$  during stochastic training. For example, spectral concentration of  $HH^\top$  and  $UU^\top$  hints similar phenomena in their interlaced

product  $\Delta K^{l,t} (\Delta K^{l,t})^\top$ , which, however, is not yet formally proved. Moreover, applying Theorem 6 assumes SGD instead of adaptive optimizers is used due to Eq. (122). Filling these gaps is left for future works because we have established spectral concentration’s empirical supports in Section 7.2.

Finally, we have discussed the spectral concentration of  $K^l (K^l)^\top$ . To put everything together, assuming moderate projection of  $\eta^l$  into non-null space of  $K^l (K^l)^\top$ , and considering the increasing trace of  $K^l (K^l)^\top$ , the only way to suppress  $\text{tr}(H_{\theta_D}) \geq (\gamma^l)^\top (K^l (K^l)^\top \odot M^l) \gamma^l = (\eta^l)^\top K^l (K^l)^\top \eta^l \geq \lambda r (\eta^l)^\top \eta^l$  is to reduce  $\|\eta^l\|_2^2 = \|g^l \odot \gamma^l\|_2^2$ . To see gradient-sparsity-induced activation sparsity’s emergence, given empirically that  $\text{tr}(M^l) = \text{tr}((g^l)^\top g^l) = \|g^l\|_2^2$  will not decrease during training, the only way to suppress  $\|\eta^l\|_2^2$  is to decrease  $\gamma^l$ , at least at entries where  $g^l$  has large magnitudes.

After theoretical analyses, we conduct experiments to verify our explanation in Section 5, show the benefits of our architectural modification in Section 6. Based on checkpoints in Section 6, evidences for theoretical assumptions are demonstrated in Section 7.

## 5 Experiments for Verification

The experiments for verification are designed to rule out other possible explanations and show that gradient sparsity is the main cause of of activation sparsity, at least in DB-MLP.

Although comprehensively demonstrated in [1], the sparsity emerging in MLP blocks has still a lot of confusions. This is because a lot of coincidences exist in ReLU. For example, ReLU and its derivatives share the same zero-valued intervals, and they are both monotonically increasing. Previous works [1], [4] consider that it is value or norm of activations that are reduced to produce sparsity. And there are more possible explanations, such as the absolute value of activations as well as all similar explanation based on pre-activations. We show none of them is the essential source of observed activation sparsity but the gradient sparsity, by designing weird activation functions, using which activations or pre-activations are not consistently decreased, increased or moved toward zero point, but the norm of derivatives is.

Our construction includes an activation function Weird-ReLU and 4 shifting operations. Weird-ReLU is defined as

$$\text{Weird-ReLU}(x) := \begin{cases} x + w_{\text{half}} & x \leq -w_{\text{half}}, \\ 0 & -w_{\text{half}} < x < w_{\text{half}}, \\ x - w_{\text{half}} & x \geq w_{\text{half}}, \end{cases} \quad (132)$$

where  $w_{\text{half}} > 0$  is a parameter. Weird-ReLU and its derivatives are illustrated in Fig. 2a. We shift it around along  $x$ - or  $y$ -direction, i.e., use  $\text{Weird-ReLU}(\cdot - \Delta x) + \Delta y$  in MLP layers, to decorrelate between activations and pre-activations, values and absolute values or norms. If gradient sparsity is indeed essential, then the activations and pre-activations will concentrate around the flat area instead of zero point or any half planes and will follow it well if it is shifted in another way. To have enough space for all pre-activations, we choose  $w_{\text{half}} = 1.5$ , i.e., the width of the flat area is 3, which is approximately the width of majority pre-activations in Fig. B.2(c) in [1]. To exclude flat area from zero point, we shift Weird-ReLU horizontally and vertically by  $(\Delta x, \Delta y) \in \{+1.6, -1.6\} \times \{+1.6, -1.6\}$ . This family of shifted Weird-ReLU is illustrated in

Fig. 2b-Fig. 2e. From theory we expect that most pre-activations and activations will fall around  $[\Delta x - w_{\text{half}}, \Delta x + w_{\text{half}}] \times \{\Delta y\}$ .

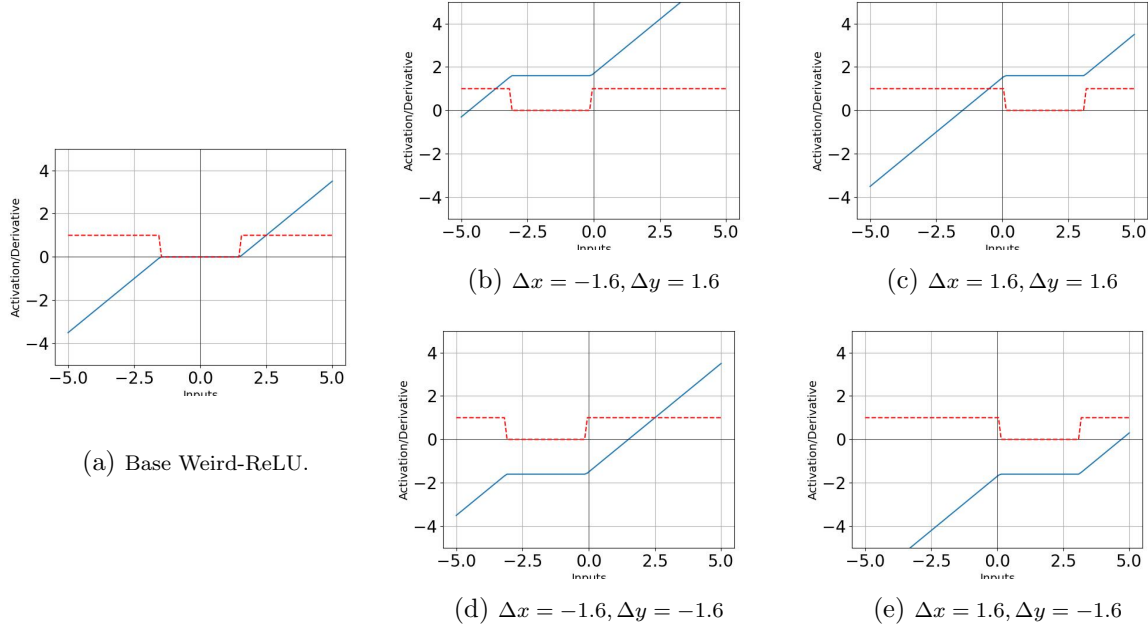


Figure 2: The illustration of base and shift Weird-ReLU and their derivatives, indicated by blue lines and red dashed lines, respectively.

We train ViT-Base with DB-MLP and J-SquaredReLU-like modified Weird-ReLU (non-zero values of base Weird-ReLU is sign-keepingly squared and shifted the same way as non-zero values of J-SquaredReLU) on CIFAR-10 [35] for 100 epochs. Training details are listed in Appendix E. The gradient sparsities during training, measured simply by the percentage [1] of activations not falling in  $[\Delta x - w_{\text{half}}, \Delta x + w_{\text{half}}] \times [\Delta y - 10^{-6}, \Delta y + 10^{-6}]$ , are illustrated in Fig. 3. In Fig. 3, deep layers have at least 70% activations concentrating at the flat area as expected, which not only indicates that activation is currently not sparse, but also is a strong evidence that gradient sparsity dominates the sparsity among other potential factors. Fig. 3 rules out other potential activation or pre-activation explanations, because Fig. 3b, Fig. 3a and Fig. 3d rule out the explanations that activation or pre-activation are decreased, Fig. 3c, Fig. 3d and Fig. 3a rule out any explanations that activations or pre-activations are increased, while all of them rule out the explanations that activations or pre-activations' norms are optimized toward zero. Furthermore, in Fig. 3, where the spurious correlation between activation and gradient sparsity is broken, activation sparsity is gone while gradient sparsity survives and follows the expected area well, indicating that gradient sparsity is more stable and essential than the activation one and thus deserves more research attention.

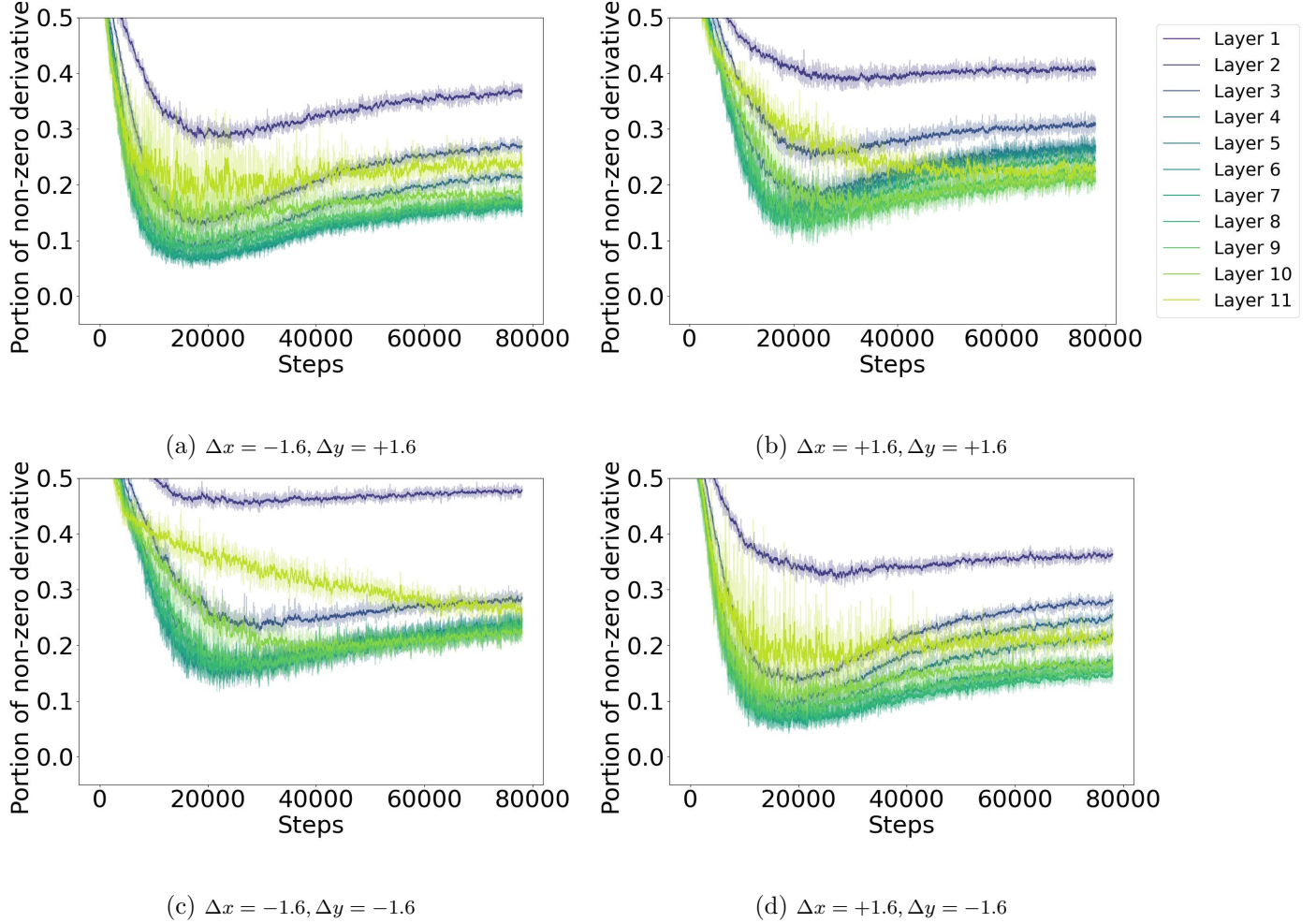


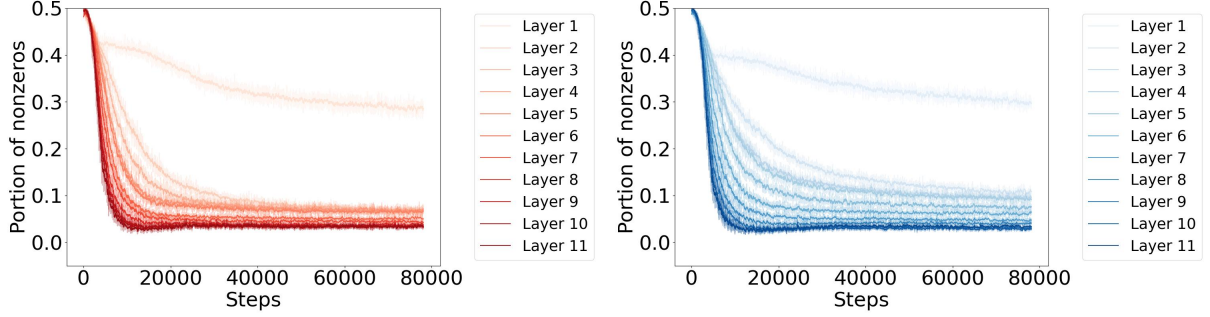
Figure 3: Gradient sparsity during training of ViT-Base with DB-MLP and differently shifted Weird-ReLU on CIFAR-10.

## 6 Experiments for Productivity

In this section, we conduct experiments with non-weird activation functions on larger scaled datasets to examine the effectiveness our modifications and verify the theoretical guidance behind them. Aside from modified models, vanilla ViTs are used for comparison. Since it is hard to define (or to achieve) sparsity on GELU activations [1], even in “vanilla” ViTs ReLU are used through out this section.

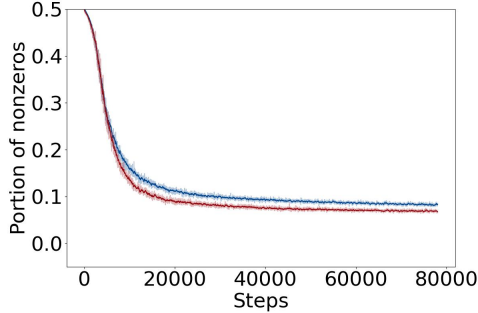
### 6.1 Training from Scratch

Although distinguished in Section 5, gradient and activation sparsity should better coincide to allow aggressive dynamic neuron pruning during both training and inference. To show its effectiveness in such practical scenarios, we test our modifications of DB-MLP and non-weird J-SquaredReLU on CIFAR-10 as well as ImageNet-1k [36], whose results are displayed in Figs. 4 and 5 and Table 1.

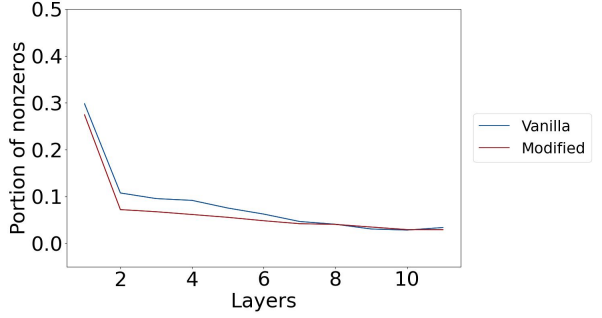


(a) ViT-Base/16 with DB-MLP and J-SquaredReLU.

(b) Vanilla ViT-Base/16.



(c) Comparison of layer-average sparsity between vanilla ViT and ViT with DB-MLP and J-SquaredReLU.

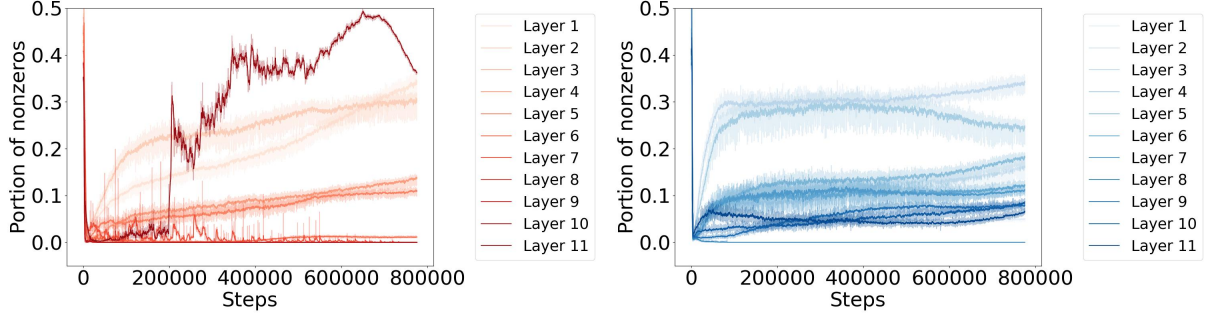


(d) Comparison of layerwise sparsity between vanilla and modified ViT during the last 100 steps.

Figure 4: Sparsity during training of ViT-Base/16 with CIFAR-10. Red is used for modified ViT while blue indicates vanilla ViT. Fig. 5a and Fig. 5b shows sparsity trending of vanilla and modified ViT in a layerwise manner. Fig. 5c compares the sparsities after averaging them across layers. Fig. 4d compares layerwise sparsity by averaging that of the last 100 steps

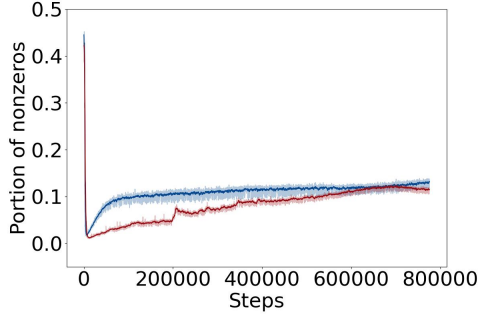
We train vanilla and modified ViT-Base/16 on CIFAR-10 for 100 epochs and show results in Fig. 4. From Fig. 4 we can see that our modification improves sparsity in shallow and middle layers. This improvement is expected because perturbations on vanilla parameters before these layers have limited expressivity compared to deeper layers and DB-MLP can improve the diversity of these perturbations. These improvements in shallow and middle layers leads to about 0.017 absolute, or 13.8% relative sparsity improvement compared to vanilla ViT across all layers.

On ImageNet-1k, we generally follow PyTorch’s recipe[37] for ViT-Base/16 to train from scratch, except that we turn off model EMA and increase gradient clipping’s global norm to 10 for larger gradient noises and better flatness. The sparsity along the training of vanilla and modified model is shown in Fig. 5b and Fig. 5a, respectively. From Fig. 5a we can see that our modification greatly improves activation/gradient sparsity in middle and deep layers, with extreme effects in Layer 3 and most deep (6–10) layers. In vanilla ViT their sparsities lie in  $[0.0, \sim 0.1]$  while in modified ViT they are squeezed into an almost-zero interval  $[0.0, 0.03]$ . Layer 11, however, sees a catastrophic drop in sparsity in early training but also a rapid compensation at the end of training. Since automatic mixed precision is used to accelerate training, we consider this to be related to numerical instability

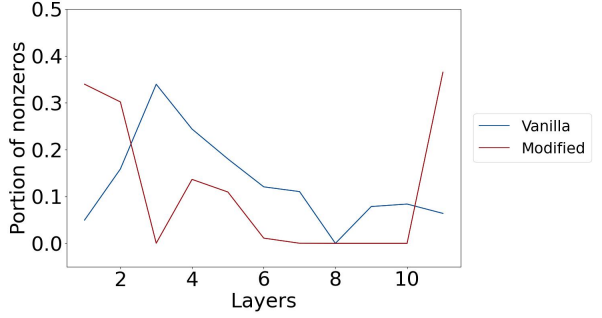


(a) ViT-Base/16 with DB-MLP and J-SquaredReLU.

(b) Vanilla ViT-Base/16.



(c) Comparison of layer-average sparsity between vanilla ViT and ViT with DB-MLP and J-SquaredReLU during training.



(d) Comparison of layerwise sparsity between vanilla and modified ViT during the last 100 steps.

Figure 5: Sparsity during training of ViT-Base/16 with ImageNet-1k. Red is used for modified ViT while blue indicates vanilla ViT. Fig. 5a and Fig. 5b shows sparsity trending of vanilla and modified ViT in a layerwise manner. Fig. 5c compares the sparsities after averaging them across layers. Fig. 5d compares layerwise sparsity by averaging that of the last 100 steps. Since there are all-zero layers, log scale presents the results poorly and the non-log scale is used.

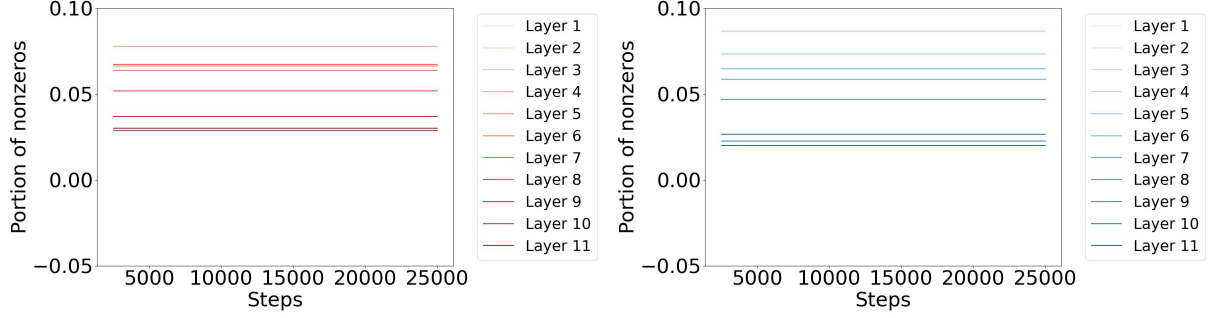
due to the squaring modification in the new activation function. Another potential reason is that we did not restrict value of zeroth biases, and Eq. (75) suggests this unboundedness is damaging the effects of LayerNorm layers. The improved version with numerical stability control and bounded zeroth biases by parameter clipping will come in the next version. In shallow and middle layers there is no significant advantage or disadvantages compared to vanilla ViT. To see whether our modification has positive or negative overall effects, sparsities are compared after being averaged across layers in Fig. 5c. It can be seen that modified ViT’s sparsity is at least as good as the vanilla one, while the modification introduces large cost reduction in the early stage of the training and provides slightly better sparsity after Layer 11 recovers from the catastrophic dropping. By averaging sparsities of all layers and steps, we conclude that our modification gains 0.028 absolute or 25.5% relative improvements on theoretical MLP training costs. We summarize absolute and relative theoretical improvements in Table 1.

	CIFAR-10		ImageNet-1k		Finetuning	
	Sparsity	Relative	Sparsity	Relative	Testing Sparsity	Relative
Vanilla	0.124		0.110		0.081	
Modified	<b>0.107</b>	↓ 13.8%	<b>0.082</b>	↓ 25.5%	<b>0.078</b>	↓ 3.4%

Table 1: Sparsities and relative improvements on CIFAR-10 and ImageNet-1k.

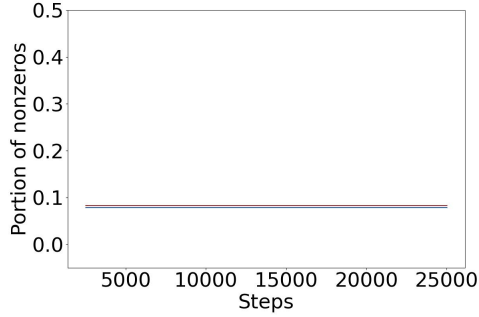
## 6.2 Finetuning for Sparsity

Apart from training from scratch, we finetune existing weights for sparsity to show a cheaper usage of our modification, given that our modification is nearly plug-and-play as analyzed in Section 4.1. We download PyTorch’s weight that has been trained for 300 epochs and train it for another 10 epochs after applying the modification. We use the same configuration as training from scratch, except that we change total epoch parameter of the learning rate scheduler into 350 and finetune from epoch 300 to epoch 310 to have higher learning rate. Since finetuning is relative short and serves for later inference, we instead measure the testing sparsity rather than training sparsity in this section. The testing sparsity of modified and vanilla ViT-Base is compared in Fig. 6. Since learning rate is small at the end of training, both of the models do not show drastic change in sparsity. According to Fig. 6d, our modification encourages sparsity in shallow and middle layers but impairs sparsity in deep layers. Overall, the modified model has a slight advantage of absolutely 0.0027 or relatively 3.4% improvements at the end of finetuning. Acknowledging that this improvement is not large, we suspect this is because the learning rate is small, which traps the optimization within the same basin determined by the loaded weight [38]. It may be resolved by learning with at first a small learning rate to adapt the parameters to the new activation function, then a larger learning rate to escape current basin toward a flatter one, and finally a small learning rate again to reach local minima.

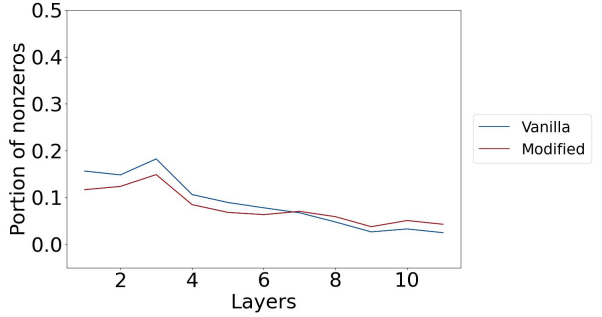


(a) ViT-Base with DB-MLP and J-SquaredReLU.

(b) Vanilla ViT-Base.



(c) Testing sparsity averaged across layers during finetuning.



(d) Layerwise testing sparsity during the last 100 steps.

Figure 6: Testing sparsity during finetuning for sparsity on ImageNet-1k. Red is used for the modified model while blue indicates the vanilla one. Fig. 6a and Fig. 6b shows changes of testing sparsity in a layerwise manner. Fig. 6c averages sparsity across layers to show overall sparsity. Fig. 6d shows layerwise sparsity at the end of finetuning by averaging sparsities of the last testing for each layer. Sparsity measure is conducted during testing at the end of each epoch, so although two models start from the same epoch, they have different sparsity at the starts of these diagrams.



## 7 Empirical Supports for Assumptions

In this section, evidences of assumptions required in Section 4.5 and Section 4.6 are empirically examined. The observation are taken during or after training from scratch or finetuning discussed in Section 6. The experiment settings are roughly similar to those in Section 6, except that gradient clipping norm is reduced to 1 as a numerical stability control when training from scratch, and better scheduling is used during finetuning. Some experiments are re-run under these modifications. We plan to replace experiments in Section 6 in later versions when the re-runs finish.

### 7.1 Spectral Increase in $K^l (K^l)^\top \odot M$

The traces of  $K^l (K^l)^\top$ ,  $M$  and  $K^l (K^l)^\top \odot M$  during (a new run of) finetuning for sparsity are displayed in Fig. 7, as well as those in the early stage of training modified ViT from scratch on ImageNet-1k in Fig. 8.

From Fig. 7 it can be seen that the trace of  $K^l (K^l)^\top$  does not drop drastically. The trace of  $M$ , i.e.,  $\|g^l\|_2^2$ , drastically increases, and so does  $K^l (K^l)^\top \odot M$ 's. Similar things happen in Fig. 8 except that traces of  $K^l (K^l)^\top$  in Fig. 8a do not change as much as in Fig. 7a. Fig. 9a indicates that the portion of non-near-zero eigenvalues are quite stable, so Fig. 7 and Fig. 8 demonstrate that the average non-near-zero eigenvalue does not drop and implicit adversarial robustness cannot be obtained by shrinking  $K^l (K^l)^\top \odot M$ ,  $K^l (K^l)^\top$  or  $\|g^l\|_2^2$ . These phenomena are related to be parameter growth discussed by [7] and those about  $M^l$  and  $g^l$  are conjectured to be related to normalization layers. It is interesting from Fig. 7a that the trace of  $K^l (K^l)^\top$  correlates well with the scheduled learning rate (we are using a  $(1 - \cos)/2$ -like learning rate scheduling for new finetuning experiments), despite the fact that both update step size and weight decay are subject to learning rate.

The results for ImageNet-1k and C4 are left in later version, because previous experiments are based on even former theories and did not observe traces.

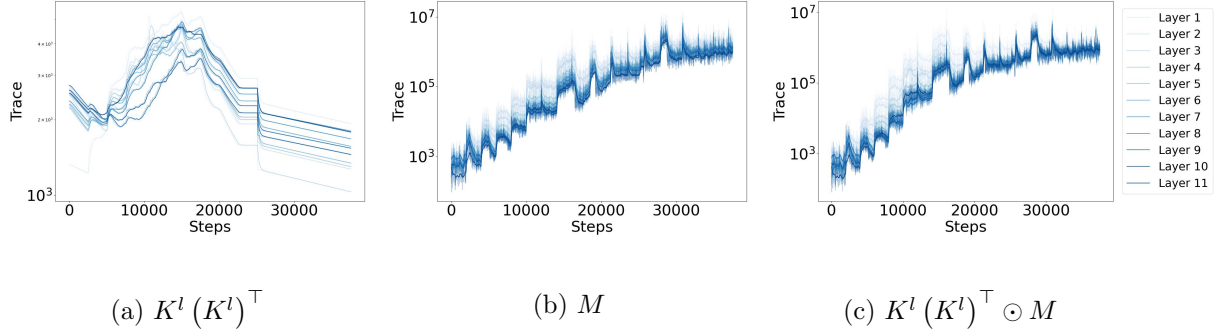


Figure 7: The traces of  $K^l (K^l)^\top$ ,  $M$  and  $K^l (K^l)^\top \odot M$  of vanilla ViT-Base during finetuning for sparsity.

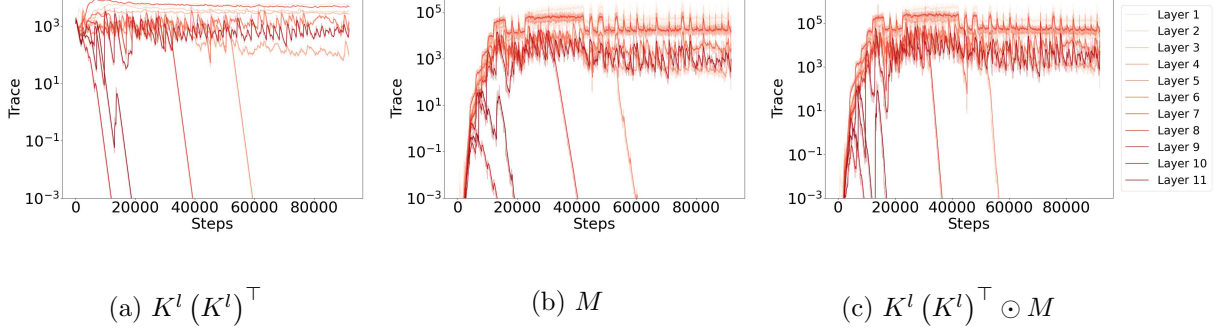


Figure 8: The traces of  $K^l (K^l)^\top$ ,  $M$  and  $K^l (K^l)^\top \odot M$  of modified ViT-Base during training from scratch on ImageNet-1k. The drop in layer 4, 7, 8, 10 is because they are totally pruned during training.

## 7.2 Spectral Concentration of $K^l (K^l)^\top$

The log-scaled histograms of eigenvalues of  $K^l (K^l)^\top$  at several epochs of vanilla ViT’s entire training on ImageNet-1k are displayed in Fig. 9. It can be seen that there is a portion of near-zero ( $< 10^{-3}$ ) eigenvalues, which are clearly separated with non-near-zero ones. For non-near-zero eigenvalues, shallow layers tend to have non-concentrating eigenvalues, but most of them still vary within the ratio of 200, despite that there are about  $3072 * \frac{1}{4} = 768$  non-near-zero eigenvalues. For deep layers, the majority varies within a ratio of  $< 100$ , and the ratio decreases to about 40 during the ending phase of training. The clear separation of near-zero eigenvalues and approximate concentration of non-zero eigenvalues are quite similar to the prediction of Theorem 1. There is also a tendency toward concentration as the training proceeds.

The results of modified ViT and those on NLP tasks will come in later versions.

## 7.3 Assumptions for Theorem 6

We measure anisotropy  $\sqrt{\text{ptr} \left( (T - I)^\top (T - I) \right)} / p$  and  $a/p$  empirically, as required in Section 4.6. They are compared to hidden dimension  $p = d$  or  $n$  to build empirical evidences for application of Theorem 6.

Since hidden dimension has to be altered, the experiment is conducted on small dataset MNIST[39] and a tiny pure MLP with 1 input layer, 1 classifier layer and 4 hidden layers, each of hidden dimension  $d$  to be altered. Skip connections are equipped. The models are trained using Cross Entropy Loss and SGD, according to the implicit assumption of Theorem 6. Inputs of the hidden layers and gradients w.r.t. linear layers’ outputs, which coincide with those w.r.t.  $K^l u$ , are collected as  $x_k$  vectors and are used to compute  $as$ , after which  $u_k$ s are computed by rescaling. Theorem 6 requires normalization on  $x_k$  but it is inefficient to re-normalize after every step. Observing  $aS^p$  is scaling invariant w.r.t.  $S^p$  and  $a$  essentially captures the expected norm upperbound in  $u_k$  in the proof, we directly compute  $T^p = aS^p$  without normalizing  $S^p$  and compute the expected norms in  $u_k$ , or  $\text{tr}(T^p)$  to illustrate  $a$ .

Fig. 10-Fig. 13 show anisotropies, norms and spectral concentration bounds computed by effective window sizes under weight decay of 0.0, 0.01, 0.1 and 0.3. From subfigures (a) and (b) in

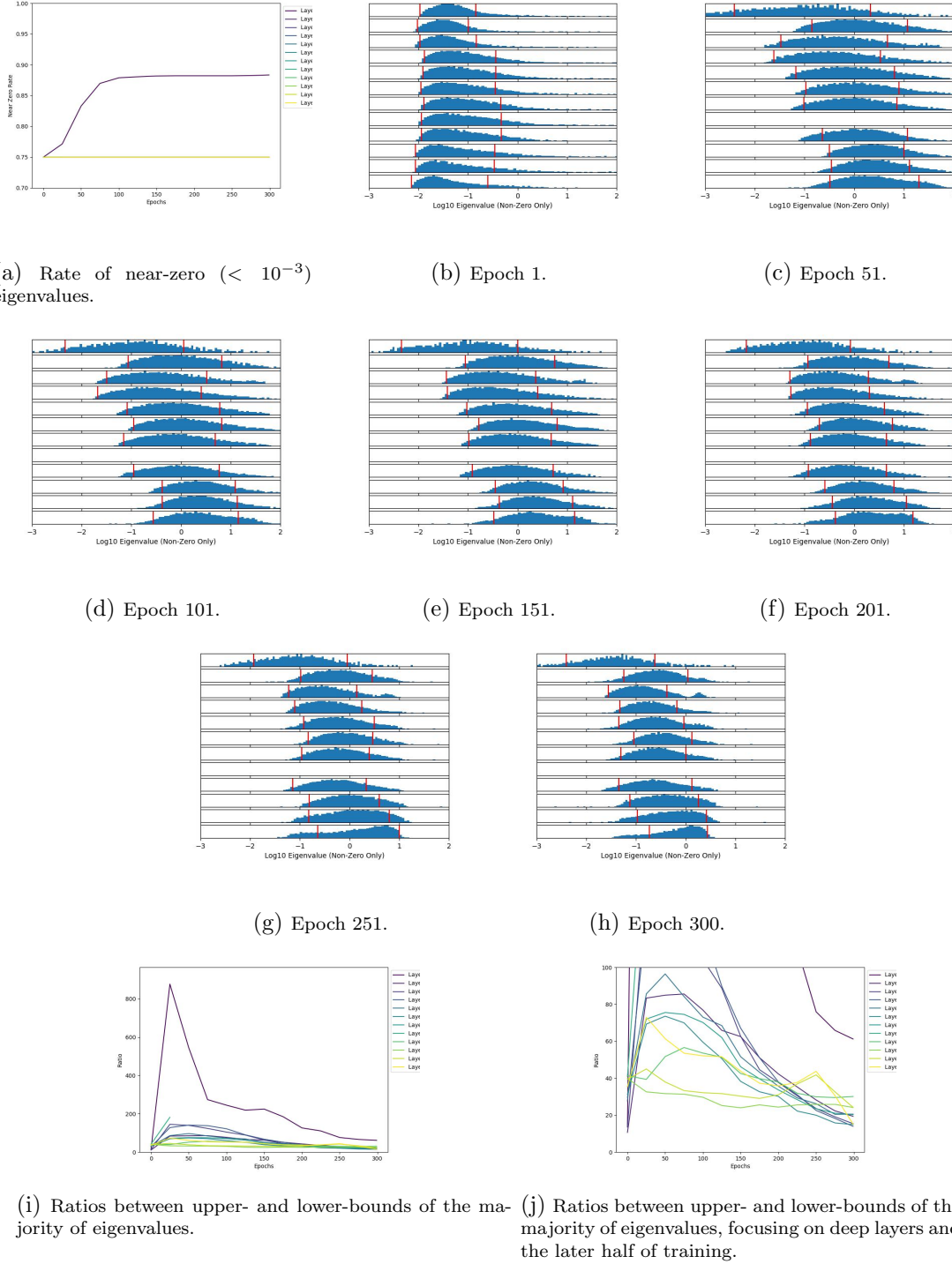


Figure 9: Empirical spectral properties of the first weight matrices in MLP blocks, observed in vanilla ViT-Base/16 trained on ImageNet-1k with PyTorch’s recipe[37]. We consider eigenvalues  $< 10^{-3}$  as near-zero eigenvalues. Fig. 9a displays the portion of near-zero eigenvalues during training. Fig. 9b-Fig. 9h display layerwise distributions of *non-near-zero* eigenvalues at different checkpoints by showing the histograms of  $\log_{10} \lambda_i$ . The top row indicates Layer 1 while the bottom one represents Layer 12. In these distributions, we annotate the majority, i.e., the shortest interval that covers at least 70% (approximately one sigma) of eigenvalues, with red vertical lines. We compute the width of majority and un-log it, illustrating ratio within which the majority varies in Fig. 9i and Fig. 9j.

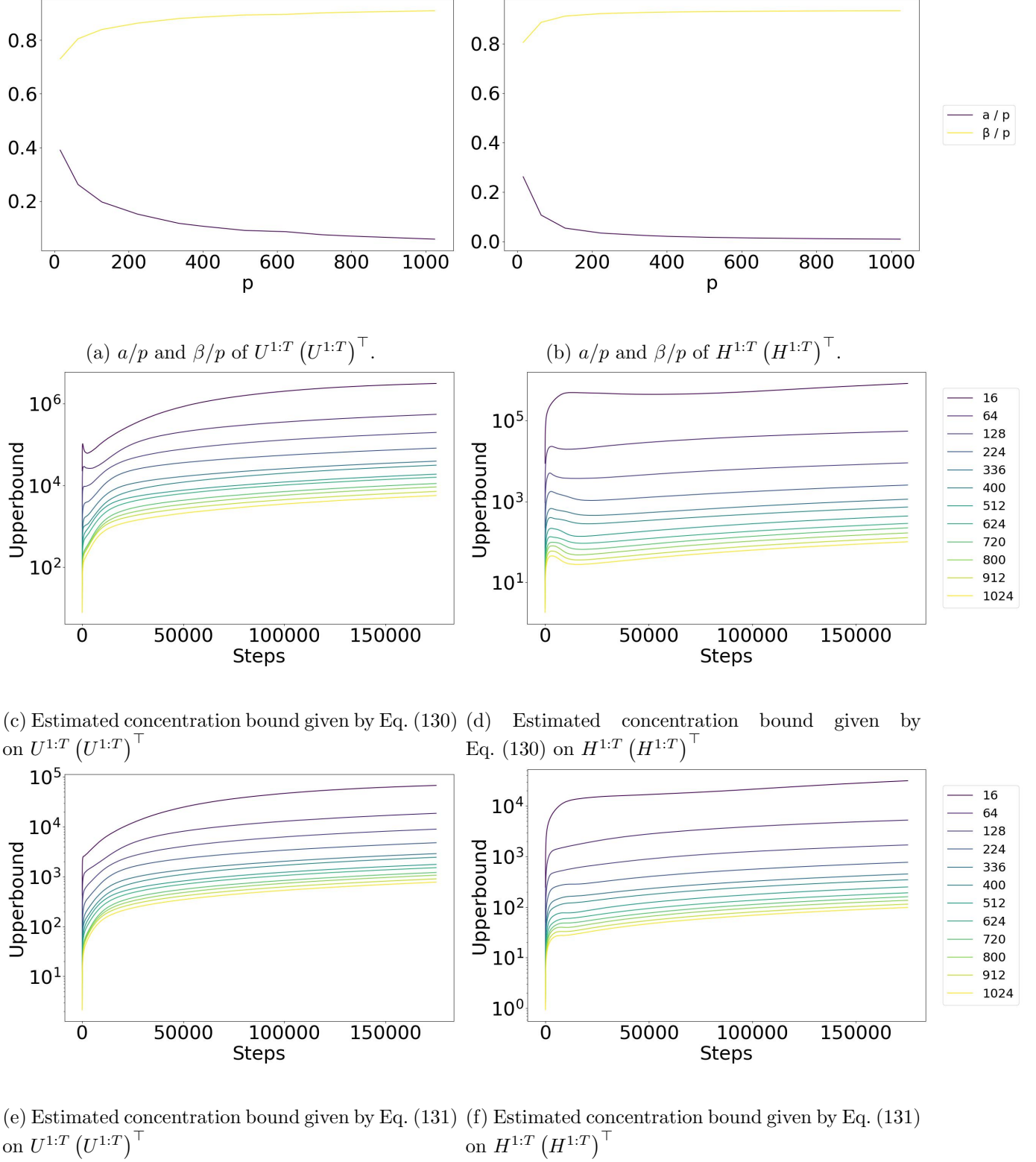


Figure 10: When weight decay is 0.0, values of  $a/p, \beta/p$  required by Theorem 6 and concentration bounds of tiny pure MLPs with different choice of hidden dimension on MNIST.  $a/p$  and  $\beta/p$  do not change much during training so for each hidden dimension, values of  $a/p$  and  $\beta/p$  are averaged across steps to ease presentation. Layers are also averaged for the same reason.

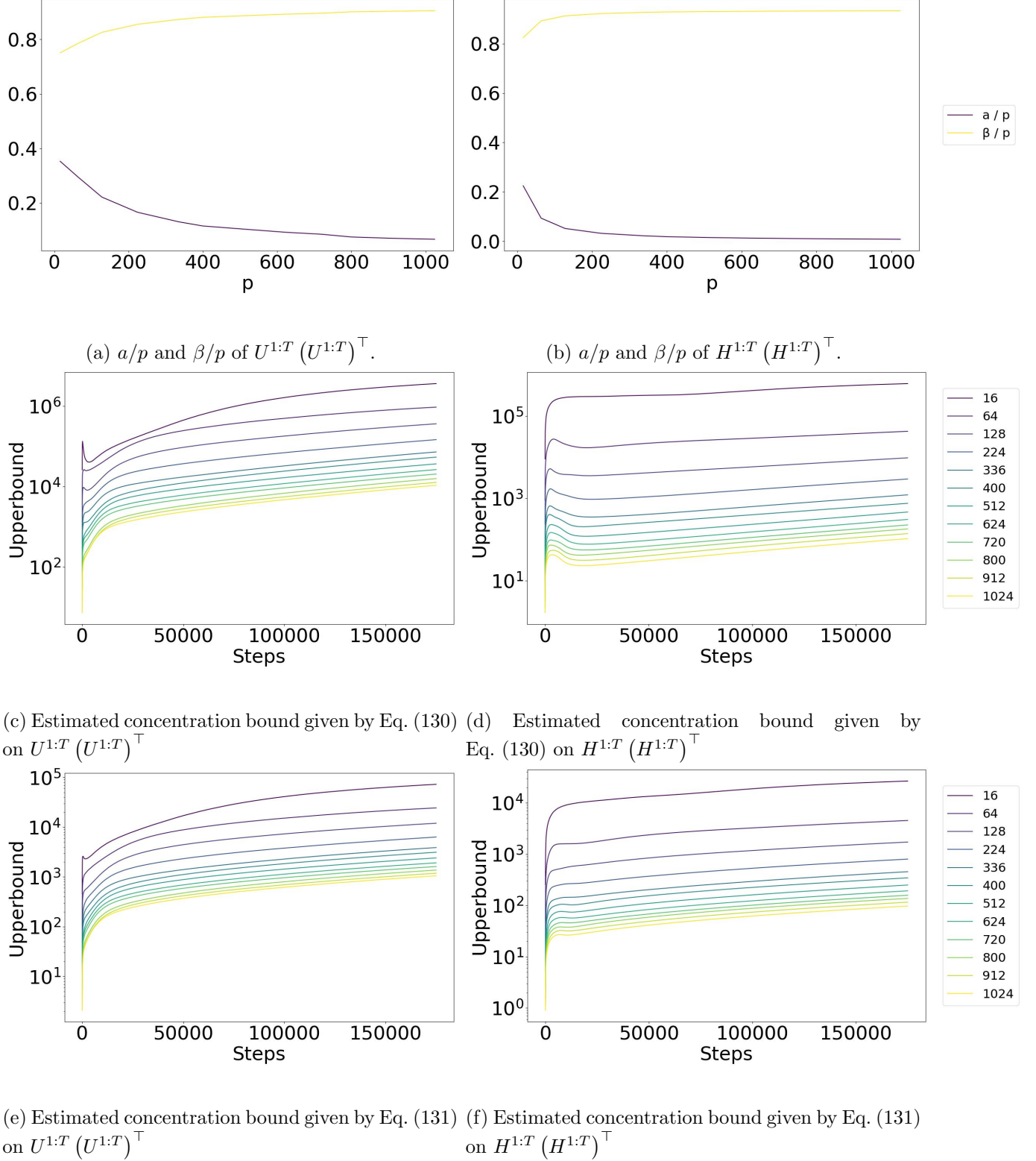


Figure 11: When weight decay is 0.01, values of  $a/p, \beta/p$  required by Theorem 6 and concentration bounds of tiny pure MLPs with different choice of hidden dimension on MNIST.  $a/p$  and  $\beta/p$  do not change much during training so for each hidden dimension, values of  $a/p$  and  $\beta/p$  are averaged across steps to ease presentation. Layers are also averaged for the same reason.

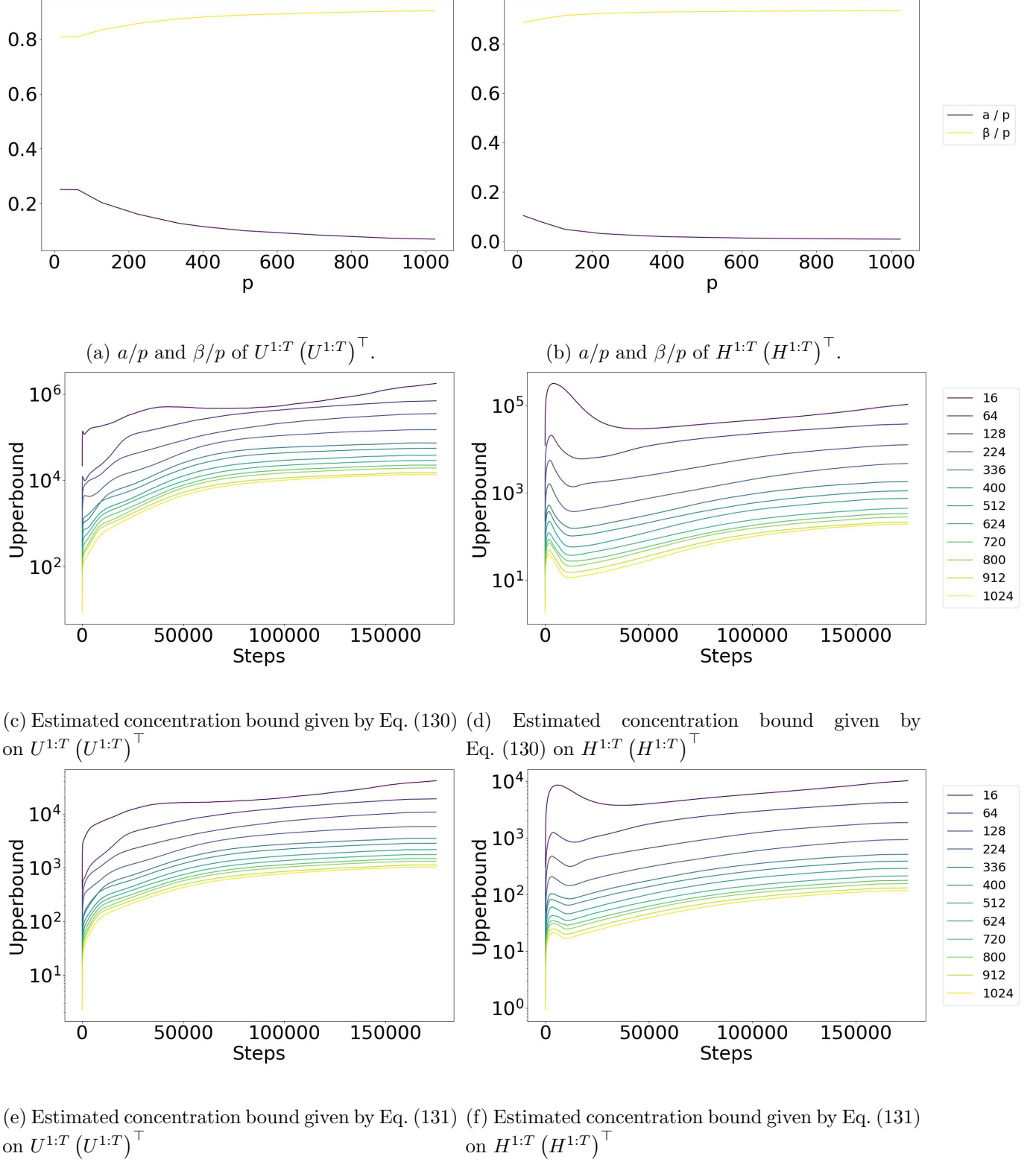
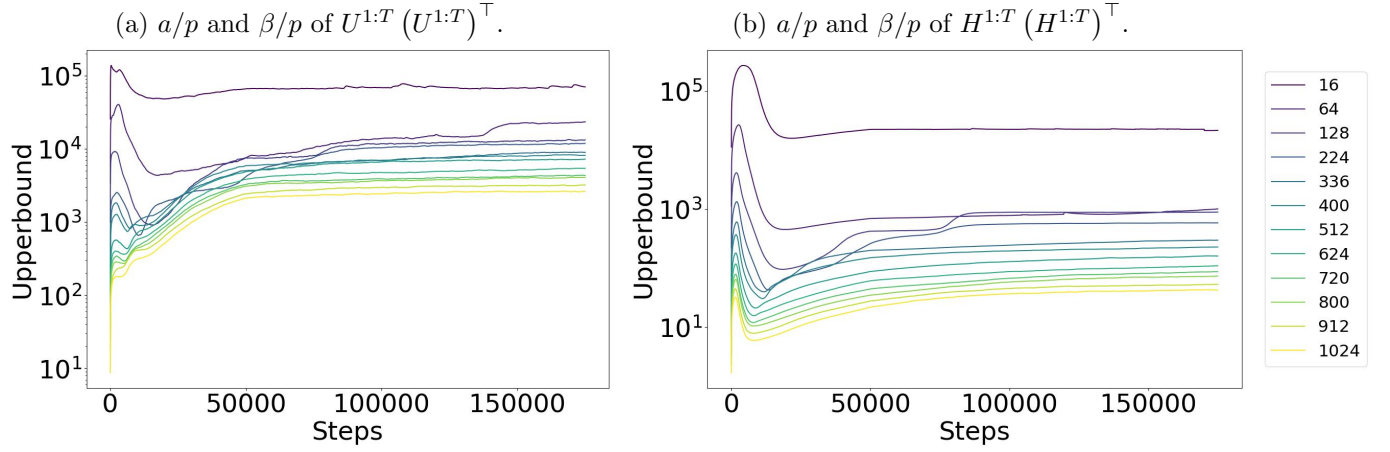
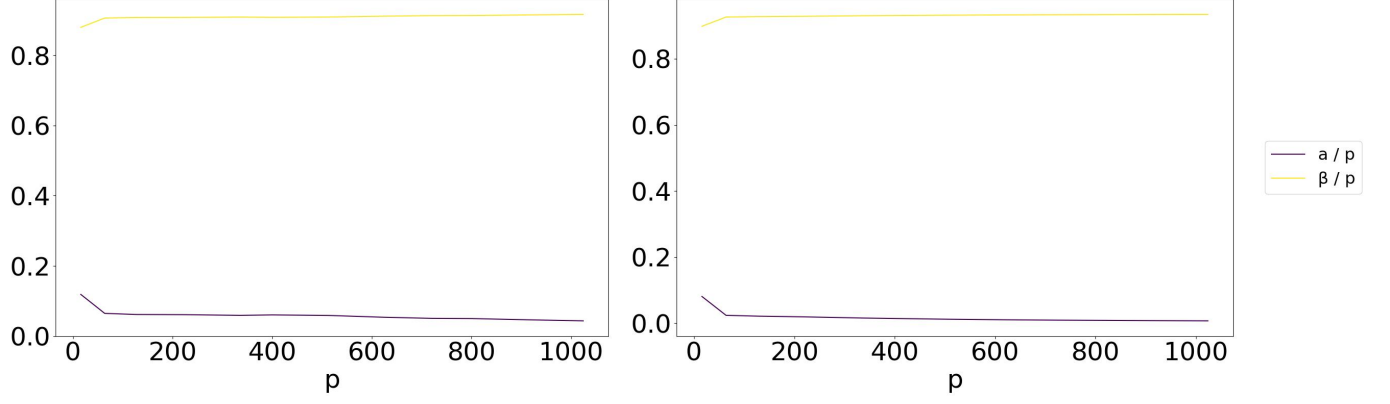
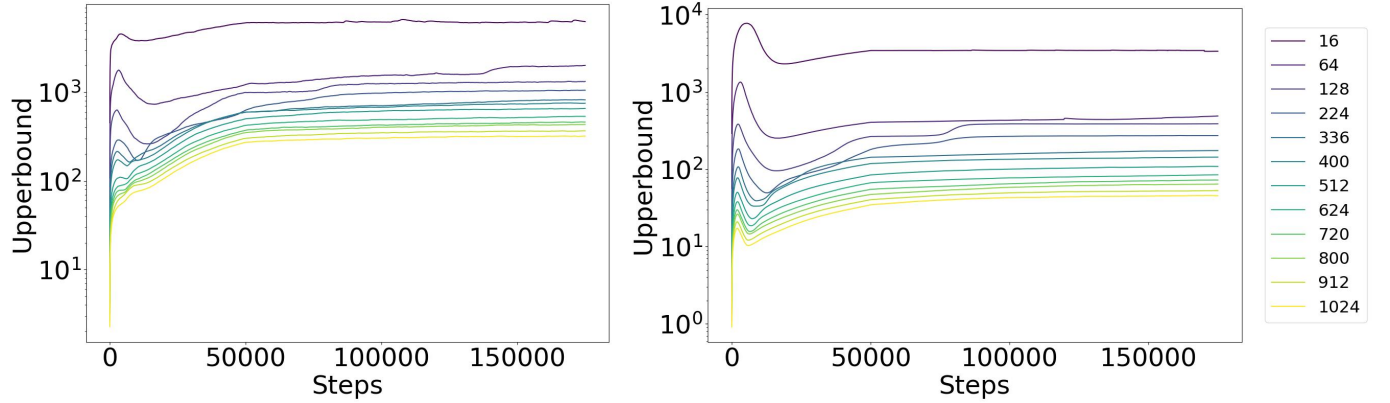


Figure 12: When weight decay is 0.1, values of  $a/p, \beta/p$  required by Theorem 6 and concentration bounds of tiny pure MLPs with different choice of hidden dimension on MNIST.  $a/p$  and  $\beta/p$  do not change much during training so for each hidden dimension, values of  $a/p$  and  $\beta/p$  are averaged across steps to ease presentation. Layers are also averaged for the same reason.





(c) Estimated concentration bound given by Eq. (130) on  $U^{1:T} (U^{1:T})^\top$  (d) Estimated concentration bound given by Eq. (130) on  $H^{1:T} (H^{1:T})^\top$



(e) Estimated concentration bound given by Eq. (131) on  $U^{1:T} (U^{1:T})^\top$  (f) Estimated concentration bound given by Eq. (131) on  $H^{1:T} (H^{1:T})^\top$

Figure 13: When weight decay is 0.3, values of  $a/p, \beta/p$  required by Theorem 6 and concentration bounds of tiny pure MLPs with different choice of hidden dimension on MNIST.  $a/p$  and  $\beta/p$  do not change much during training so for each hidden dimension, values of  $a/p$  and  $\beta/p$  are averaged across steps to ease presentation. Layers are also averaged for the same reason.

them,  $a/p$  significantly drops as  $p$  increases while  $\beta/p$  increases but never exceeds 1. Since in bounds Eq. (130) and Eq. (131),  $\beta/p$  is only found within the square root, the increase of  $\beta/p$  has relatively small effects on the bounds. As a result, in subfigures (c)-(f), the estimated bounds decrease as hidden dimension increases under all experimented weight decay intensities. Among the two bounds, it is theoretically and empirically observed that Eq. (131) based on real parts is more desirable.

As discussed in Section 4.6, weight decay effectively limits  $T$  and stops bounds' divergence. From Fig. 10 to Fig. 13 we can see that as weight decay intensifies, the bounds computed by effective windows size drop significantly, especially in Fig. 13 where  $w = 0.3$ . Weight decay not only upperbounds  $\frac{1}{c}$ , which happens at approximately 50,000 steps in Fig. 13, but also decreases  $a/p$ . Note this is not trivial because  $\text{tr}(aS^p)$  is scaling invariant. How weight decay causes this drop is worth investigation in future works. When training ViTs, weight decay is usually as large as 0.1 or 0.3 [37], [40], so Fig. 12 and Fig. 13 suit the practices best, where both  $U^{1:T} (U^{1:T})^\top$  and  $H^{1:T} (H^{1:T})^\top$  have relatively low spectral ratio bounds smaller than 400 or 100 when hidden dimension is relatively large, which is a low value even though there are hundreds of dimensions.

## 8 Conclusion

In this work, we explain the activation sparsity observed in [1] with gradient sparsity and effective gradient sparsity, which emerges from flatness and implicit adversarial robustness. Proofs are done for pure MLPs and other architectures including Transformers, under hypothetical massively perturbed training. To argue the effectiveness of zeroth biases, we analyze the phenomenon of spectral concentration in weight matrices using random matrix theory. We propose two sparsity oriented architectural plug-and-play modifications and one radical modification. Experiments for verification, where our theory predicts well, are conducted to rule out potential zeroth-order explanations. We test our modification on CIFAR-10 and ImageNet-1k to demonstrate its practical effectiveness. Finetuning for sparsity demonstrates a cheaper way toward better sparsity. Assumptions made during analyses are empirically validated.

Having demonstrated how sparsity emerges from noises and the robustness against them, we wildly conjecture that a similar explanation applies to sparsity, and thus energy efficiency, in human brains and cognition, which face enormous environmental and sensory noises everyday and exhibit great robustness against them. Our work also demonstrates that some architectural designs may greatly ease theoretical analysis in deep neural networks, and more theoretically oriented architectures can be proposed in the future. We introduce random matrix theory as a powerful tool in analyzing training dynamics, hoping for its broader application in machine learning community.

Several experiments, including finetuning for sparsity with better learning rate scheduling, training from scratch on ImageNet1-k with numerical stability controls, NLP tasks with similarly modified T5-Base on C4 dataset, experiments on ViT-Base-Wide and T5-Base-Wide, are still being prepared and running. Although theoretically ensured, the effectiveness of MagicSynapse in Appendix G is still under empirical examination. They are coming, probably, soon in later versions.



## References

- [1] Z. Li, C. You, S. Bhojanapalli, *et al.*, “The lazy neuron phenomenon: On emergence of activation sparsity in transformers,” presented at the The Eleventh International Conference on Learning Representations, Sep. 29, 2022. [Online]. Available: <https://openreview.net/forum?id=TJ2nxcYCK-> (visited on 08/17/2023).
- [2] D. Dai, L. Dong, Y. Hao, Z. Sui, B. Chang, and F. Wei, “Knowledge neurons in pretrained transformers,” in *Proceedings of the 60th Annual Meeting of the Association for Computational Linguistics (Volume 1: Long Papers)*, Dublin, Ireland: Association for Computational Linguistics, 2022, pp. 8493–8502. DOI: 10.18653/v1/2022.acl-long.581. [Online]. Available: <https://aclanthology.org/2022.acl-long.581> (visited on 03/24/2023).
- [3] M. Geva, R. Schuster, J. Berant, and O. Levy, “Transformer feed-forward layers are key-value memories,” in *Proceedings of the 2021 Conference on Empirical Methods in Natural Language Processing*, Online and Punta Cana, Dominican Republic: Association for Computational Linguistics, 2021, pp. 5484–5495. DOI: 10.18653/v1/2021.emnlp-main.446. [Online]. Available: <https://aclanthology.org/2021.emnlp-main.446> (visited on 08/17/2023).
- [4] M. Andriushchenko, D. Bahri, H. Mobahi, and N. Flammarion, *Sharpness-aware minimization leads to low-rank features*, May 25, 2023. arXiv: 2305.16292[cs]. [Online]. Available: <http://arxiv.org/abs/2305.16292> (visited on 06/02/2023).
- [5] M. Andriushchenko, A. V. Varre, L. Pillaud-Vivien, and N. Flammarion, “SGD with large step sizes learns sparse features,” in *Proceedings of the 40th International Conference on Machine Learning*, ISSN: 2640-3498, PMLR, Jul. 3, 2023, pp. 903–925. [Online]. Available: <https://proceedings.mlr.press/v202/andriushchenko23b.html> (visited on 07/23/2023).
- [6] T. Bricken, R. Schaeffer, B. Olshausen, and G. Kreiman, “Emergence of sparse representations from noise,” presented at the International Conference on Machine Learning, PMLR, Jun. 15, 2023. [Online]. Available: <https://openreview.net/forum?id=cxYaBAXVKg> (visited on 07/23/2023).
- [7] W. Merrill, V. Ramanujan, Y. Goldberg, R. Schwartz, and N. A. Smith, “Effects of parameter norm growth during transformer training: Inductive bias from gradient descent,” in *Proceedings of the 2021 Conference on Empirical Methods in Natural Language Processing*, Online and Punta Cana, Dominican Republic: Association for Computational Linguistics, Nov. 2021, pp. 1766–1781. DOI: 10.18653/v1/2021.emnlp-main.133. [Online]. Available: <https://aclanthology.org/2021.emnlp-main.133> (visited on 08/17/2023).
- [8] J. Puigcerver, R. Jenatton, C. Riquelme, P. Awasthi, and S. Bhojanapalli, “On the adversarial robustness of mixture of experts,” in *Advances in Neural Information Processing Systems*, S. Koyejo, S. Mohamed, A. Agarwal, D. Belgrave, K. Cho, and A. Oh, Eds., vol. 35, Curran Associates, Inc., 2022, pp. 9660–9671. [Online]. Available: [https://proceedings.neurips.cc/paper\\_files/paper/2022/file/3effb91593c4fb42b1da1528328eff49-Paper-Conference.pdf](https://proceedings.neurips.cc/paper_files/paper/2022/file/3effb91593c4fb42b1da1528328eff49-Paper-Conference.pdf).
- [9] Q. Ren, J. Gao, W. Shen, and Q. Zhang, *Where we have arrived in proving the emergence of sparse symbolic concepts in AI models*, May 3, 2023. DOI: 10.48550/arXiv.2305.01939. arXiv: 2305.01939[cs]. [Online]. Available: <http://arxiv.org/abs/2305.01939> (visited on 07/08/2023).

- [10] D. So, W. Mañke, H. Liu, Z. Dai, N. Shazeer, and Q. V. Le, “Searching for efficient transformers for language modeling,” in *Advances in Neural Information Processing Systems*, vol. 34, Curran Associates, Inc., 2021, pp. 6010–6022. [Online]. Available: [https://proceedings.neurips.cc/paper\\_files/paper/2021/hash/2f3c6a4cd8af177f6456e7e51a916ff3-Abstract.html](https://proceedings.neurips.cc/paper_files/paper/2021/hash/2f3c6a4cd8af177f6456e7e51a916ff3-Abstract.html) (visited on 08/17/2023).
- [11] S. Liu and Z. Wang, *Ten lessons we have learned in the new "sparseland": A short handbook for sparse neural network researchers*, Jun. 24, 2023. DOI: 10.48550/arXiv.2302.02596. arXiv: 2302.02596[cs]. [Online]. Available: <http://arxiv.org/abs/2302.02596> (visited on 07/03/2023).
- [12] F. Chen, D. Kunin, A. Yamamura, and S. Ganguli, *Stochastic collapse: How gradient noise attracts SGD dynamics towards simpler subnetworks*, Jun. 7, 2023. DOI: 10.48550/arXiv.2306.04251. arXiv: 2306.04251[cs,stat]. [Online]. Available: <http://arxiv.org/abs/2306.04251> (visited on 07/11/2023).
- [13] G. M. Correia, V. Niculae, and A. F. T. Martins, “Adaptively sparse transformers,” in *Proceedings of the 2019 Conference on Empirical Methods in Natural Language Processing and the 9th International Joint Conference on Natural Language Processing (EMNLP-IJCNLP)*, Hong Kong, China: Association for Computational Linguistics, Nov. 2019, pp. 2174–2184. DOI: 10.18653/v1/D19-1223. [Online]. Available: <https://aclanthology.org/D19-1223> (visited on 08/17/2023).
- [14] K. Lin, L. Li, C.-C. Lin, *et al.*, “SwinBERT: End-to-end transformers with sparse attention for video captioning,” presented at the Proceedings of the IEEE/CVF Conference on Computer Vision and Pattern Recognition, 2022, pp. 17949–17958. [Online]. Available: [https://openaccess.thecvf.com/content/CVPR2022/html/Lin\\_SwinBERT\\_End-to-End\\_Transformers\\_With\\_Sparse\\_Attention\\_for\\_Video\\_Captioning\\_CVPR\\_2022\\_paper.html](https://openaccess.thecvf.com/content/CVPR2022/html/Lin_SwinBERT_End-to-End_Transformers_With_Sparse_Attention_for_Video_Captioning_CVPR_2022_paper.html) (visited on 08/09/2023).
- [15] S. Liu, J. Ye, S. Ren, and X. Wang, “DynaST: Dynamic sparse transformer for exemplar-guided image generation,” in *Computer Vision – ECCV 2022*, S. Avidan, G. Brostow, M. Cissé, G. M. Farinella, and T. Hassner, Eds., ser. Lecture Notes in Computer Science, Cham: Springer Nature Switzerland, 2022, pp. 72–90, ISBN: 978-3-031-19787-1. DOI: 10.1007/978-3-031-19787-1\_5.
- [16] C. Riquelme, J. Puigcerver, B. Mustafa, *et al.*, “Scaling vision with sparse mixture of experts,” in *Advances in Neural Information Processing Systems*, vol. 34, Curran Associates, Inc., 2021, pp. 8583–8595. [Online]. Available: <https://proceedings.neurips.cc/paper/2021/hash/48237d9f2dea8c74c2a72126cf63d933-Abstract.html> (visited on 08/17/2023).
- [17] W. Fedus, B. Zoph, and N. Shazeer, “Switch transformers: Scaling to trillion parameter models with simple and efficient sparsity,” *The Journal of Machine Learning Research*, vol. 23, no. 1, pp. 5232–5270, 2022.
- [18] B. Li, Y. Shen, J. Yang, *et al.*, “Sparse mixture-of-experts are domain generalizable learners,” presented at the The Eleventh International Conference on Learning Representations, Sep. 29, 2022. [Online]. Available: <https://openreview.net/forum?id=RecZ9nB9Q4> (visited on 08/17/2023).

- [19] N. S. Keskar, D. Mudigere, J. Nocedal, M. Smelyanskiy, and P. T. P. Tang, *On large-batch training for deep learning: Generalization gap and sharp minima*, Feb. 9, 2017. DOI: 10.48550/arXiv.1609.04836. arXiv: 1609.04836[cs,math]. [Online]. Available: <http://arxiv.org/abs/1609.04836> (visited on 08/09/2023).
- [20] P. Zhou, J. Feng, C. Ma, C. Xiong, S. C. H. Hoi, and W. E, “Towards theoretically understanding why sgd generalizes better than adam in deep learning,” in *Advances in Neural Information Processing Systems*, vol. 33, Curran Associates, Inc., 2020, pp. 21 285–21 296. [Online]. Available: <https://proceedings.neurips.cc/paper/2020/hash/f3f27a324736617f20abfb2ffd806f6d-Abstract.html> (visited on 08/17/2023).
- [21] U. Simsekli, L. Sagun, and M. Gurbuzbalaban, “A tail-index analysis of stochastic gradient noise in deep neural networks,” in *Proceedings of the 36th International Conference on Machine Learning*, ISSN: 2640-3498, PMLR, May 24, 2019, pp. 5827–5837. [Online]. Available: <https://proceedings.mlr.press/v97/simsekli19a.html> (visited on 08/17/2023).
- [22] P. Chaudhari and S. Soatto, “Stochastic gradient descent performs variational inference, converges to limit cycles for deep networks,” in *2018 Information Theory and Applications Workshop (ITA)*, Feb. 2018, pp. 1–10. DOI: 10.1109/ITA.2018.8503224.
- [23] A. Achille, G. Paolini, and S. Soatto, *Where is the information in a deep neural network?* Jun. 21, 2020. arXiv: 1905.12213[cs,math,stat]. [Online]. Available: <http://arxiv.org/abs/1905.12213> (visited on 03/24/2023).
- [24] A. Achille and S. Soatto, *Emergence of invariance and disentanglement in deep representations*, Jun. 28, 2018. arXiv: 1706.01350[cs,stat]. [Online]. Available: <http://arxiv.org/abs/1706.01350> (visited on 03/24/2023).
- [25] V. A. Marčenko and L. A. Pastur, “DISTRIBUTION OF EIGENVALUES FOR SOME SETS OF RANDOM MATRICES,” *Mathematics of the USSR-Sbornik*, vol. 1, no. 4, pp. 457–483, Apr. 30, 1967, ISSN: 0025-5734. DOI: 10.1070/SM1967v001n04ABEH001994. [Online]. Available: <https://iopscience.iop.org/article/10.1070/SM1967v001n04ABEH001994> (visited on 08/24/2023).
- [26] F. Götze and A. Tikhomirov, “Rate of convergence in probability to the marchenko-pastur law,” *Bernoulli*, vol. 10, no. 3, pp. 503–548, Jun. 2004, Publisher: Bernoulli Society for Mathematical Statistics and Probability, ISSN: 1350-7265. DOI: 10.3150/bj/1089206408. [Online]. Available: <https://projecteuclid.org/journals/bernoulli/volume-10/issue-3/Rate-of-convergence-in-probability-to-the-Marchenko-Pastur-law/10.3150/bj/1089206408.full> (visited on 08/13/2023).
- [27] D. Stutz, M. Hein, and B. Schiele, “Relating adversarially robust generalization to flat minima,” presented at the Proceedings of the IEEE/CVF International Conference on Computer Vision, 2021, pp. 7807–7817. [Online]. Available: [https://openaccess.thecvf.com/content/ICCV2021/html/Stutz\\_Relating\\_Adversarially\\_Robust\\_Generalization\\_to\\_Flat\\_Minima\\_ICCV\\_2021\\_paper.html](https://openaccess.thecvf.com/content/ICCV2021/html/Stutz_Relating_Adversarially_Robust_Generalization_to_Flat_Minima_ICCV_2021_paper.html) (visited on 08/17/2023).
- [28] G. Zhang, C. Wang, B. Xu, and R. Grosse, “Three mechanisms of weight decay regularization,” presented at the International Conference on Learning Representations, Sep. 27, 2018. [Online]. Available: <https://openreview.net/forum?id=B1lz-3Rct7> (visited on 08/17/2023).

- [29] J. Bryson, R. Vershynin, and H. Zhao, *Marchenko-pastur law with relaxed independence conditions*, Feb. 2, 2021. DOI: 10.48550/arXiv.1912.12724. arXiv: 1912.12724[math]. [Online]. Available: <http://arxiv.org/abs/1912.12724> (visited on 08/14/2023).
- [30] P. Yaskov, “A short proof of the marchenko–pastur theorem,” *Comptes Rendus Mathematique*, vol. 354, no. 3, pp. 319–322, Mar. 1, 2016, ISSN: 1631-073X. DOI: 10.1016/j.crma.2015.12.008. [Online]. Available: <https://www.sciencedirect.com/science/article/pii/S1631073X15003362> (visited on 08/22/2023).
- [31] F. Gotze and A. Tikhomirov, “Limit theorems for spectra of positive random matrices under dependence,” *Journal of Mathematical Sciences*, vol. 133, no. 3, pp. 1257–1276, Mar. 2006, ISSN: 1072-3374, 1573-8795. DOI: 10.1007/s10958-006-0035-8. [Online]. Available: <http://link.springer.com/10.1007/s10958-006-0035-8> (visited on 08/22/2023).
- [32] J. Yao, “A note on a marčenko–pastur type theorem for time series,” *Statistics [?] Probability Letters*, vol. 82, pp. 22–28, Jan. 31, 2012. DOI: 10.1016/j.spl.2011.08.011.
- [33] H. Liu, A. Aue, and D. Paul, “On the mar\{c}enko-pastur law for linear time series,” *The Annals of Statistics*, vol. 43, no. 2, Apr. 1, 2015, ISSN: 0090-5364. DOI: 10.1214/14-AOS1294. arXiv: 1310.7270[math, stat]. [Online]. Available: <http://arxiv.org/abs/1310.7270> (visited on 08/22/2023).
- [34] J. Kaplan, S. McCandlish, T. Henighan, *et al.*, *Scaling laws for neural language models*, Jan. 22, 2020. arXiv: 2001.08361[cs, stat]. [Online]. Available: <http://arxiv.org/abs/2001.08361> (visited on 03/24/2023).
- [35] A. Krizhevsky, G. Hinton, *et al.*, “Learning multiple layers of features from tiny images,” 2009.
- [36] J. Deng, W. Dong, R. Socher, L.-J. Li, K. Li, and L. Fei-Fei, “Imagenet: A large-scale hierarchical image database,” in *2009 IEEE Conference on Computer Vision and Pattern Recognition*, 2009, pp. 248–255. DOI: 10.1109/CVPR.2009.5206848.
- [37] “Vision/references/classification at main · pytorch/vision,” GitHub. (), [Online]. Available: <https://github.com/pytorch/vision/tree/main/references/classification> (visited on 08/05/2023).
- [38] G. Stoica, D. Bolya, J. Bjorner, T. Hearn, and J. Hoffman, *ZipIt! merging models from different tasks without training*, May 4, 2023. DOI: 10.48550/arXiv.2305.03053. arXiv: 2305.03053[cs]. [Online]. Available: <http://arxiv.org/abs/2305.03053> (visited on 08/08/2023).
- [39] L. Deng, “The mnist database of handwritten digit images for machine learning research,” *IEEE Signal Processing Magazine*, vol. 29, no. 6, pp. 141–142, 2012.
- [40] A. Dosovitskiy, L. Beyer, A. Kolesnikov, *et al.*, “An image is worth 16x16 words: Transformers for image recognition at scale,” presented at the International Conference on Learning Representations, Oct. 2, 2020. [Online]. Available: [https://openreview.net/forum?id=YicbFdNTTy&utm\\_campaign=f86497ed3a-EMAIL\\_CAMPAIGN\\_2019\\_04\\_24\\_03\\_18\\_COPY\\_01&utm\\_medium=email&utm\\_source=Deep%20Learning%20Weekly&utm\\_term=0\\_384567b42d-f86497ed3a-72965345](https://openreview.net/forum?id=YicbFdNTTy&utm_campaign=f86497ed3a-EMAIL_CAMPAIGN_2019_04_24_03_18_COPY_01&utm_medium=email&utm_source=Deep%20Learning%20Weekly&utm_term=0_384567b42d-f86497ed3a-72965345) (visited on 08/17/2023).

- [41] 23rd (<https://math.stackexchange.com/users/46120/23rd>), *Sum of eigenvalues and singular values*, Mathematics Stack Exchange, URL:<https://math.stackexchange.com/q/386872> (version: 2013-05-09). eprint: <https://math.stackexchange.com/q/386872>. [Online]. Available: <https://math.stackexchange.com/q/386872>.
- [42] A. F. Murray and P. J. Edwards, "Enhanced mlp performance and fault tolerance resulting from synaptic weight noise during training," *IEEE Transactions on neural networks*, vol. 5, no. 5, pp. 792–802, 1994.
- [43] A. F. Murray and P. J. Edwards, "Synaptic weight noise during multilayer perceptron training: Fault tolerance and training improvements," *IEEE Transactions on Neural Networks*, vol. 4, no. 4, pp. 722–725, 1993.

# Appendices

## A Proof of Lemmas

*Proof of Lemma 3.* Expanding definitions and simple rearrangement give

$$H_\theta = \nabla_\theta^2 \mathbf{E}_{(X,Y) \sim \mathcal{D}} [\mathcal{L}_{\text{CE}}(f_\theta, (X, Y))] = -\mathbf{E}_{(X,Y) \sim \mathcal{D}} [\nabla_\theta^2 \log f(Y | \theta, X)]. \quad (133)$$

We first deal with the Hessian within the expectation, i.e., for any  $(y, x)$  there is

$$\nabla_\theta^2 \log f(y | \theta, x) = J_\theta \left( \frac{\nabla_\theta f(y | \theta, x)}{f(y | \theta, x)} \right) \quad (134)$$

$$= \frac{(\nabla_\theta^2 f(y | \theta, x)) f(y | \theta, x) - (\nabla_\theta f(y | \theta, x)) (\nabla_\theta f(y | \theta, x))^\top}{f(y | \theta, x) f(y | \theta, x)} \quad (135)$$

$$= \frac{\nabla_\theta^2 f(y | \theta, x)}{f(y | \theta, x)} - \left( \frac{\nabla_\theta f(y | \theta, x)}{f(y | \theta, x)} \right) \left( \frac{\nabla_\theta f(y | \theta, x)}{f(y | \theta, x)} \right)^\top \quad (136)$$

$$= \frac{\nabla_\theta^2 f(y | \theta, x)}{f(y | \theta, x)} - (\nabla_\theta \log f(y | \theta, x)) (\nabla_\theta \log f(y | \theta, x))^\top. \quad (137)$$

Plugging this equality back to Eq. (133) gives

$$H_\theta = -\mathbf{E}_{(X,Y) \sim \mathcal{D}} \left[ \frac{\nabla_\theta^2 f(Y | \theta, X)}{f(Y | \theta, X)} - (\nabla_\theta \log f(Y | \theta, X)) (\nabla_\theta \log f(Y | \theta, X))^\top \right] \quad (138)$$

$$= \mathbf{E}_{(X,Y) \sim \mathcal{D}} \left[ (\nabla_\theta \log f(Y | \theta, X)) (\nabla_\theta \log f(Y | \theta, X))^\top \right] - \mathbf{E}_{(X,Y) \sim \mathcal{D}} \left[ \frac{\nabla_\theta^2 f(Y | \theta, X)}{f(Y | \theta, X)} \right], \quad (139)$$

the trace of which is

$$\text{tr}(H_\theta) = \mathbf{E}_{(X,Y) \sim \mathcal{D}} \left[ \text{tr} \left( (\nabla_\theta \log f(Y | \theta, X)) (\nabla_\theta \log f(Y | \theta, X))^\top \right) \right] \quad (140)$$

$$- \mathbf{E}_{\mathcal{D}(X)} \left[ \text{tr} \left( \mathbf{E}_{\mathcal{D}(Y|X)} \left[ \frac{\nabla_\theta^2 f(Y | \theta, X)}{f(Y | \theta, X)} \right] \right) \right] \quad (141)$$

$$= \mathbf{E}_{(X,Y) \sim \mathcal{D}} \left[ \text{tr} \left( (\nabla_\theta \log f(Y | \theta, X))^\top (\nabla_\theta \log f(Y | \theta, X)) \right) \right] \quad (142)$$

$$- \mathbf{E}_{\mathcal{D}(X)} \left[ \text{tr} \left( \mathbf{E}_{\mathcal{D}(Y|X)} \left[ \frac{\nabla_\theta^2 f(Y | \theta, X)}{f(Y | \theta, X)} \right] \right) \right] \quad (143)$$

$$= \mathbf{E}_{(X,Y) \sim \mathcal{D}} \left[ \|\nabla_\theta \log f(Y | \theta, X)\|_2^2 \right] \quad (144)$$

$$- \mathbf{E}_{\mathcal{D}(X)} \left[ \text{tr} \left( \mathbf{E}_{\mathcal{D}(Y|X)} \left[ \frac{\nabla_\theta^2 f(Y | \theta, X)}{f(Y | \theta, X)} \right] \right) \right]. \quad (145)$$

For well learned model, there is  $f(Y | \theta, X) \approx \mathcal{D}(Y | X)$ , so given the finiteness of label space there is

$$\mathbf{E}_{\mathcal{D}(Y|X)} \left[ \frac{\nabla_\theta^2 f(Y | \theta, X)}{f(Y | \theta, X)} \right] = \sum_y \mathcal{D}(y | X) \cdot \frac{\nabla_\theta^2 f(y | \theta, X)}{f(y | \theta, X)} \quad (146)$$

$$\approx \sum_y \nabla_\theta^2 f(y | \theta, X) = \nabla_\theta^2 \sum_y f(y | \theta, X) \quad (147)$$

$$= \nabla_\theta^2 1 = 0, \quad (148)$$

where Eq. (148) follows the assumption that  $f$  outputs a distribution over label space that sums to 1.  $\square$

## B More Preliminaries

In this section, we introduce more preliminary and notation used when proving Theorem 6.

Recall from Section 3 that  $\|\cdot\|_p$  for matrices is Schatten norms, or  $L_p$  norm conducted on singular values. Additionally, let  $\|\cdot\| := \|\cdot\|_\infty$  indicates the spectral norm, i.e.  $L_\infty$  norm or the maximum magnitude of singular values. One major difference with the main text is that complex matrices are involved (although most vectors are still real vectors). So conjugate transposition is substituted for transposition in trace's connection to  $L_2$  norm. More properties of trace are involved, for example, Lemma 8 is used to introduce Schatten 1-norm to bound approximation errors.

**Lemma 8** (Absolute Trace and Schatten 1-norm). *For real or complex  $n \times n$  matrix  $A \in \mathbb{C}^{n \times n}$ ,*

$$|\text{tr}(A)| \leq \sum_i |\lambda_i(A)| \leq \sum_i |\sigma_i(A)| =: \|A\|_1, \quad (149)$$

where  $\sigma_i(A)$  indicates singular values of  $A$  and equals to the absolute value of the  $i$ -th eigenvalue in normal matrices.

*Proof.* This proof is from [41]. By Schur decomposition, there exists unitary  $S$  and upper triangular matrix  $T$  such that  $A = STS^{-1}$ . Note that  $T$  shares the same eigenvalues, which are its diagonal entries, as  $A$ . There exists  $d_i$  such that  $\lambda_i(A) = |\lambda_i(A)|d_i$  and  $|d_i| = 1$ . Let  $D := \text{Diag}(\bar{d}_i)$  and note that  $D$  is unitary. As a result, there exist unitary matrices  $D^*S^*$  and  $S$  such that

$$\text{tr}(D^*S^*AS) = \sum_{i=1}^n |\lambda_i(A)|. \quad (150)$$

On the other hand, the sum of singular values is also

$$\sum_i \sigma_i(A) = \max_{X,Y \in U_n} |\text{tr}(XAY)|, \quad (151)$$

where  $U_n$  is the set of all unitary matrices in  $\mathbb{C}^{n \times n}$ . To see this, first notice that the singular value decomposition  $A = U\Sigma V^*$  naturally provides a pair of  $X, Y$  that achieve  $\sum_i \sigma_i(A)$ . For other unitary matrices,  $\text{tr}(XAY) = \text{tr}(V^*YXU\Sigma) = \sum_i (V^*YXU)_{i,i} \sigma_i$  and

$$|\text{tr}(XAY)| = \left| \sum_i (V^*YXU)_{i,i} \sigma_i \right| \leq \sum_i |(V^*YXU)_{i,i}| \sigma_i. \quad (152)$$

Note that  $V^*YXU$  is also unitary, whose entries' magnitudes are no greater than 1, which implies  $|\text{tr}(XAY)| \leq \sum_i \sigma_i$  and Eq. (151) is proved.

With  $D^*S^*$  and  $S$  also unitary, the lemma directly follows.  $\square$

Schatten 1-norms are usually not direct from assumptions and conditions, so we apply Hölder's inequality on Schatten norms to produce

$$\|XY\|_1 \leq \|X\|_1 \|Y\|_\infty, \quad (153)$$

where  $\frac{1}{p} + \frac{1}{q} = \frac{1}{1} + \frac{1}{\infty} = 1$ . If  $X$  is real symmetric positive semi-definite then  $\|X\|_1 = \sum_i |\lambda_i| = \sum_i \lambda_i = \text{tr}(X)$ . If  $X$  is further an outer product of real vectors, then  $\|X\|_1 = \text{tr}(X)$  can be bounded by upperbounds of vector norms. One can also prove

$$\|x\|_1 \leq \sqrt{\dim x} \|x\|_2 \quad (154)$$

to relate  $L_1$  and  $L_2$  norms, and thus Schatten 1-norms and 2-norms by seeing them as  $L_p$  norms conducted on singular values. The bound on  $\|Y\|_\infty = \|Y\|$  is often provided by Lemma 11 introduced later.

## C Proof of Theorem 6

More notations and preliminary information are used in the proof, which are listed in Appendix B.

To have a clear goal, we first point out how the ratio in Theorem 6 emerges. In random matrix theory (RMT), a powerful tool is Stieltjes transform when it comes to spectral distribution. Stieltjes transform of a distribution  $\mu$  is

$$s^\mu(z) := \int_{\mathbb{R}} \frac{1}{\lambda - z} \mu(d\lambda), \forall z \in \mathbb{C}^+, \quad (155)$$

where  $\mathbb{C}^+ := \{u + vi : u, v \in \mathbb{R}, v > 0\} \subset \mathbb{C}$ . It can be seen as expected value of inverse. So if the Stieltjes transform of the spectral distribution' bound is computed and multiplied with the average eigenvalue that can be computed by trace as the sum of eigenvalues, then the expected fraction is bounded. Lemma 9 fulfills this intuition.

**Lemma 9** (Stieltjes transform and eigenvalue ratio). *For any density  $\mu$  over real numbers that is only supported on positive numbers, there is*

$$\text{Re}(s^\mu(vi)) = \int \frac{1}{\lambda + \frac{v^2}{\lambda}} \mu(d\lambda) = \mathbf{E} \left[ \frac{1}{\lambda + \frac{v^2}{\lambda}} \right], \quad (156)$$

$$\text{Im}(s^\mu(vi)) = \int \frac{1}{\left(\frac{\lambda}{\sqrt{v}}\right)^2 + v} \mu(d\lambda) = \mathbf{E} \left[ \frac{1}{\left(\frac{\lambda}{\sqrt{v}}\right)^2 + v} \right], \quad (157)$$

*As a result, if upperbound or mean of  $\lambda$  is obtained, one can estimate the averaged ratio between eigenvalues.*



*Proof.* By definition,

$$s^\mu(z) := \int \frac{1}{\lambda - z} \mu(d\lambda) \quad (158)$$

$$= \int \frac{\lambda - \bar{z}}{(\lambda - z)(\lambda - \bar{z})} \mu(d\lambda) \quad (159)$$

$$= \int \frac{\lambda - u + vi}{\lambda^2 - 2u\lambda + u^2 + v^2} \mu(d\lambda), \quad (160)$$

$$\operatorname{Re}(s^\mu(z)) = \int \frac{\lambda - u}{\lambda^2 - 2u\lambda + u^2 + v^2} \mu(d\lambda) \quad (161)$$

$$= \int \frac{1}{\lambda - u + \frac{v^2}{\lambda - u}} \mu(d\lambda), \quad (162)$$

$$\operatorname{Im}(s^\mu(z)) = \int \frac{v}{(\lambda - u)^2 + v^2} \mu(d\lambda). \quad (163)$$

By setting  $z = 0 + vi$ , there is

$$\operatorname{Re}(s^\mu(z)) = \int \frac{1}{\lambda + \frac{v^2}{\lambda}} \mu(d\lambda), \quad (164)$$

$$\operatorname{Im}(s^\mu(z)) = \int \frac{1}{\left(\frac{\lambda}{\sqrt{v}}\right)^2 + v} \mu(d\lambda). \quad (165)$$

□

We adapt the proof of Theorem 2.1 in [30], where a quadratic equation  $\frac{\mathbf{E}[S_p]}{1 + \mathbf{E}[S_p]} - z\mathbf{E}[S_p] = c + o(1) = \frac{p}{bT} + o(1)$  bridges the Stieltjes transform of the spectral distribution and value  $c$ . We follow a similar path, but in a non-asymptotic and dependent scenario where it is hard to obtain an  $o(1)$  residual. So we turn to a generalized form where the residual term is bounded. Lemma 10 explores how we can bound  $\mathbf{E}[S_p]$ , which is scaled Stieltjes transform of the empirical spectral distribution, by  $c$  and the magnitude of the residual term.

**Lemma 10** (Bounds of on Stieltjes transform). *Suppose  $S$  is a function of  $z, p, b, T$  such that*

$$\frac{S}{1 + S} - zS = c + t, \quad (166)$$

where  $z = 0 + vi \in \mathbb{C}^+(v \in \mathbb{R}^+)$ ,  $c = p/bT \in \mathbb{R}^+$ , and  $t \in \mathbb{C}$  is also a function of  $z, p, b, T$ . Assume  $S$  is continuous w.r.t.  $z$  and further assume  $S$  always has non-negative real part. Assume  $|t|$  is upperbounded by function  $h(z, p, b, T)$  which monotonically decreases w.r.t.  $v$  when  $p, b, T$  is fixed and  $v$  increases. Then, there is

$$|\operatorname{Im}(S)|, |\operatorname{Re}(S)| \leq |S| \leq 2\sqrt{2}\sqrt{c + |t|}. \quad (167)$$

*Proof.* Assume  $p, b, T$  is fixed.

First of all, since  $t = \frac{S}{1+S} - zS - c$ , where  $S$  is continuous w.r.t.  $z$ , so  $t$  is also continuous w.r.t.  $z$ .

$\frac{S}{1+S} - zS = c + t$  implies

$$S^2 + \frac{z-1+c+t}{z}S + \frac{c+t}{z} = (S-b)^2 - b^2 + \frac{c+t}{z} = 0, \quad (168)$$

where  $b = \frac{z-1+c+t}{2z}$ . Consider a modified version of this quadratic equation by altering the zeroth order term

$$(R+b)^2 - b^2 + \frac{c+t}{z}u = 0. \quad (169)$$

where  $R = R(z, p, T, u)$  is the solution of the modified equation arranged so that  $R$  is continuous (it is possible because  $b, b^2$  and  $\frac{c+t}{z}u$  rely on  $z, u$  in a continuous way via  $b$  and  $t$ ). There are at most two solution at the same time, so let  $R_1$  and  $R_2$  be two solutions continuous w.r.t.  $z, u$ . Then  $S = R_1(u=1)$  or  $S = R_2(u=1)$ .

Consider  $R$ 's behaviour when  $u = 0$ .  $R$  is either 0 or  $-2b$ . By their continuity,  $R_1$  and  $R_2$  can only be universally one of them otherwise there would be discontinuity. Without loss of generality, let

$$R_1(z, p, T, 0) = 0, \quad (170)$$

$$R_2(z, p, T, 0) = -2b = \frac{1-z-c-t}{z} = \frac{-i-v+ci+ti}{v}. \quad (171)$$

Assume  $S = R_2(u=1)$  for contradiction. If so,  $\lim_{v \rightarrow \infty} \text{Re}(R_2(u=1)) \geq 0$ . Consider the following trajectory of  $(z, u)$  to conclude that  $\lim_{v \rightarrow \infty} \text{Re}(R_2(u=1)) \leq -0.5$ :

1. Start from  $z = i, u = 0$ , where  $R_2 = -\frac{i}{v} - 1 + \frac{c+t}{v}i$ .
2. Increase  $v$  alone until  $v \geq 100(c + h(z, b, p, T))$ . After this step, term  $\frac{c+t}{v}i$  will not flip the sign of  $-1$  given that  $|\frac{c+t}{v}i| \leq \frac{c+b}{v} \leq \frac{1}{100}$ . Therefore, after this step  $\text{Re}(R_2) \leq -0.99$ .
3. Increase  $u$  alone to 1. During this step, the term  $\frac{c+t}{z}u$  in Eq. (169), which appears under squared root in  $R_2$ , changes  $R_2$  at most by  $\sqrt{|\frac{c+t}{z}|} \leq \sqrt{\frac{c+h}{v}} \leq \frac{1}{10}$ . Therefore, it will not flip the sign and  $\text{Re}(R_2) \leq -0.89$ .
4. Increase  $v$  to infinity. The influences of  $\frac{c+t}{v}$  and  $\frac{c+t}{v}u$  will further drop to ignorable. So  $R_2 \leq -0.5$  in later parts of the trajectory.

Note since  $h$  monotonically decreases as  $v$  increases, step (3) will happen when  $v < \infty$  and the limit following this trajectory equals to  $\lim_{v \rightarrow \infty} R_2(z)$ . Therefore,  $\lim_{v \rightarrow \infty} R_2(z) \leq -0.5$ ,  $S \neq R_2$  and  $S = R = R_1(u=1)$ . As a result,  $S$  can be approximated by  $R_1 = 0$  from  $u = 0$ .

To this end, taking differentiation gives

$$2(R(u) + b)dR + \frac{c+t}{z}du = 0. \quad (172)$$

or

$$\left| \frac{dR}{du} \right| = \left| -\frac{c+t}{2z(R(u)+b)} \right| = \frac{|c+t|}{2v\sqrt{|b^2 - \frac{c+t}{z}u|}} \leq \frac{|c+t|}{2\sqrt{|v^2b^2 - v(c+t)u|}}. \quad (173)$$

Starting from  $R(u=0) = 0$ , there is

$$|S - R(u=0)| = \left| \int_0^1 \frac{dS}{du} du \right| \quad (174)$$

$$\leq \int_0^1 \frac{|c+t|}{2\sqrt{|v^2b^2 - v(c+t)u|}} du \leq \frac{1}{2v} \int_0^1 \frac{v|c+t|}{\sqrt{|v^2|b^2| - v|c+t|u|}} du \quad (175)$$

$$= \frac{1}{2v} \int_{v^2|b|^2 - v|c+t|}^{v^2|b|^2} \frac{1}{\sqrt{|w|}} dw \leq \frac{1}{2v} \int_{-v|c+t|/2}^{v|c+t|/2} \frac{1}{\sqrt{|w|}} dw = \sqrt{\frac{2}{v}} |c+t|, \quad (176)$$

where the second inequality follows the triangle inequality for subtracting edges. The third inequality is done by moving  $[v^2|b|^2 - v|c+t|, v^2|b|^2]$  toward zero until it is symmetric, during which the end with the largest absolute value is moved to the other end and its absolute value is decreased, enlarging the inverted square root.  $\square$

As a result, if the residual term is bounded, so are the Stieltjes transform and the expected fraction. In [30] this quadratic equation is extracted by convergence, which is hard in non-asymptotic analysis. We extract it with approximation, whose error is bounded by vector norm bound  $\alpha/p$ , anisotropy bound  $\beta/p$ .

Some matrices are also involved in the approximation, where a technical lemma in [30] is very useful. Lemma 11 states that a special matrix, which we will encounter many times in the following proof, has bounded spectral norm. Combined with Hölder's inequality, bounds on matrices' spectral norms and vector norms ( $\alpha/p$ ) will suppress the approximation error.

**Lemma 11** (Lemma 3.1 in [30]). *Let  $C \in \mathbb{R}^{p \times p}$  be a real symmetric positive semi-definite matrix and  $x \in \mathbb{R}^p$ . If  $z \in \mathbb{C}$  is such that  $v = \text{Im}(z) > 0$ , then*

1.  $\|(C - zI)^{-1}\| \leq 1/v$  ;
2.  $|\text{tr}(C + xx^\top - zI)^{-1} - \text{tr}(C - zI)^{-1}| \leq 1/v$ ;
3.  $|x^\top (C + xx^\top - zI)^{-1} x| \leq 1 + |z|/v$ ;
4.  $\text{Im}(z + z \text{tr}(C - zI)^{-1}) \geq v$  and  $\text{Im}(\text{tr}(C - zI)^{-1}) > 0$ ;
5.  $\text{Im}(z + zx^\top (C - zI)^{-1} x) \geq v$ .

With these three lemmas, we can begin the proof of Theorem 6. Following [30], we relate Stieltjes transform of the spectral distribution with the quadratic equation. The quadratic equation is formed by approximation, whose error becomes  $t$  in Lemma 10. After concluding bounds of the Stieltjes transform, applying Lemma 9 gives the final conclusion.

**Theorem 6** (Spectral property of accumulated steps). *Let  $X^{p,b} \in \mathbb{R}^{p \times b}$  be a random matrix whose columns are  $X_{:,j}^{p,b} \in \mathbb{R}^p$ . Assume columns in  $X^{p,bT} \in \mathbb{R}^{p \times bT} = X^p$  are not necessarily independent but forms a batch dependence model as in Definition 4 with step count  $T$  and batch size  $b$ .*

*Let  $x_k^p := X_{:,k}^{p,b}$  be the  $k$ -th column of  $X^p$  and  $x_{t,l}^p := X_{:,l}^{p,b}$  be the  $l$ -th column of batch  $t$  or equivalently the  $k = ((t-1)*b + l)$ -th column  $x_k$  in  $X^{p,b}$ . Superscription  $p$  maybe dropped for convenience.*

Let  $S^p := \frac{1}{bT} \sum_{k=1}^{bT} x_k x_k^\top$  be the empirical covariance matrix of all random vectors, and  $I_p$  be the compatible identity matrix. Assume  $x_{t,l}$ 's norm is bounded, say by 1, and scale it with

$$u_{t,l}^p := \sqrt{\alpha} x_{t,l}^p, \quad (127)$$

obtaining  $U^{p,b} = [U^1 \ \dots \ U^t \ \dots \ U^T] = \sqrt{a} \cdot X^p$ , where  $a := \frac{\text{tr}(S^p)}{\text{tr}(S^p S^p)}$ . Let

$$T^p := \frac{1}{bT} \sum_{k=1}^{bT} u_k u_k^\top = a \cdot S^{p,t} \quad (128)$$

be the empirical covariance matrix of all  $u_k^p$ 's.

Assume  $a$  is bounded by  $\alpha(p) = O(p)$  and  $\mathbf{E} \left[ \sqrt{\text{ptr}((T^p - I^p)(T^t - I^p))} \right]$  also is upperbounded by  $\beta(p) = O(p)$ .

Further assume that the following function of  $z \in \mathbb{C}^+$  and  $p, b, T \in \mathbb{N}^+$

$$\mathbf{E} \left[ \sum_i \frac{1}{\lambda_i(UU^\top) - z} \right] \quad (129)$$

is always continuous w.r.t.  $z$  for any  $p, b, T$ .

If the above assumptions are satisfied, the non-zero eigenvalue concentrates. To be more specific, let  $\overline{\lambda^{>0}}$  be the mean of non-zero eigenvalues of  $\frac{1}{bT} U^p (U^p)^\top$  and use  $\mathbf{E} \left[ \overline{\lambda^{>0}} \right]^2$  to represent the overall situation of non-zero eigenvalues. Then there is

$$\mathbf{E} \left[ \frac{\mathbf{E} \left[ \overline{\lambda^{>0}} / \sqrt{v} \right]^2}{\left( \frac{\lambda}{\sqrt{v}} \right)^2 + v} \right] \leq \frac{\sqrt{2}}{cv\sqrt{v}} \frac{\alpha^2}{\min(bT, p)^2} \sqrt{c + \frac{(2\sqrt{2} + 2) c\alpha}{vp} + \frac{c\beta}{vp} + \frac{c}{vp}}, \quad (130)$$

$$\mathbf{E} \left[ \frac{\mathbf{E} \left[ \overline{\lambda^{>0}} \right]}{\lambda + \frac{v^2}{\lambda}} \right] \leq \frac{\sqrt{2}}{c\sqrt{v}} \frac{\alpha}{\min(bT, p)} \sqrt{c + \frac{(2\sqrt{2} + 2) c\alpha}{vp} + \frac{c\beta}{vp} + \frac{c}{vp}}. \quad (131)$$

for any  $v > 0$ , where  $\lambda$  is a randomly selected eigenvalue of  $\frac{1}{bT} U^p (U^p)^\top$  and  $c = p/bT$ .

*Proof of Theorem 6.* The proof is adapted from [30] where independence condition is replaced with new regularities.

Cauchy-Stieltjes transform method is used. When applied to empirical spectral density, by definition there is

$$s^{FA}(z) = \text{tr}(A - zI)^{-1} / p := \text{tr}((A - zI)^{-1}) / p. \quad (177)$$

for positive semi-definite  $A \in \mathbb{R}^{p \times p}$ . Specifically,  $\frac{1}{bT} U^p (U^p)^\top = \frac{1}{bT} U U^\top$ 's Stieltjes transform is

$$s_p(z) = \text{tr} \left( \frac{1}{bT} U U^\top - zI \right)^{-1} / p = bT / \text{ptr} \left( U U^\top - zbTI \right)^{-1}. \quad (178)$$

To ease presentation, we define  $\Xi(g)$  to indicate (complex) functions whose magnitudes are bounded by positive real function  $g$ , i.e.,

$$h \in \Xi(g) \iff \forall x, y, |h(x, y)| \leq g(x), \quad (179)$$

where  $y$  indicates variables other than  $x$  that  $h$  relies.  $\Xi(\cdot)$  will be used combined with “=” imitating  $O(\cdot)$ . Since  $\Xi(\cdot)$  does not hide constant scaling factors and biases in it, unlike  $O(\cdot)$  it can be freely added, averaged, multiplied and divided, i.e.,

$$\Xi(g_1) + \Xi(g_2) \in \Xi(g_1 + g_2) \quad (180)$$

$$\frac{1}{n} \sum_{i=1}^n \Xi(g_i) \in \Xi\left(\frac{1}{n} \sum_{i=1}^n g_i\right), \quad (181)$$

$$\Xi(g_1) \cdot \Xi(g_2) \in \Xi(g_1 \cdot g_2), \quad (182)$$

$$\frac{\Xi(g_1)}{g_2} \in \Xi\left(\frac{g_1}{g_2}\right), \quad (183)$$

Consistent with final conclusion, fix  $z = 0 + vi$  ( $v \in \mathbb{R}^+$ ) throughout the proof. Define  $A^p := \sum_k u_k u_k^\top$ . Sample an auxiliary vector  $u_{T,b+1} = u_{bT+1} \in \mathbb{R}^p$  so that it is sampled from the conditional distribution given the first  $T-1$  batches but it is conditionally independent with other samples in  $U^T$ , i.e., an extra sample for the last batch. This dependence relation can be expressed by only adding edges  $U^{1:T-1} \rightarrow u_{T,b+1}$  to the SCMs of Batch Dependence Model. With the auxiliary vector, define  $B^p := A^p + u_{T,b+1} u_{T,b+1}^\top$ .

By Lemma 11(1),  $B^p - zbTI$  is non-degenerate and

$$p = \text{tr} \left( (B^p - zbTI) (B^p - zbTI)^{-1} \right) \quad (184)$$

$$= \sum_{t=1}^T \sum_{l=1}^{b+I[t=T]} u_{t,l}^\top (B^p - zbTI)^{-1} u_{t,l} - zbT \text{tr} (B^p - zbTI)^{-1}. \quad (185)$$

Taking expectation and using the exchangeability within each batch give

$$p = \sum_{t=1}^T (b + I[t=T]) \mathbf{E} \left[ u_t^\top (B^p - zbTI)^{-1} u_t \right] - zbT \mathbf{E} \left[ \text{tr} (B^p - zbTI)^{-1} \right]. \quad (186)$$

Define  $S_p(z) := \text{tr} (A^p - zbTI)^{-1}$  and note that  $S_p(z) = (p/bT) s_p(z)$ .

By Lemma 11(2), there are

$$\mathbf{E} \left[ \text{tr} (B^p - zbTI)^{-1} \right] = \mathbf{E} [S_p(z)] + \Xi(1/vbT) = \mathbf{E} [S_p(z)] + \Xi(c/vp), \quad (187)$$

We now prove,

$$\frac{1}{T} \sum_{t=1}^T \mathbf{E} \left[ u_t^\top (B^p - zbTI)^{-1} u_t \right] = \frac{\mathbf{E} [S_p(z)]}{1 + \mathbf{E} [S_p(z)]} + t, \quad (188)$$

where  $|t|$  is bounded by a function of  $c, \alpha, \beta, v, p$ .

A complex function  $\frac{x}{1+x} = 1 - \frac{1}{x+1}$  emerges many times. We will approximate it to the first order so its complex derivative should be computed and bounded.

$$\left| \left( \frac{x}{1+x} \right)' \right| = \left| \frac{1}{(x+1)^2} \right| = \frac{1}{|x+1|^2} \quad (189)$$

Therefore, if  $x_1, x_2$  both stay away from  $-1$ , then  $\left| \left( \frac{x'}{1+x'} \right)' \right| = \Xi(1)$  on the line connecting  $x_1, x_2$  and we can approximate  $\frac{x_2}{1+x_2}$  by  $\frac{x_1}{1+x_1} + O(1)\Delta x$ , where  $\Delta x = x_1 - x_2$ . In latter application,  $x$ , both the start and the end of approximation, is often of form  $\frac{1}{n} \sum_{i=1}^n \mathbf{E} \left[ u_i^\top (C - zbTI)^{-1} u_i \right]$  possibly with averaging or expectation missing, where  $C$  is real symmetric positive semi-definite and  $u_i$  is real vector. The eigenvalues in  $(C - zbTI)^{-1}$  are

$$\frac{1}{\lambda_i(C) - vbTi} = \frac{\lambda_i(C) + vbTi}{\lambda_i(C)^2 + (vbT)^2}, \quad (190)$$

whose real part is

$$\operatorname{Re} \left( \frac{1}{\lambda_i(C) - vbTi} \right) = \frac{\lambda_i(C)}{\lambda_i(C)^2 + (vbT)^2} \geq 0. \quad (191)$$

As a result, the real part of inner products is always non-negative and  $x$  stays away from  $-1$ , and the magnitude of derivatives are  $\Xi(1)$ .

Another approximation is done between  $C_k^p$  and  $A_p$ , whose difference is outer products of a constant number of random vectors, and it should be minor considering there are  $bT$  of them. Formally, for real symmetric positive semi-definite  $C$  with eigenvalue decomposition  $C = V\Lambda V^\top$  by real matrices  $V$  and  $\Lambda$ ,  $(C - zI)$  can be decomposed to  $(C - zI) = V(\Lambda - zI)V^\top$ , and non-degenerate  $(C - zI)^{-1}$  to  $(C - zI)^{-1} = V(\Lambda - zI)^{-1}V^\top =: V\Sigma\Sigma V^\top$  where  $\Sigma := \sqrt{(\Lambda - zI)^{-1}}$ . Let  $S := V\Sigma V^\top$  to have  $S^\top S = SS = (C - zI)^{-1}$ . After that, there is

$$\left| y^\top \left( C + xx^\top - zI \right)^{-1} y - y^\top (C - zI)^{-1} y \right| \quad (192)$$

$$= \left| y^\top \left( \left( C + xx^\top - zI \right)^{-1} - (C - zI)^{-1} \right) y \right| \quad (193)$$

$$= \left| \frac{y^\top (C - zI)^{-1} xx^\top (C - zI)^{-1} y}{1 + x^\top (C - zI)^{-1} x} \right| = \left| \frac{(y^\top S^\top S x) (x^\top S^\top S y)}{1 + x^\top (C - zI)^{-1} x} \right| \quad (194)$$

$$= \left| \frac{(a^\top \bar{b}) (\bar{b}^\top a)}{1 + x^\top (C - zI)^{-1} x} \right| = \frac{|a^* b| |a^* b|}{\left| 1 + x^\top (C - zI)^{-1} x \right|} \quad (195)$$

$$\leq \frac{\|a^*\|_2 \|b\|_2 \|a^*\|_2 \|b\|_2}{\left| 1 + x^\top (C - zI)^{-1} x \right|} = \frac{|a^* a| |b^* b|}{\left| 1 + x^\top (C - zI)^{-1} x \right|} \quad (196)$$

$$= \frac{|\operatorname{tr}(yy^\top S^* S)| |b^* b|}{\left| 1 + x^\top (C - zI)^{-1} x \right|} \leq \frac{\|yy^\top S^* S\|_1 |b^* b|}{\left| 1 + x^\top (C - zI)^{-1} x \right|} \quad (197)$$

$$\leq \frac{\|yy^\top\|_1 \|S^* S\|_\infty |b^* b|}{\left| 1 + b^\top b \right|} = \frac{\|y\|_2^2}{\operatorname{Im}(z)} \frac{|b^* b|}{\left| 1 + b^\top b \right|}, \quad (198)$$

where  $a := Sy, b := \bar{S}\bar{x} = \bar{S}x$ , the second step is from Sherman-Morrison formula, and the second last inequality is due to Lemma 8. The facts, that  $S^*S$  is positive semi-definite whose largest eigenvalue is smaller than the upperbound  $\frac{1}{v}$  of  $S^\top S$ 's eigenvalue magnitude, is also used. To bound the fraction between  $|b^*b|$  and  $|1 + b^\top b|$ , recall the eigenvalue decomposition on  $(C - zI)^{-1}$

$$(C - zI)^{-1} = V\Sigma\Sigma^\top V^\top \quad (199)$$

and  $S = V\Sigma^\top V^\top$ . Then

$$b^\top b = v^\top \Sigma \Sigma v, \quad (200)$$

$$b^*b = v^\top \bar{\Sigma} \Sigma v, \quad (201)$$

where  $v := V^\top x$  is a real vector. Notice that  $\Sigma\Sigma = \text{Diag}\left(\frac{1}{\lambda_i(C) - vi}\right) = \text{Diag}\left(\frac{\lambda_i(C) + vi}{\lambda_i(C)^2 + v^2}\right)$  where both real and imaginary parts are non-negative, and that  $\Sigma^*\Sigma = \text{Diag}\left(\frac{|\lambda_i(C) + vi|}{\lambda_i(C)^2 + v^2}\right)$ . With this, the inner products simplify to

$$b^\top b = \sum_i \frac{v_i^2 \lambda_i(C)}{\lambda_i(C)^2 + v^2} + i \sum_i \frac{v_i^2 v}{\lambda_i(C)^2 + v^2}, \quad (202)$$

$$b^*b = \sum_i \left| \frac{v_i^2}{\lambda_i(C)^2 + v^2} \lambda_i(C) + i \frac{v_i^2 v}{\lambda_i(C)^2 + v^2} \right| \quad (203)$$

Representing complex numbers by 2-dimensional vectors  $w_i := \begin{bmatrix} \frac{v_i^2 \lambda_i(C)}{\lambda_i(C)^2 + v^2} & \frac{v_i^2 v}{\lambda_i(C)^2 + v^2} \end{bmatrix}^\top$ , there is

$$|b^\top b| = \left\| \sum_i w_i \right\|_2, \quad (204)$$

$$|b^*b| = \sum_i \|w_i\|_2. \quad (205)$$

Noting that all entries of  $w_i$ 's are non-negative, there is

$$|b^*b| = \sum_i \|w_i\|_2 \leq \sum_i \|w_i\|_1 = \left\| \sum_i w_i \right\|_1 \leq \sqrt{2} \left\| \sum_i w_i \right\|_2 = \sqrt{2} |b^\top b|. \quad (206)$$

So  $\frac{|b^*b|}{|b^\top b|} \leq \sqrt{2}$ . Given that the real part of  $b^\top b$  is non-negative, adding 1 will only increase its magnitude. As a result, there is

$$\left| y^\top (C + xx^\top - zI)^{-1} y - y^\top (C - zI)^{-1} y \right| \leq \frac{\sqrt{2} \|y\|_2^2}{\text{Im}(z)}, \quad (207)$$

When  $zbT$  is substituted, there is

$$\left| y^\top (C + xx^\top - zbTI)^{-1} y - y^\top (C - zbTI)^{-1} y \right| = \frac{\sqrt{2} \|y\|_2^2}{vbT}. \quad (208)$$

In later use,  $y$  is instantiated by  $u_k$  and there is  $\|u_k\|_2^2 = a\|x\|_2^2 \leq \alpha = O(p)$  for any  $t$ , so by assumption the approximation error is always bounded by

$$\left| u_k^\top \left( C + xx^\top - zbTI \right)^{-1} u_k - u_k^\top (C - zbTI)^{-1} u_k \right| \leq \Xi \left( \frac{\sqrt{2}c\alpha}{vp} \right) \quad (209)$$

even after averaging.

With these two approximation techniques, we first approximate the LHS of Eq. (188). To this end, let  $C_k^p := B^p - u_k u_k^\top$  and by Sherman-Morrison formula there is

$$u_k^\top (B^p - zbTI)^{-1} u_k = u_k^\top \left( C_k^p + u_k u_k^\top - zbTI \right)^{-1} u_k \quad (210)$$

$$= u_k^\top \left( (C_k^p - zbTI)^{-1} - \frac{(C_k^p - zbTI)^{-1} u_k u_k^\top (C_k^p - zbTI)^{-1}}{1 + u_k^\top (C_k^p - zbTI)^{-1} u_k} \right) u_k \quad (211)$$

$$= \frac{u_k^\top (C_k^p - zbTI)^{-1} u_k}{1 + u_k^\top (C_k^p - zbTI)^{-1} u_k} \quad (212)$$

$$= \frac{u_k^\top (A^p - zbTI)^{-1} u_k}{1 + u_k^\top (A^p - zbTI)^{-1} u_k} + \Xi(1) \cdot \Xi \left( \frac{2\sqrt{2}c\alpha}{vp} \right). \quad (213)$$

After that, there is

$$\frac{1}{T} \sum_{t=1}^T \mathbf{E} \left[ u_t^\top (B^p - zbTI)^{-1} u_t \right] \quad (214)$$

$$= \frac{1}{T} \sum_{t=1}^T \frac{1}{b} \sum_{l=1}^b \mathbf{E} \left[ \frac{u_{t,l}^\top (A^p - zbTI)^{-1} u_{t,l}}{1 + u_{t,l}^\top (A^p - zbTI)^{-1} u_{t,l}} \right] + \Xi(1) \cdot \Xi \left( \frac{2\sqrt{2}c\alpha}{vp} \right) \quad (215)$$

$$= \frac{1}{bT} \sum_k \mathbf{E} \left[ \frac{\mathbf{E} \left[ \frac{1}{bT} \sum_k u_k^\top (A^p - zbTI)^{-1} u_k \right]}{1 + \mathbf{E} \left[ \frac{1}{bT} \sum_k u_k^\top (A^p - zbTI)^{-1} u_k \right]} \right] + \Xi \left( \frac{2\sqrt{2}c\alpha}{vp} \right) \quad (216)$$

$$+ \frac{1}{bT} \sum_k \mathbf{E} \left[ \Xi(1) \left| u_k^\top (A^p - zbTI)^{-1} u_k - \mathbf{E} \left[ \frac{1}{bT} \sum_k u_k^\top (A^p - zbTI)^{-1} u_k \right] \right| \right] \quad (217)$$

$$= \frac{\mathbf{E} \left[ \frac{1}{bT} \sum_k u_k^\top (A^p - zbTI)^{-1} u_k \right]}{1 + \mathbf{E} \left[ \frac{1}{bT} \sum_k u_k^\top (A^p - zbTI)^{-1} u_k \right]} + \Xi \left( \frac{2\sqrt{2}c\alpha}{vp} \right) \quad (218)$$

$$+ \Xi(1) \frac{1}{bT} \sum_k \mathbf{E} \left[ \left| u_k^\top (A^p - zbTI)^{-1} u_k - \mathbf{E} \left[ \frac{1}{bT} \sum_k u_k^\top (A^p - zbTI)^{-1} u_k \right] \right| \right] \quad (219)$$

$$= \frac{\mathbf{E} \left[ \frac{1}{bT} \sum_k u_k^\top (A^p - zbTI)^{-1} u_k \right]}{1 + \mathbf{E} \left[ \frac{1}{bT} \sum_k u_k^\top (A^p - zbTI)^{-1} u_k \right]} \quad (220)$$

$$+ \Xi(1) \mathbf{E} \left[ \left| u_r^\top (A^p - zbTI)^{-1} u_r - \mathbf{E} \left[ u_r^\top (A^p - zbTI)^{-1} u_r \right] \right| \right] \quad (221)$$

$$+ \Xi \left( \frac{2\sqrt{2}c\alpha}{vp} \right), \quad (222)$$



where  $r$  in the last line is an uniformly randomly selected index from  $\{1, \dots, bT\}$  independent to training process.

Notice that  $S_p(z) = \text{tr}(A^p - zbTI)^{-1}$ ,  $\mathbf{E}[S_p(z)] = \mathbf{E}[\text{tr}(A^p - zbTI)^{-1}]$ . So for the term in Eq. (220) we proceed by proving  $\frac{1}{b} \sum_{l=1}^b \mathbf{E}[u_{t,l}^\top (A^p - zbTI)^{-1} u_{t,l}]$  approximates  $\mathbf{E}[\text{tr}(A^p - zbTI)^{-1}]$ . For convenience let  $D := bT(A^p - zbTI)^{-1}$  be an alias to it, whose spectral norm satisfies  $\|D\|_\infty \leq bT \frac{1}{vbT} = \frac{1}{v}$ , then

$$\left| \mathbf{E} \left[ \frac{1}{bT} \sum_k u_k^\top (A^p - zbTI)^{-1} u_k \right] - \mathbf{E}[S_p(z)] \right| \quad (223)$$

$$= c \left| \frac{\mathbf{E} \left[ \frac{1}{bT} \sum_k u_k^\top bT (A^p - zbTI)^{-1} u_k \right]}{p} - \frac{\mathbf{E}[bTS_p(z)]}{p} \right| \quad (224)$$

$$= \frac{c}{p} \left| \frac{1}{bT} \sum_k \mathbf{E}[u_k^\top D u_k] - \mathbf{E}[\text{tr}(D)] \right| = \frac{c}{p} \left| \mathbf{E} \left[ \text{tr} \left( \left( \frac{1}{bT} \sum_k u_k u_k^\top - I \right) D \right) \right] \right| \quad (225)$$

$$\leq \frac{c}{p} \mathbf{E} \left[ \left\| \left( \frac{1}{bT} \sum_k u_k u_k^\top - I \right) D \right\|_1 \right] \leq \frac{c}{p} \mathbf{E} \left[ \left\| \left( \frac{1}{bT} \sum_k u_k u_k^\top - I \right) \right\|_1 \|D\|_\infty \right] \quad (226)$$

$$\leq \frac{c}{vp} \mathbf{E} \left[ \left\| \left( \frac{1}{bT} \sum_k u_k u_k^\top - I \right) \right\|_1 \right] \leq \frac{c}{vp} \mathbf{E} \left[ \sqrt{p \text{tr}((T_t^p - I)^\top (T_t^p - I))} \right] \quad (227)$$

$$= \Xi \left( \frac{c\beta}{vp} \right), \quad (228)$$

where the last inequality is because

$$\|A\|_1 = \sum_{i=1}^p |\lambda_i(A)| = \left\| [\lambda_1(A) \ \dots \ \lambda_i(A) \ \dots \ \lambda_p(A)]^\top \right\|_1 \quad (229)$$

$$\leq \sqrt{p} \left\| [\lambda_1(A) \ \dots \ \lambda_i(A) \ \dots \ \lambda_p(A)]^\top \right\|_2 \quad (230)$$

$$= \sqrt{p} \|A\|_2 = \sqrt{p \text{tr}(A^\top A)}, \quad (231)$$

given that  $A = (\frac{1}{bT} \sum_k u_k u_k^\top - I)$  is symmetric so that its singular values are absolute eigenvalues. With approximation on complex function  $\frac{x}{1+x}$ , this  $\Xi \left( \frac{c\beta}{vp} \right)$ -boundedness implies  $\Xi(1) \cdot \Xi \left( \frac{c\beta}{vp} \right) = \Xi \left( \frac{c\beta}{vp} \right)$  approximation of in Eq. (220).

For the difference term in Eq. (221), we prove its diminishment by  $\frac{1}{v}$ -bounded variance of  $u_{t,l}^\top (A^p - zbTI)^{-1} u_{t,l}$ , or formally

$$\mathbf{E} [|X - \mathbf{E}[X]|^2] - \mathbf{E} [|X - \mathbf{E}[X]|]^2 = \mathbf{E} [ (|X - \mathbf{E}[X]| - \mathbf{E} [|X - \mathbf{E}[X]|])^2 ] \geq 0 \quad (232)$$

$$\mathbf{E} [|X - \mathbf{E}[X]|] \leq \sqrt{\mathbf{E} [|X - \mathbf{E}[X]|^2]} = \sqrt{\mathbf{Var}[X]}, \quad (233)$$

and

$$\mathbf{Var} \left[ u_r^\top (A^p - zbTI)^{-1} u_r \right] \quad (234)$$

$$= \frac{c^2}{p^2} \mathbf{Var} \left[ u_r^\top Du_r \right] = \frac{c^2}{p^2} \left( \mathbf{E} \left[ \text{tr} \left( u_r^\top Du_r u_r^\top Du_r \right) \right] - \mathbf{E} \left[ \text{tr} \left( u_r^\top Du_r \right) \right]^2 \right) \quad (235)$$

$$\leq \frac{c^2}{p^2} \alpha^2 \left( \mathbf{E} \left[ \text{tr} \left( x_r^\top Dx_r x_r^\top Dx_r \right) \right] - \mathbf{E} \left[ \text{tr} \left( x_r^\top Dx_r \right) \right]^2 \right) \quad (236)$$

$$\leq \frac{c^2 \alpha^2}{p^2} \mathbf{E} \left[ \text{tr} \left( x_r^\top Dx_r x_r^\top Dx_r \right) \right] \leq \frac{c^2 \alpha^2}{p^2} \mathbf{E} \left[ \|x^p\|_2^4 \|D\|_\infty^2 \right] \quad (237)$$

$$= \frac{c^2 \alpha^2}{v^2 p^2}, \quad (238)$$

where the last step follows that  $x^p$ 's norm is bounded and that  $\|D\|$  is also uniformly bounded.

To sum up, we have obtained

$$\frac{1}{T} \sum_{t=1}^T \mathbf{E} \left[ u_t^\top (B^p - zbTI)^{-1} u_t \right] = \frac{\mathbf{E} [S_p(z)]}{1 + \mathbf{E} [S_p(z)]} + t, \quad (239)$$

where  $|t| = \Xi \left( \frac{2\sqrt{2}c\alpha}{vp} + \frac{c\beta}{vp} + \frac{c\alpha}{vp} \right)$ .

With Eq. (188), Eq. (187), one can reduce Eq. (186) to

$$p = T(b + O(1)) \left( \frac{\mathbf{E} [S_p(z)]}{1 + \mathbf{E} [S_p(x)]} + t \right) - zbT (\mathbf{E} [S_p(z)] + \Xi (c/vp)), \quad (240)$$

and

$$\frac{\mathbf{E} [S_p(z)]}{1 + \mathbf{E} [S_p(x)]} - z\mathbf{E} [S_p(z)] = \frac{p}{bT} + s = c + s, \quad (241)$$

where  $s = \Xi \left( \frac{2\sqrt{2}c\alpha}{vp} + \frac{c\beta}{vp} + \frac{c\alpha}{vp} + \frac{c}{vp} + \frac{c\alpha}{vp} \right)$ .

$\mathbf{E} [S_p(p)]$  always have non-negative real part because real parts of eigenvalues of  $(UU^\top - vbTI)$  are always non-negative by argument similar to previous ones. Since  $\alpha, \beta, c$  depend only on  $p, b, T$  instead of  $v$ ,  $s = \Xi \left( \frac{2\sqrt{2}c\alpha}{vp} + \frac{c\beta}{vp} + \frac{c\alpha}{vp} + \frac{c}{vp} + \frac{c\alpha}{vp} \right)$  is bounded by a function that monotonically decreases when  $p, b, T$  are fixed and  $v$  increases. By Lemma 10, there is

$$|\text{Im} (\mathbf{E} [S_p(vi)])| \leq |\mathbf{E} [S_p(vi)]| \quad (242)$$

$$\leq \sqrt{\frac{2}{v} \left( c + \frac{2\sqrt{2}c\alpha}{vp} + \frac{c\beta}{vp} + \frac{c\alpha}{vp} + \frac{c}{vp} + \frac{c\alpha}{vp} \right)}. \quad (243)$$

The similar bound for  $s_p(z) = (bT/p)S_p(z) = \frac{1}{c}S_p(z)$  is

$$|\text{Im} (\mathbf{E} [s_p(vi)])| \leq \frac{1}{c} \sqrt{\frac{2}{v} \left( c + \frac{2\sqrt{2}c\alpha}{vp} + \frac{c\beta}{vp} + \frac{c\alpha}{vp} + \frac{c}{vp} + \frac{c\alpha}{vp} \right)}. \quad (244)$$

The expected mean  $\mathbf{E} \left[ \overline{\lambda^{>0}} \right]$  of  $\frac{1}{bT} U^p (U^p)^\top$ 's non-zero eigenvalue is

$$\mathbf{E} \left[ \frac{\text{tr} \left( \frac{1}{bT} U^p (U^p)^\top \right)}{\min(bT, p)} \right] = \frac{\frac{1}{bT} \sum_{k=1}^{bT} \mathbf{E} [\text{tr} (u_k u_k^\top)]}{\min(bT, p)} \quad (245)$$

$$= \frac{\frac{1}{bT} \sum_{k=1}^{bT} \mathbf{E} [\|u_k\|_2^2]}{\min(bT, p)} \leq \frac{\alpha}{\min(bT, p)}. \quad (246)$$

Finally, the desired conclusion is obtained through Lemma 9 by

$$\mathbf{E} \left[ \frac{\mathbf{E} \left[ \overline{\lambda^{>0}} / \sqrt{v} \right]^2}{\left( \frac{\lambda}{\sqrt{v}} \right)^2 + v} \right] \leq \frac{1}{v} \mathbf{E} \left[ \overline{\lambda^{>0}} \right]^2 |\text{Im} (s_p(vi))| \quad (247)$$

$$\leq \frac{1}{vc} \frac{\alpha^2}{\min(bT, p)^2} \sqrt{\frac{2}{v} \left( c + \frac{2\sqrt{2}c\alpha}{vp} + \frac{c\beta}{vp} + \frac{c\alpha}{vp} + \frac{c}{vp} + \frac{c\alpha}{vp} \right)}, \quad (248)$$

$$\mathbf{E} \left[ \frac{\mathbf{E} \left[ \overline{\lambda^{>0}} \right]}{\lambda + \frac{v^2}{\lambda}} \right] \leq \mathbf{E} \left[ \overline{\lambda^{>0}} \right] |\text{Re} (s_p(vi))| \quad (249)$$

$$\leq \frac{1}{c} \frac{\alpha}{\min(bT, p)} \sqrt{\frac{2}{v} \left( c + \frac{2\sqrt{2}c\alpha}{vp} + \frac{c\beta}{vp} + \frac{c\alpha}{vp} + \frac{c}{vp} + \frac{c\alpha}{vp} \right)}. \quad (250)$$

□

## D Effective Window Size

We argue that the effective window size should be considered by  $r = 1 - \eta w$  instead of  $\sqrt{r} = \sqrt{1 - \eta w}$  to have better results, where  $\eta$  is learning rate and  $w$  is the strength of weight decay. The argument relies on another formulation of eigenvalues:  $\lambda_i(A)$  corresponds to critical points of Rayleigh quotient

$$\max_{v \in \mathbb{R}^n \setminus \{0\}} \frac{v^\top A v}{v^\top v} = \max_{v \in \mathbb{R}^n: \|v\|=1} v^\top A v. \quad (251)$$

Particularly for weight decayed sample covariances where  $S = UU^\top = \sum_{t,l} \sqrt{r}^{T-t} u_{t,l} \sqrt{r}^{T-t} u_{t,l}^\top$ , its eigenvalues are given by critical points of

$$\max_{v \in \mathbb{R}^n: \|v\|=1} v^\top U U^\top v = \max_{v \in \mathbb{R}^n} \sum_{t,l} r^{T-t} \langle u_{t,l}, v \rangle^2. \quad (252)$$

So terms are weighted by  $r$  instead of  $\sqrt{r}$ . Now consider situation where effective window  $k$  is used to produce  $S'$ , whose eigenvalues are given by

$$\max_{v \in \mathbb{R}^n: \|v\|_2=1} \sum_{t=T-k+1}^T \sum_l r^{T-t} \langle u_{t,l}, v \rangle^2, \quad (253)$$

and consider its difference with those of all samples.

For the smallest non-zero eigenvalues, there is  $\lambda_{\min(p,bT)}(S) \geq \lambda_{\min(p,bT)}(S')$  since adding a real symmetric positive semi-definite matrix to  $S'$  to obtain  $S$  increases all eigenvalues. So we will not be overoptimistic in smallest non-zero eigenvalues, when it comes bounding the fraction between the largest and smallest non-zero eigenvalues.

For the largest eigenvalues, there is  $\lambda_1(S) \leq \lambda_1(S') + \sum_{t=1}^{T-k} \sum_l r^{T-t} \|u_{t,l}\|_2^2$ . To see this, let  $v_{\max}$  be the unit vector that achieves  $\lambda_1(S)$ .

$$\lambda_1(S) = \sum_{t=1}^T \sum_l r^{T-t} \langle u_{t,l}, v_{\max} \rangle^2 = \sum_{t=T-k+1}^T \sum_l r^{T-t} \langle u_{t,l}, v_{\max} \rangle^2 + \sum_{t=1}^{T-k} \sum_l r^{T-t} \langle u_{t,l}, v_{\max} \rangle^2 \quad (254)$$

$$\leq \max_{\|v\|_2=1} v^\top S' v + \sum_{t=1}^{T-k} \sum_l r^{T-t} \|u_{t,l}\|_2^2 = \lambda_1(S') + \sum_{t=1}^{T-k} \sum_l r^{T-t} \|u_{t,l}\|_2^2. \quad (255)$$

So at most will be overoptimistic by  $\sum_{t=1}^{T-k} \sum_l r^{T-t} \|u_{t,l}\|_2^2$ .

As a result, if exponential weight sum of out-of-window tail, controlled by  $r$  instead of  $\sqrt{r}$ , is small, then the overoptimism will be suppressed.

## E Experimental Details

There are 4 experiments involving massive training in our work. We summarize most their hyper-parameters in Table 2. Weights in linear layers are initialized with Xavier initialization based on uniform distribution and vanilla biases are initialized normal distribution with standard deviation of  $10^{-6}$ , inherited from PyTorch’s recipe [37].

In Section 7.2, checkpoints are from training vanilla ViT-Base on ImageNet-1k from scratch. Eigenvalues are computed by 1) feed  $K^l (K^l)^\top$  into `torch.linalg.eigvals`, and then 2) drop imaginary parts because  $K^l (K^l)^\top$  is symmetric real matrix, and finally 3) clamped into  $[0, \infty)$  given that  $K^l (K^l)^\top$  is symmetric positive semi-definite.

In Section 7.3, tiny MLPs have 4 pre-LayerNormed hidden linear layers, each with square weight matrix of shape  $p \times p$ . Residual connections are placed across hidden layers. Inputs and outputs of the model are transformed using input and classifier linear layers without LayerNorm or residual connections. Parameters are initialized using default initialization in PyTorch. Affine parameters are turned off in LayerNorm layers. Data augmentations include random clipping, which first scales digits into  $36 \times 36$  images and then clips them into  $32 \times 32$  images, and random rotation with maximum rotation of 30 degrees. SGD without momentum is used for optimization. Learning rate is set to  $10^{-3}$  and no scheduler is used to ease the computation of effective window size. Batch size is 32 and training is lasts for 100 epochs. Hidden features  $U^t$  and back-propagated gradients  $H^t$  are recorded every step. The outer products of vectors are computed, and are summed to existing empirical covariance matrix decayed by factor  $(\sqrt{1 - \eta w})^2 = 1 - \eta w =: r$ , where  $w \in \{0.0, 0.01, 0.1, 0.3\}$  is the strength of weight decay and  $\eta = 10^{-3}$  is the learning rate. When weight decay is 0.0,  $T$  equals to the current step number. When weight decay exists,  $T$  is the smallest value among the step count and the effective window size computed as in Section 4.6 with tail weight threshold  $\tau = 10^{-3}$ .

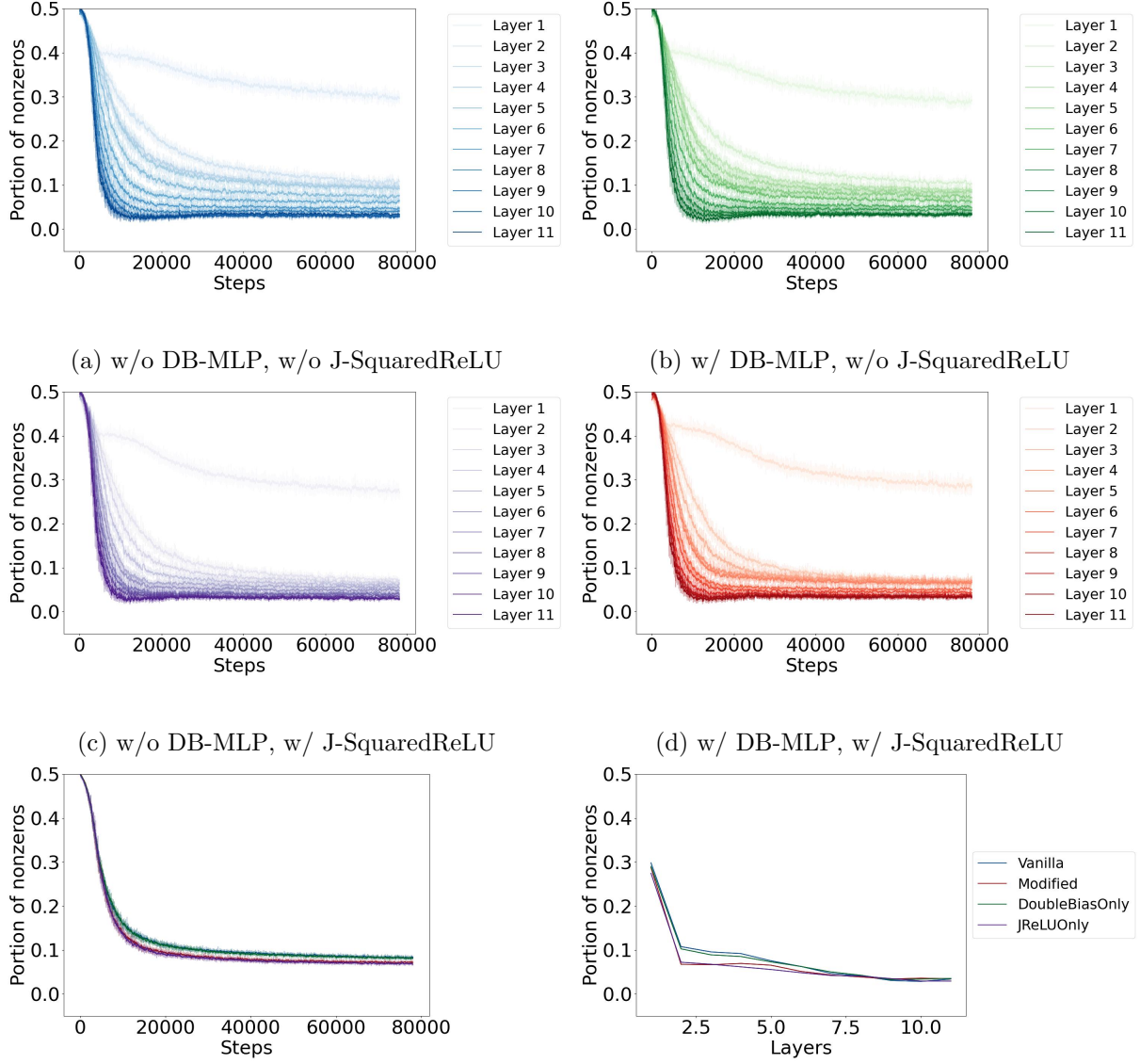
	Validation (5)	CIFAR-10 (6.1)	ImageNet-1k (6.1)	Finetuning (6.2)
Arch. and size	ViT-Base/16	ViT-Base/16	ViT-Base/16	ViT-Base/16
Optimizer	Adam	Adam	AdamW	AdamW
Epochs	100	100	300	301 – 310
Learning rate	$10^{-4}$	$10^{-4}$	$3 \times 10^{-3}$	$3 \times 10^{-3}$
Batch size	64	64	512	512
Dropout	0.0	0.0	0.0	0.0
Weight decay	0.0	0.0	0.3	0.3
Gradient Clipping	1.0	1.0	10.0	10.0
Warmup (Linear)	5 epochs	5 epochs	0 epochs	0 epochs
Scheduler			CosineAnnealing	CosineAnnealing
Label smoothing			0.11	0.11
Mixup alpha			0.2	0.2
Auto augmentation			ra	ra
Cutmix alpha			1.0	1.0
AMP			✓	✓
Model EMA			✗	✗
Based on			PyTorch’s recipe [37]	PyTorch’s recipe [37]

Table 2: Major hyperparameters of computer vision experiments.

## F More Experimental Results

Ablation study is conducted on CIFAR-10 to verify that both of our modifications improve gradient sparsity. The results are shown in Fig. 14.

From Fig. 14e we can see that J-SquaredReLU greatly improves sparsity while DB-MLP does not. After inspecting the codes we found that zeroth biases are misplaced before self-attention modules instead of MLP blocks. The experiment with this bug fixed will come in later versions.



(e) Sparsity averaged across layers during training.

(f) Layerwise sparsity during the last 100 steps.

Figure 14: Results of ablation study.

## G Theoretically Guided Magic: Massive Perturbation with Small Computation Cost and Good Parallelism

Lemma 6 and Theorem 4 state that by adding massive synaptic noises (non-massive synaptic noises for single tokens can be found in [42], [43], dated back to 1990s) to weight matrices during forward propagation as in Eq. (82), we are training a  $k$  times larger effective model and optimizing its flatness w.r.t. these  $k$  times parameters, where  $k$  is the number of tokens. These noises can potentially greatly improve the generalization of deep CNNs, Transformers, MLP-Mixers or other architectures as long as they split input into multiple tokens.

However, Eq. (82) requires adding noises to weight matrices independently for each token before matrix multiplication, which is unfriendly to GPUs who prefer stacked matrix multiplication. Direct application of Eq. (82) also requires  $k \times n \times d$  independent Gaussian noises. Therefore, here we propose an algorithm called MagicSynapse that is friendly to parallelism and only requires  $k \times n$  independent noises, which is the same number as dropout.

The core motivation of MagicSynapse is to add noises *after* matrix multiplication, which is possible by merging multiple Gaussian noises into one. Let  $Z^l$  be the result of multiplication with  $\hat{W}^{l,i}$ s in Eq. (82) and  $z_i^l := Z_{:,i}^l$  be the  $i$ -th (column) hidden vector/token in it. Then there is

$$z_i^l := \hat{W}^{l,i} x_i = W^l x_i + E^{l,i} x_i = W^l x_i + \left[ \left\langle E_j^{l,i}, x_i \right\rangle \right]_j \quad (256)$$

$$= W^l x_i + \left[ \sum_q X_{q,i}^l \cdot E_{j,q}^{l,i} \right]_j. \quad (257)$$

The summation is a linear combination of independent Gaussian variables, which is also Gaussian. Since entries in  $E^{l,i}$  are assumed to follow  $\mathcal{N}(0, \sigma^2)$ , there is

$$\sum_q X_{q,i}^l \cdot E_{j,q}^{l,i} \sim \mathcal{N} \left( 0, \sigma^2 \sum_q \left( X_{q,i}^l \right)^2 \right) = \mathcal{N} \left( 0, \sigma^2 \|x_i\|_2^2 \right). \quad (258)$$

Note that  $E_j^{l,i}$  is only used once for each  $(i, j)$ , so the linear combinations are independent and the perturbed matrix product simplifies to

$$z_i^l = W^l x_i + e^{l,i}, \quad (259)$$

where  $n$ -variate Gaussian noise  $e^{l,i} \sim \mathcal{N} \left( 0, \sigma^2 \|x_i\|_2^2 I \right)$ . Therefore, we only need to compute the norm of input tokens, then sample  $k \times n$  Gaussian noises columnly scaled by them and add the scaled noises to the matrix product, which is MagicSynapse. If zeroth biases are removed and LayerNorm layers are placed before linear layers, the squared norm further simplifies to constant  $\|x_i\|_2^2 = d$ .

Interestingly, MagicSynapse is theoretically ensured by Lemma 6 and Theorem 4 to encourage flatness if the empirical loss is small enough, even though it is only a first-order optimization and requires only one forward and one backward propagations. Moreover, by using MagicSynapse, one is magically expanding the number of parameters. Although their values are correlated, their flatness w.r.t. non-correlated perturbations is indeed optimized. To give a sense of this magical parameter expansion, for ViT-Base, MagicSynapse-ed ViT-Base is effectively 197 times larger, with approximately 17B flatness-effective parameters. In NLP tasks this expansion is even larger given

the larger number of tokens. MagicSynapse can be easily implemented as a PyTorch forward Hook that is registered on all linear layers, which is useful in almost any architectures. For CNN, which can be seen as MLPs with parameters de-duplicated, the computation of input norms can be tricky but is also possible and efficient by all-1-kernel convolution on squared input feature maps.

$\sigma^2$  is a hyperparameter that must be determined beforehand. The noise should be small compared to the magnitudes of entries in weight matrices to allow approximation. However, the norm of parameters may change drastically during training, especially under weight decay. So a more practical solution is to adjust  $\sigma^2$  dynamically. We consider a simple solution: for each weight matrix, we compute the average  $L_1$  norm of entries in that matrix and multiply it with a pre-determined  $\rho < 1$  to obtain  $\sigma^2$ . We call it AdaptiveMagicSynapse.

The experiments are still running together with all re-runs in Section 6 and will come in the next version.